Czech Technical University in Prague
Faculty of Civil Engineering
Department of Steel and Timber Structures

Stainless Steel Portal Frames

Master's thesis

Bc. Martin Kapoun

Master programme: Civil Engineering
Branch of study: Building Structures
Supervisor: Doc. Ing. Michal Jandera, Ph.D.

Stockholm, December 2018

KTH Royal Institue of Technology in Stockholm
School of Architecture and Built Environment
Department of Civil and Architectural Engineering

Stainless Steel Portal Frames

Master's thesis

Bc. Martin Kapoun

Master programme: Civil and Architectural Engineering
Branch of study: Division of Structural Engineering and Bridges
Supervisor: Doc. Ing. John Leander, Ph.D.

Stockholm, December 2018

ČESKÉ VYSOKÉ UČENÍ TECHNICKÉ V PRAZE
Fakulta stavební
Thákurova 7, 166 29 Praha 6

ZADÁNÍ DIPLOMOVÉ PRÁCE

I. OSOBNÍ A STUDIJNÍ ÚDAJE

Příjmení: Kapoun Jméno: Martin Osobní číslo: 477988

Zadávající katedra: Katedra ocelových a dřevěných konstrukcí

Studijní program: Stavební inženýrství

Studijní obor: Konstrukce pozemních staveb

II. ÚDAJE K DIPLOMOVÉ PRÁCI

Název diplomové práce: Portálové rámy z korozivzdorné oceli

Název diplomové práce anglicky: Stainless steel portal frames

Pokyny pro vypracování:
Literature review, FEM modeling in ABAQUS, recurrent meeting with supervisor

Seznam doporučené literatury:
Fiona Walport, Behaviour of Stainless Steel Frames
JANDERA, Michal, Denny SYAMSUDDIN a Bretislav ZIDLICKY. Stainless Steel Beam-Columns Behaviour. The Open Civil Engineering Journal[online]. 2017, 11(Suppl-1, M5), 358-368 [cit. 2018-10-09]. DOI: 10.2174/1874149501711010358. ISSN 1874-1495.
WALPORT, F., L. GARDNER, E. REAL, I. ARRAYAGO a D.A. NETHERCOT. Effects of material nonlinearity on the global analysis and stability of stainless steel frames. Journal of Constructional Steel Research[online]. 2018 [cit. 2018-10-09]. DOI: 10.1016/j.jcsr.2018.04.019. ISSN 0143974X.
EN 1993-1-1: General rules and rules for buildings.
EN 1993-1-4: General rules - Supplementary rules for stainless steels.

Jméno vedoucího diplomové práce: John Leander, doc. Ing. Ph.D.; Michal Jandera, doc. Ing. Ph.D.

Datum zadání diplomové práce: 1.10.2018 Termín odevzdání diplomové práce: 6.1.2019

III. PŘEVZETÍ ZADÁNÍ

Beru na vědomí, že jsem povinen vypracovat diplomovou práci samostatně, bez cizí pomoci, s výjimkou poskytnutých konzultací. Seznam použité literatury, jiných pramenů a jmen konzultantů je nutné uvést v diplomové práci a při citování postupovat v souladu s metodickou příručkou ČVUT „Jak psát vysokoškolské závěrečné práce" a metodickým pokynem ČVUT „O dodržování etických principů při přípravě vysokoškolských závěrečných prací".

1.10.2018
Datum převzetí zadání

Thesis Supervisor:
Doc. Ing. Michal Jandera, Ph.D.
Department of Steel and Timber Structures
Faculty of Civil Engineering
Czech Technical University in Prague
Thákurova 7
160 29 Prague 6
Czech Republic

Thesis Erasmus Supervisor:
Doc. Ing. John Leander, Ph.D.
Department of Civil and Architectural Engineering
School of Architecture and Built Environment
KTH Royal Institute of Technology in Stockholm
Brinellvägen 8
SE-100 44 Stockholm
Sweden

Declaration

I hereby declare that I have written this master thesis independently and quoted all the sources of information used in accordance with methodological instructions on ethical principles for writing an academic thesis. Moreover, I state that this thesis has neither been submitted nor accepted for any other degree.

In Stockholm, December 2018

.....
Bc. Martin Kapoun

Abstrakt

Stávající metodologie pro návrh konstrukcí z korozivzdorné oceli daná normou EN 1993-1-4 je založena na podobnosti s přístupy definovanými pro ocel uhlíkovou. Změny jsou například při kontrole stability nebo v uvažování elasticity ve všech výpočtech. Hlavní cíl této práce je ukázat rozdíly mezi uvažováním materiálové nelinearity v analýze v porovnání s normovým lineárním přístupem, který může vést k nadhodnoceným a konzervativním výsledkům. Plně geometrická a materiálově nelineární analýza byla provedena za pomoci softwaru pro výpočet metodou konečných prvků Abaqus pro devět různých tříd korozivzdorné oceli a pro tři různé třídy uhlíkové oceli. Tyto výsledky byly porovnány s výslednými hodnotami vypočítanými dle normy. Geometrie a průřezy jednotlivých prvků portálového rámu jsou převzaty z reálné konstrukce umístěné v kampusu technické univerzity ve Stockholmu. Závěry této práce ukazují podcenění návrhové kapacity konstrukce v případě zanedbání materiálové nelinearity.

Klíčová slova: nelineární materiál, kozorivzdorná ocel, portalový rám, MKP, ABAQUS.

Abstract

The current design methodology for structural stainless steel given by EN 1993-1-4 is based on its similarities with the carbon steel approach but with minor changes in equations for member buckling resistance and the assumption elasticity. The primary aim of this paper is to show differences between assuming material non-linearity in the analysis compared to the linear analysis code approach which can lead to over-predicted and conservative results. Fully geometric and material non-linear analysis with initial imperfections is carried out using the finite element software Abaqus for nine different grades of stainless steel and three different grades of carbon steel. These results are compared with results obtained by the code approach. The geometry and cross-sections of the portal frame is based on the real structure located in the campus of the university in Stockholm. The conclusion of this work shows the under estimation of the structure design capacity when material non-linearity is neglected.

Keywords: non-linear material, stainless steel, portal frame, FEM, ABAQUS.

Acknowledgements

I would like to express my deep gratitude to doc. Ing. John Leander, PhD. for his valuable and constructive suggestions, for his patient guidance, enthusiastic encouragement and useful critiques of this research work. I would also like to thank doc. Ing. Michal Jandera PhD., for his advice and motivation in this field of study.

Finally, I wish to thank my family for their encouragement and support throughout my study.

List of Tables

List of Figures

Contents

Chapter 1

Introduction

1.1 Background

Nowadays, architectural requirements have been increasing with clients demanding more with regards to the visual matter of the structure. Because of this, un-aesthetic bearing structures are now being constructed with materials which appear more visually pleasing. Stainless steel is one such material which fulfills this requirement due to its advantages in corrosion resistance and durability when compared to common carbon steel. On the other hand there is still a big disadvantage which is its expensiveness. This specific iron alloy is primarily divided into five groups used in structural design. Design Manual for Structural Stainless Steel [1] divides them namely into austenitic-ferritic (duplex), ferritic, martensitic and austenitic stainless steel and precipitation hardening steels differing in amounts of chromium and other chemical elements and thermomechanical treatment.

This work is focused on austenitic and austenitic-ferritic steels. Austenitic stainless steels are the most commonly used alloys in construction with a high amount of nickel content. According to [2] they have high ductility, are weldable and have a exceptional corrosion resistance. Only cold working can strengthen them. Austenitic-ferritic stainless steels have much higher mechanical strengths compared to austenitic steels and due to lower amounts of nickel in the alloy, the market price is more or less constant and not so volatile as it is in case of austenitic steels. With similar weldability and corrosion resistance they are the closest to austenitic steels from all the five groups.

There are few design approaches for structures of stainless steel, but they are generally based on the similarity with carbon steel. However, stainless steel and carbon steel have different material properties and behaviour. Carbon steel is described by a bi-linear stress-strain response meanwhile the characteristics of stainless steel is non-linear, curved. Current EN 1993-1-1 [3] states rules for designing structures from carbon steel and assumes that the material stress-strain behaviour is linear. EN 1993-1-4 [4] then supplements the

rules when the material is stainless steel but still assuming the linear behaviour which can lead to conservativeness of the design capacity.

1.2 Aim and the scope

Codes mentioned in Section 1.1 are used to examine an existing part of a building structure assumed as a portal frame. Firstly the structure is checked using the mentioned code approach for carbon steel and secondly a FE shell model is developed and full GMNIA is done using the Abaqus software for finite element calculations. This check is followed by a parametric study with different stainless steel materials, both for carbon and stainless steel with appropriate code, and its behaviour to find the difference in assuming and neglecting stainless steel material non-linearity. The overall purpose of this work is to show the differences in the material linearity and non-linearity of the stainless steel and the conservativeness of the code approach. The study objectives include:

- to investigate the structure using code approach for carbon and stainless steel
- to develop a finite element model close to the real structure
- to study the influence of stainless steel material non-linearity
- to investigate the influence of different modes for initial imperfections on theoretical load
- to assess fully geometrical and non-linear material analysis with initial imperfections for all modelled grades of steel

1.3 Outline of the thesis

In this chapter you will find a short introduction to stainless steel as well as the objectives of this thesis and outline of work.

In the second chapter you can find a literature review which was considered relevant to the study.

The third chapter contains descriptions of the methods which were used on a case study of an existing portal frame part of the structure, a description of the check using code approaches, development of the FE shell model together with finding the suitable mesh type and seed size used for the analysis, the process for finding the eigen modes of the structure, a definition of initial geometric imperfections and non-linear material modelling and its application in the software. This chapter also explains settings used in parametric studies.

The results of the different analysis are presented in chapter four and a final summary, conclusions and suggestions for further research can be found in the last chapter.

Chapter 2

Literature review

2.1 European design standards and stainless steel

To keep consistency and to have a unitary system of documents for building designs, the European Union prepared and developed a set of building approaches called Eurocodes. These standards cover the designs of all types of structures such as timber, steel or masonry. Each type of structure has its own document with parts explaining the basis of design or so called 'Principles and Application Rules'.

To distinguish between country specific variables such as modification factors, the choice of design method or whether an informative annex may be used, each of the Eurocodes have essential documents called 'National Annexes'.

In the matter of structural stainless steel there is a European stainless steel design guidance [1] firstly published by Euro Inox in 1994 which formed the basis for a European standard for stainless steel [4].

The European design standard for common carbon steel [3] gives us rules how to design steel structures, with material thicknesses $t \geq 3mm$, in a limit state design approach. The above mentioned standard [4] only supplements or supersedes the standard used for the carbon steel. Therefore during designing stainless steel structures both of the codes must be used together. Currently [4] lists a wider range of austenitic alloys but a smaller amount of ferritic and duplex, totalling 21 grades covered in three groups.

However [3] assumes in the elastic calculations that the material behavior is linear. Clause 5.4.2 states that elastic global analysis should be based on the assumption that the stress-strain behaviour of the material is linear, regardless of the stress level. Furthermore to perform calculations in the plastic state, a bi-linear material diagram is assumed as seen in Figure 2.1. Clause 5.4.3 states that the bi-linear stress-strain relationship may be used for the grades of structural steel specified in different sections of the standard. Figure 2.1b describes the carbon steel behaviour quite closely compared to the real case

up till 0.75% strain [1]. If such a diagram was simplified for higher strains, unrealistic values of stress would be obtained.

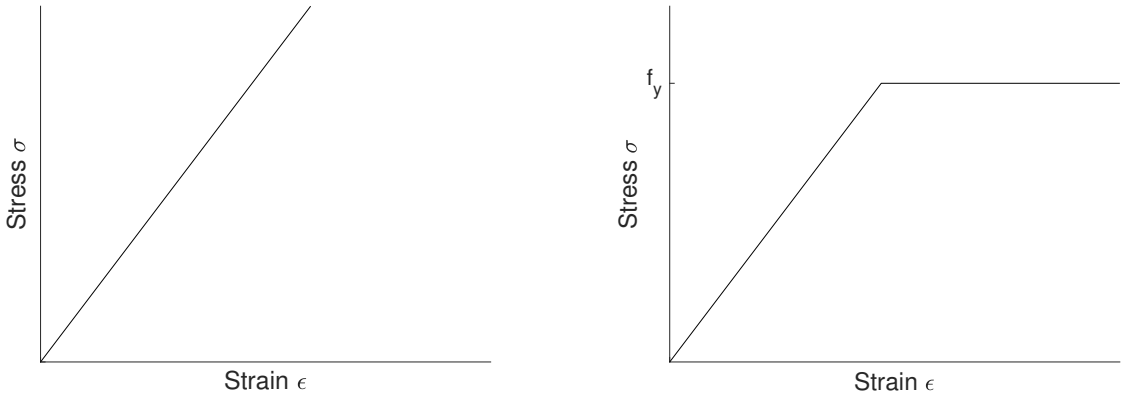

(a) Elastic relationship (b) Elastic-perfectly plastic relationship

Figure 2.1: Stress-strain relationships used in global analysis

However the behaviour of a stainless steel material is completely rounded (Figure 2.2) with no defined yield point. Furthermore assuming an elastic behaviour of a stainless steel material by using material characteristics according to the code will neglect a plastic redistribution of loads and material strain hardening, leading to underestimation of the material capacity.

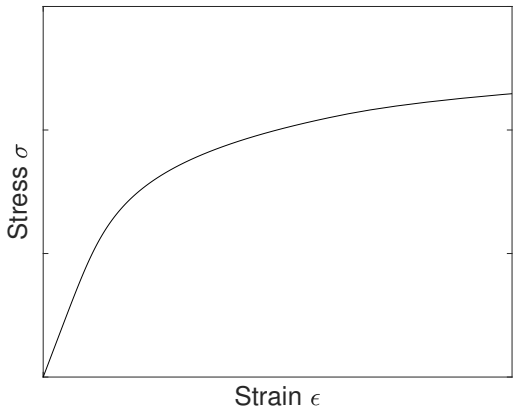

Figure 2.2: Stress-strain relationships for stainless steel

Annex C of [4] gives us an alternative method of how to model the material stress-strain behaviour when there is a need for material modelling. Otherwise this standard gives us a table in Clause 2.1.2 with values of material strengths used for a global analysis and material coefficients in Clause 2.1.3 for determining resistances of members and cross-sections.

2.2 Stress-strain non-linear behaviour

Due to the mentioned differences in the shapes of the stress-strain relationship in stainless and carbon steel, there are few methods of material models which have been developed. It should be noted that the bi-linear relationship acceptable for carbon steel is not acceptable for stainless steel as it is discussed later. In Figure 2.3 we can see a comparison of different relationships between stainless steels and carbon steel as it is showed in [1].

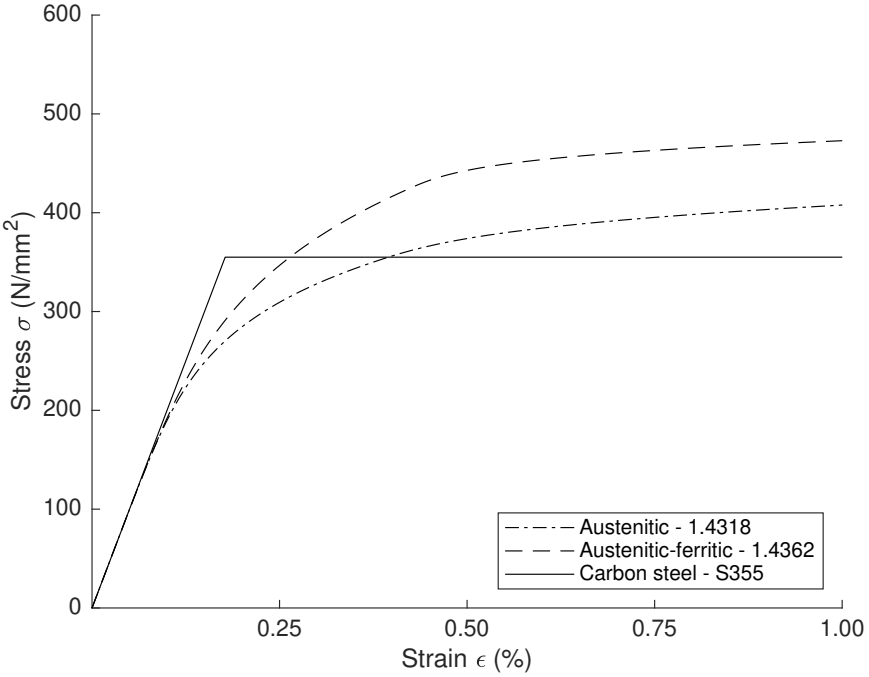

Figure 2.3: Comparision of carbon and stainless steel relationships

One of the first formulas of material model describing the non-linear stress-strain relationship is the Ramberg-Osgood one stage Equation (2.1), where ϵ is the strain, E is the Young's modulus of elasticity, σ is the stress, n is the strain hardening exponent and $\sigma_{0.2}$ is the material 0.2% proof stress, which has been developed into the more and widely used two-stage model because it was not provided enough accuracy.

$$\epsilon = \frac{\sigma}{E} + 0.002 \left(\frac{\sigma}{\sigma_{0.2}} \right)^n \tag{2.1}$$

The previously mentioned Ramberg-Osgood two-stage modification given by the Annex C of [4] (Equation 2.2, where n, m are strain hardening coefficients in which $R_{p0.01}$ is the 0.01% proof stress, f_y is the yield stress, E_y is the tangent modulus of the stress strain curve at the yield strength defined, ϵ_u is the ultimate strain) is found to accurately represent the stress-strain behavior of the different stainless steel grades according to the study made by Arrayago et al. [5]. The accuracy is especially imminent at the material

strains above 0.2% proof strength (a more accurate description of a strain hardening), a comparison is shown in Figure 2.4. Having a more accurate representation of the strain hardening is important because a non-linear response may then increase the ultimate strength of the material.

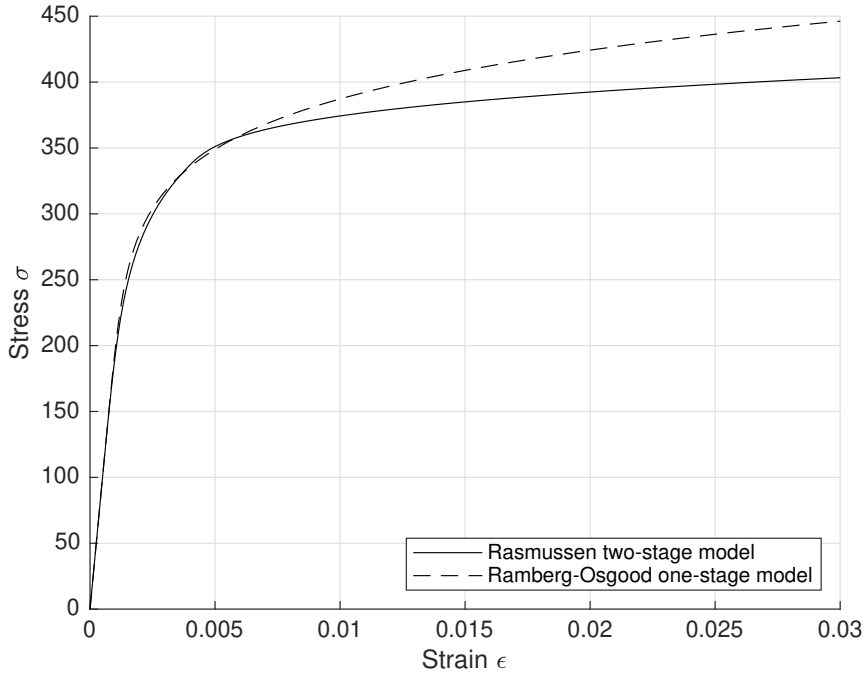

Figure 2.4: Comparision of one and two-stage material models

$$\epsilon = \begin{cases} \frac{\sigma}{E} + 0.002 \left(\frac{\sigma}{f_y}\right)^n & \text{for } \sigma \leq f_y \\ 0.002 + \frac{f_y}{E} + \frac{\sigma - f_y}{E_y} + \epsilon_u \left(\frac{\sigma - f_y}{f_u - f_y}\right)^m & \text{for } f_y \leq \sigma \leq f_u \end{cases} \tag{2.2}$$

$$n = \frac{ln(20)}{ln(f_y/R_{p0.01})} \tag{2.3}$$

2.3 Beam-column behaviour

Portal frames are very efficient and inexpensive for building and producing structures consisting of columns and rafters (beams). When applying a load at a portal frame (for example wind, snow and dead load), column members will be always subjected to a combination of a bending and axial force. This kind of applied loading may lead to lateral-torsional and flexural buckling of the member.

As noted in Section 2.1 the supplementing part for stainless steels [4] provides a modified equation for this kind of behaviour. Unfortunately, the current formula was

developed around 10 years ago (Jandera et al. [6]) and interaction buckling factors, which cover the material's non-linearity and its gradual yielding, have improved since then.

Relevant interaction factors for stainless steel beam-columns, proposed by [3], [4] and other researchers were studied in [6]. The study was performed on three column lengths of three different stainless steel grades and two types of open and hollow cross-sections. Fully GMNIA was carried out and the extracted interaction factor was compared with the interaction factor calculated by the code definition. In case of a non-uniform moment distribution along the member length, the results showed conservativeness for members loaded mostly by bending.

Walport et al. [7] carried out analysis of different design approaches used to assess stainless steel portal frames. Settings of the portal frames in the study was done in a way that the members (cross-section HE340B) were under both axial load and bending and ratio of GMNIA to design resistance was calculated for 10 considered design approaches, from which five of them were the Eurocode based. The results in these design approaches in [4] showed that the design predictions are highly scattered and excessively conservative in elastic global analysis.

2.4 Global analysis and stability

[3] states two methods for determining the internal forces and moments of the analysed structure. Using an initial geometry of the structure is called a first-order analysis and a second-order analysis is when the influence of the deformed structure is taken into account. A second-order analysis should be considered only if the effects of the deformed geometry increase the action effects or modify the structural behaviour significantly. Moreover, portal frames and frames with a large length to height ratio usually take into account these kind of effects unlike frames with a low length to height ratio.

The standard provides us with guidelines when it is necessary to take the second order effects into account based on the value α_{cr}, a critical load factor by which the design loading would have to be increased to cause an elastic instability in a global mode.

Concerning portal frames, following the Clause 5.2.1(4)B portal frames with shallow roof slopes and beam-column type plane frames α_{cr} should be calculated using Equation (2.4), where H_{Ed} is the total design horizontal load, V_{Ed} is the total design vertical load, h is the storey height and $\delta_{H,Ed}$ is the horizontal displacement when the frame is loaded with horizontal loads.

$$\alpha_{cr} = \left(\frac{H_{Ed}}{V_{Ed}}\right)\left(\frac{h}{\delta_{H,Ed}}\right) \tag{2.4}$$

If the influence of the deformation of the structure plays role ($\alpha_{cr} \leq 10$) then we have

to assess the structure considering the second order effects and imperfections which can be accounted both totally in global analysis or partially by a global analysis and partially through individual stability checks of members as it is stated in Clause 5.2.2(3). There is also possibility of a simpler method using a first-order analysis and to amplify the results of relevant action effects by a factor but α_{cr} has to satisfy a condition $3 \leq \alpha_{cr} \leq 10$. In case of $\alpha_{cr} < 3$ a more accurate second order analysis has to be done.

In [7] a new approach is presented which assesses the necessity of second-order effects for a stainless steel material. For all frames with $\alpha_{cr} < 15$ a second order plastic analysis should be carried out. There is also proposed a new elastic buckling load factor $\alpha_{cr,mod}$ based on the ratio of the load-lateral deflection curve from a first order plastic analysis. When $\alpha_{cr,mod} < 10$ a second order analysis may be performed otherwise a first order analysis may be carried out.

2.5 Residual stresses

Residual stresses were not incorporated in the study, following the results of the finite element study in [7] done on portal frame of a height 5 m and a width of 10 m from austenitic stainless steel. The residual stresses showed small reductions in the stiffness and little influence on overall behaviour and therefore negligible effects on the behaviour of such frame. Similarly published in [6] the influence of residual stresses was assumed negligible in beam-column behaviour even though more research may be done in a matter of residual stresses in stainless steel open sections.

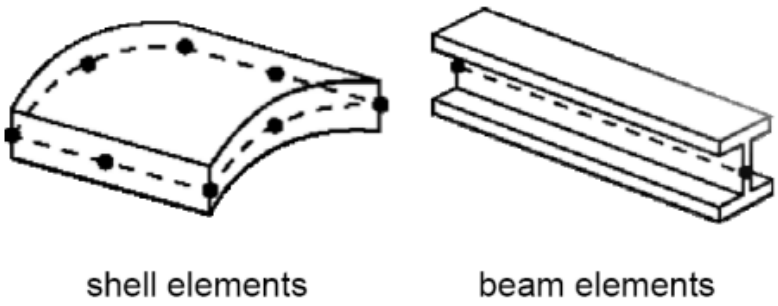

Figure 2.5: Beam and shell elements [8]

2.6 Beam and shell approach difference

Following the Abaqus manual [8], the choice of elements is based on the study's analysis type. In this case, any of the stress/displacement elements such as beam or shell (also

called structural elements - Figure 2.5) in the Abaqus can be used. The behaviour of both of them can be linear or non-linear and may or may not require numerical integration over the section.

As [7] states in the conclusion linear beam elements in the Abaqus used for the numerical modelling do not allow the member to deform locally. An Euler-Bernoulli beam formulation only has uniaxial behaviour and neglects shear deformation. This can lead to over-predicting of the load capacity of the section. By using shell elements which carry forces in biaxial bending plus in-plane shear and axial forces, local buckling can be accounted for in the study.

Chapter 3

Case study analysis

Figure 3.1: Exterior of the U-building

Figure 3.1 shows that the selected structure used for numerical analysis and parametric study is a steel substructure of the existing U-building in the campus of KTH Royal Institute of Technology in Stockholm. KTH's U-building is one of the latest buildings built in the campus with a reinforced concrete core surrounded by a steel frame carrying concrete floors as well as the rest of the structure. It is one of the buildings in the campus with the newest equipment and intelligent behaviour and maintenance.

Due to a relatively thick concrete roof desk the building provides an interesting choice in a matter of actions and loading on the bearing structure. Further motivation for the selection comes from the visible parts from inside (Figure 3.2a), having moment resisiting connections (Figure 3.2b), and realistic dimensions as very widely used Class 1 cross sections.

As seen on the Figure 3.2 the frame is composed of two columns from the cross-section HE300B with its main axis rotated 90° to obtain a higher stiffness as discussed later, supporting a beam from the cross-section HE550A. This beam is extended on one side with a length $\frac{1}{3}$ of the distance between the columns. There are two stiffener plates above the column closer to the cantilever part of the beam (more on geometry development in Section 3.1.1).

(a) Frame part of the structure

(b) Connection beam-column detail

Figure 3.2: Analyzed part of the steel structure

3.1 Code based approach

There are several stages a civil engineer or a designer should follow when it comes to designing a steel structure. Based on these stages it is possible to do a verification check to see if the structure was correctly designed. Following the EN 1990 [9], [3], and then publication the Design of Steel Frame Buildings to Eurocode 3 [10] and its basis of design and process recommendation, one of the first things in designing a structure is defining a client's geometry requirements whilst being a little conservative to have and allow enough space in changes in a member size.

Afterwards, the actions should be stated acting on the analyzed structure defined by the EN 1991 [11], [12], [13], depending on the location, site altitude and local topography together with the self-weight of the structure and permanent loading.

Next step is a determination of internal forces of the simplified structure model and initial member selection based on their cross-section resistance and buckling resistance. As explained later, for columns subjected to a combination of bending and axial forces (according to portal frames internal forces) usually the most critical check may be lateral-torsional buckling resistance.

Frames must be assessed on their sensitiveness to the second order effects. In case the second order effects should be assumed, it could be done by amplifying the first order

analysis results or by completing a second order analysis.

Each member is verified afterwards, following the member cross-section classification, the resistance to bending, shear, compression and buckling resistance.

Finally the value of the largest deflection is compared to the defined limits or to the requirements of the client.

The whole procedure of the structure assessment done by hand and described later in the following sections is attached as an Appendix B.

3.1.1 Geometry, loading, imperfections and internal forces

The geometry model was based on a BIM model (Figure 3.3) of KTH's whole U-building in which it was possible to get the most accurate and real dimensions of the structure. As explained in the general description of the structure, all bearing steel structures are made from the steel grade S355, cross-section properties of the columns (members no. $1, 3$ in Figure 3.4b) are HE300B and cross-section properties of the beam (members no. $2, 4$ in Figure 3.4b) are HE550A. Total length of the structure is $L = 9.61$ m and the height is $h = 4.21$ m. The dimensions were related to the center lines of cross-sections and stiffener plates were neglected in the code based approach analysis of the structure. The boundary conditions were fixed supports in the points a, b and the points c, d were classified as rigid, moment resisting joints. The movement constraint in the point e, available in a real case scenario, was neglected.

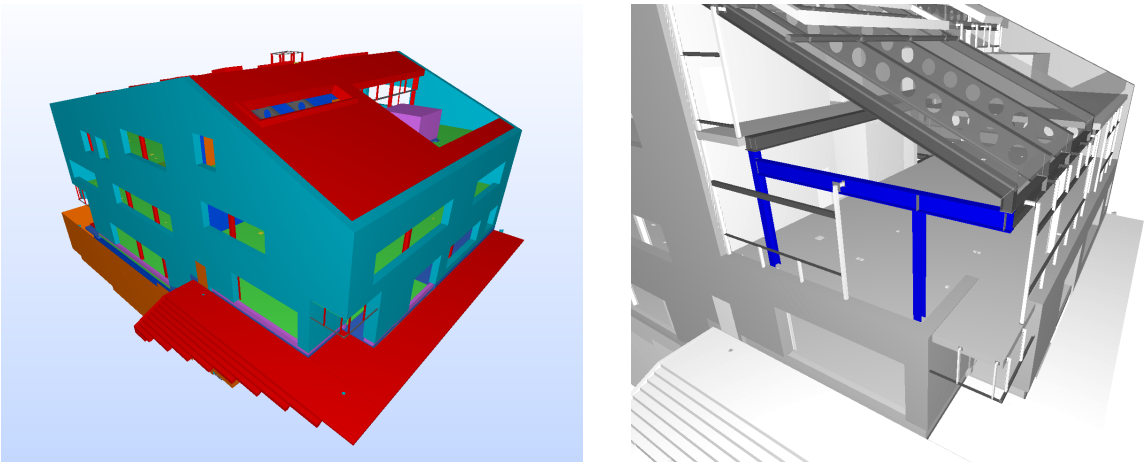

(a) Overview of the whole building (b) Detail of the analyzed part

Figure 3.3: BIM model of the building *(provided by KTH)*

The acting loading was calculated based on the materials in the BIM model - for permanent actions (self-weight of the structures - roof, other bearing structures, floors and walls) and following the Swedish National Annex of [12] - for defining snow load and

live load acting (technology, maintenance, people and furniture). These forces were placed in points c and e as described in Figure 3.4b as vertical concentrated forces V.

For a global analysis of the frame according to Clause 5.3.1 of [3] global imperfections for the frames were incorporated as a global initial sway imperfection stated in Clause 5.3.2 using Equation 3.1, where ϕ_0 is initial basic value of imperfections, α_h is the reduction factor for a height h and α_m is the reduction factor for number of columns in a row.

$$\phi = \phi_0 \alpha_h \alpha_m \tag{3.1}$$

The sum of all vertical forces V was therefore multiplied by this coefficient and the result was applied as a horizontal force H. Local imperfections were not introduced as Clause 5.3.2 states that during performing a global analysis for determining the end forces and the end moments used in member checks according to Section 6.3 local imperfections may be neglected.

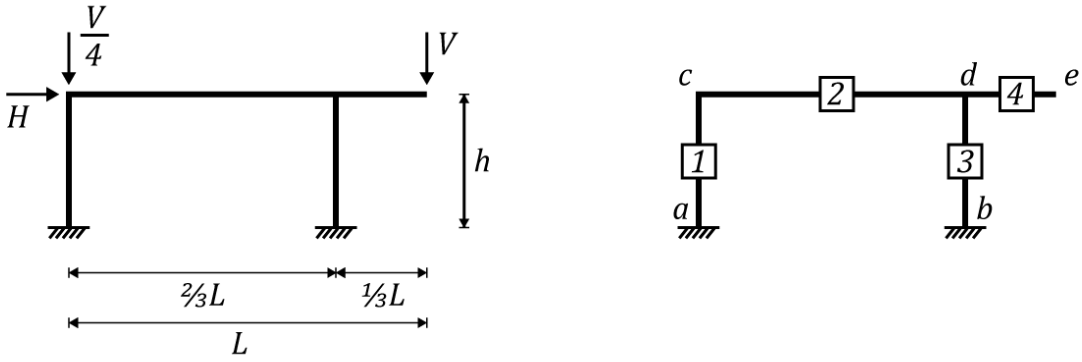

(a) Geometry and loading (b) Numbering of members and points

Figure 3.4: Details of the analyzed frame

The internal forces were firstly determined manually using a method of virtual work for the calculation of indeterminate structures. Determining the $\alpha_{cr} = 15.236$ assumed a first order analysis to be used as it is stated in Clause 5.2.1 of [3]. The results of the manual approach were compared and verified together with the results produced from the software.

3.1.2 Cross-section and member verification

As mentioned earlier, a cross-sectional resistance and a member buckling resistance were verified following Clause 6.2 and 6.3 of [3].

3.1.2.1 Cross-sectional resistance

Cross-section classification Each cross-section was classified according to Table 5.2 of [3]. The reason for this is to identify the extent to which the resistance and rotation capacity of cross sections is limited by its local buckling resistance as it is explained in Clause 5.5.1. The classification of a cross-section depends on the width to thickness ratio of the parts subjected to compression. [3] defines four cross-sections classes and in this case study all of the members are in Class 1. This can be defined as those which can form a plastic hinge with the rotation capacity required from plastic analysis without reduction of the resistance.

Cross-section verification According to the diagram of the internal forces of the structure, the effects of bending and axial forces were verified on the column's cross-section as specified in Clause 6.2.9.1 in [3]. The effects of bending (Clause 6.2.5), bending and shear (Clause 6.2.8) and bending and axial force were verified for the beam's cross-section.

3.1.2.2 Buckling resistance of members

Firstly the members sensitive to buckle were defined. The members no. 2 and 4 are sensitive to flexural buckling characterized by Equation (3.2), where M_{Ed} is the design value of the moment, $M_{b,Rd}$ is the design buckling resistance moment, and the member no. 3 is sensitive to buckling resistance in combination of axial compression force and bending moment characterized by Equations (3.3), (3.4), where $N_{Ed}, M_{y,Ed}, M_{z,Ed}$ are the design values of the compression force and the maximum moments about the y-y and z-z axis along the member, $\Delta M_{y,Ed}, \Delta M_{z,Ed}$ are the moments due to the shift of the centroidal axis, χ_y, χ_z are the reduction factors due to flexural buckling, χ_{LT} is the reduction factor due to lateral torsional buckling, $k_{yy}, k_{zy}, k_{yz}, k_{zz}$ are the interaction factors.

$$\frac{M_{Ed}}{M_{b,Rd}} \leq 1.0 \tag{3.2}$$

$$\frac{N_{Ed}}{\frac{\chi_y N_{Rk}}{\gamma_{M1}}} + k_{yy}\frac{M_{y,Ed} + \Delta M_{y,Ed}}{\chi_{LT}\frac{M_{y,Rk}}{\gamma_{M1}}} + k_{yz}\frac{M_{z,Ed} + \Delta M_{z,Ed}}{\frac{M_{z,Rk}}{\gamma_{M1}}} \leq 1.0 \tag{3.3}$$

$$\frac{N_{Ed}}{\frac{\chi_z N_{Rk}}{\gamma_{M1}}} + k_{zy}\frac{M_{y,Ed} + \Delta M_{y,Ed}}{\chi_{LT}\frac{M_{y,Rk}}{\gamma_{M1}}} + k_{zz}\frac{M_{z,Ed} + \Delta M_{z,Ed}}{\frac{M_{z,Rk}}{\gamma_{M1}}} \leq 1.0 \tag{3.4}$$

Out of these two buckling resistance checks, the most critical one was selected, which was the bending resistance. The forces were then amplified to the level where the ratio of the moments in Equation (3.2) was equal to unity.

Critical moment finding To obtain the design buckling resistance moment $M_{b,Rd}$ given by Equation (3.5), where W_y is the section modulus, χ_{LT} is the reduction factor for lateral-torsional buckling given by Equation (3.6), it was necessary to calculate the non-dimensional slenderness $\overline{\lambda}_{LT}$ characterized in Equation (3.8) where the elastic critical moment for lateral-torsional buckling M_{cr} is used. The greater the imperfection parameter Φ_{LT} is, the smaller the value of the reduction factor. The symbol α_{LT} is the imperfection factor and β is the correction factor for the lateral-torsional buckling curves. The symbol $\overline{\lambda}_{LT,0}$ is the plateau length of the lateral torsional buckling curves.

$$M_{b,Rd} = \chi_{LT} W_y \frac{f_y}{\gamma_{M1}} \tag{3.5}$$

$$\chi_{LT} = \frac{1}{\Phi_{LT} + \sqrt{\Phi_{LT}^2 - \beta\overline{\lambda}_{LT}^2}} \tag{3.6}$$

$$\phi_{LT} = 0.5[1 + \alpha_{LT}(\overline{\lambda}_{LT} - \overline{\lambda}_{LT,0}) + \beta\overline{\lambda}_{LT}^2] \tag{3.7}$$

$$\overline{\lambda}_{LT} = \sqrt{\frac{W_y f_y}{M_{cr}}} \tag{3.8}$$

$$M_{cr} = \mu_{cr} \frac{\pi\sqrt{EI_z GI_t}}{L} \tag{3.9}$$

$$G = E/2(1+\nu) \tag{3.10}$$

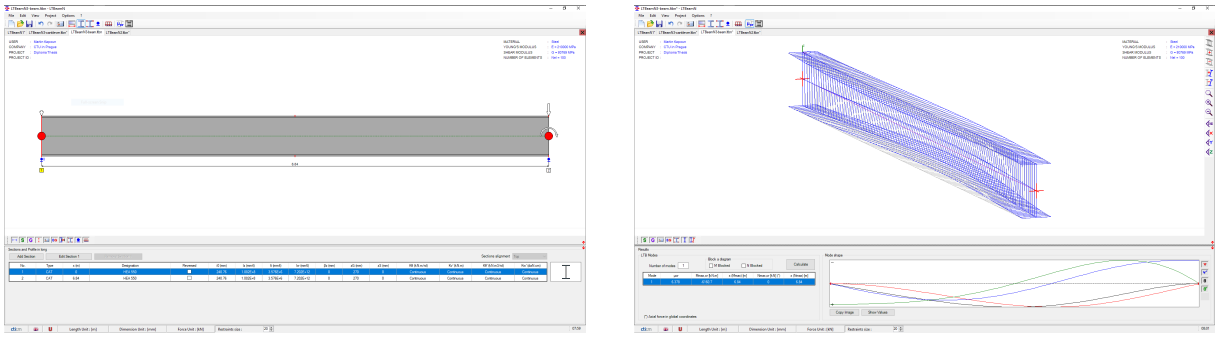

(a) Input data (b) Results

Figure 3.5: Screenshots of the LTBeamN GUI

To obtain the elastic critical moment there exists two ways, one of them is to use the software LTBeamN and the second one is to calculate it by hand following Equation (3.9), where E is the Young's modulus of elasticity, I_z is the second moment of inertia about the minor axis, G is the shear modulus given by Equation 3.10, ν is the Poisson's

ratio, I_t is the torsional constant, L is the length of the member and μ_{cr} is the relative non-dimensional critical moment.

To have the smallest elastic critical moment means that the non-dimensional slenderness will be larger and therefore the reduction factor χ_{LT} will be smaller. In this case study both approaches of obtaining the elastic critical moment were done and compared.

3.1.3 Parametric settings for stainless steel

As explained in Section 1.1, there are minor changes in [4] in the formulas when the structure is made of the stainless steel. All code based checks were done for nine types of stainless steel grades. The material properties used in the calculations for the different grades of a stainless steel were taken from Table 2.1 and the material coefficients were taken from Clause 2.1.3.

The cross-sections were classified based on their material grade following Table 5.2. The formula used in a flexural buckling resistance check was improved - Equation 3.6 changes its denominator to Equation 3.11 and Equation 3.7 is changed to Equation 3.12 and the formulas used in a buckling resistance during bending and axial compression (Equation (3.3), Equation (3.4)) are changed to Equation (3.13), Equation (3.14) when the uniaxial moment is about the major axis and to Equation (3.15) when the uniaxial moment is about the minor axis, where N_{Ed}, $M_{y,Ed}$ and $M_{z,Ed}$ are the design values of the compression force and the amximum moments about the y-y and z-z axis along the member, respectively, $(N_{b,Rd})_{min}$ is the smallest value of $N_{b,Rd}$ for the four buckling modes, $(N_{b,Rd})_{min1}$ is the smallest value of $N_{b,Rd}$ for the three buckling modes, $\beta_{W,y}$, $\beta_{W,z}$ are the factors that allows for the classification of a cross-section, $W_{pl,y}$, $W_{pl,z}$ are the plastic moduli for the y and z axes respectively, $M_{b,Rd}$ is the lateral-torsional buckling resistance and k_y, k_z, k_{LT} are the interaction factors and e_{Ny}, e_{Nz} are the shifts in the neutral axes when the cross-section os subject to uniform compression.

$$\chi_{LT} = \frac{1}{\Phi_{LT} + \sqrt{\Phi_{LT}^2 - \overline{\lambda}_{LT}^2}} \tag{3.11}$$

$$\phi_{LT} = 0.5[1 + \alpha_{LT}(\overline{\lambda}_{LT} - 0.4) + \overline{\lambda}_{LT}^2] \tag{3.12}$$

$$\frac{N_{Ed}}{(N_{b,Rd})_{min}} + k_y \left(\frac{M_{y,Ed} + N_{Ed} e_{Ny}}{\beta_{W,y} W_{pl,y} f_y / \gamma_{M1}} \right) \leq 1 \tag{3.13}$$

$$\frac{N_{Ed}}{(N_{b,Rd})_{min1}} + k_{LT} \left(\frac{M_{y,Ed} + N_{Ed} e_{Ny}}{M_{b,Rd}} \right) \leq 1 \tag{3.14}$$

$$\frac{N_{Ed}}{(N_{b,Rd})_{min}} + k_y \left(\frac{M_{z,Ed} + N_{Ed} e_{Nz}}{\beta_{W,z} W_{pl,z} f_y / \gamma_{M1}} \right) \leq 1 \tag{3.15}$$

All iterations were done using developed MATLAB scripts with variable parameters to obtain the ultimate loading of the different materials as it can be seen in Figure 3.6.

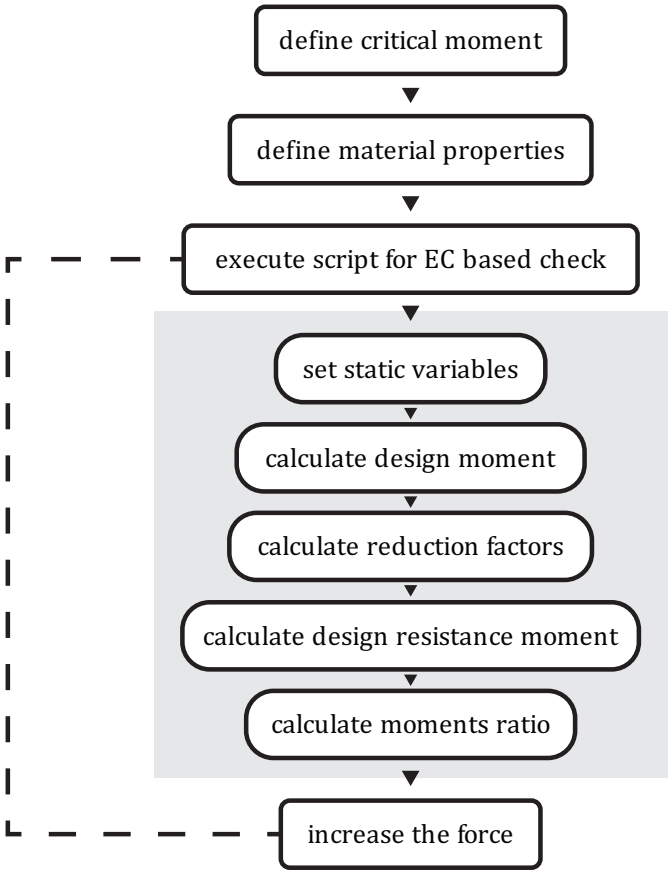

Figure 3.6: Diagram of parametric approach in EC analysis

Firstly, the parametric study was done for Class 1 cross-sections, HE300B, HE550A. Secondly the Class 1 was changed to Class 4, where the dimensions of the column cross-section were $b = 300$ mm, $h = 300$ mm, $t_f = 12$ mm, $t_w = 6$ mm, where t_f is the flange thickness and t_w is the web thickness and the dimensions of the beam cross-section were $b = 300$ mm, $h = 540$ mm, $t_f = 12$ mm, $t_w = 5$ mm.

3.2 FEM approach

To analyze the structure under full geometrical and material nonlinear conditions with initial imperfections, finite element (FE) analysis was performed in the general-purpose FE software Abaqus.

The FE method works by dividing the parts into smaller subdivisions and reconnecting these elements in nodes with results in a set of algebraic equations. It consists of three step; pre-processing or defining geometry, element type, material properties etc., solution or computing the unknown values and post-processing of the results.

The calculation of the ultimate critical force acting in point e (Figure 3.4a) was performed using two models. The first one calculates the eigenvalue (using linear perturbation and buckle step) of the structure, extracts the resulted displacement and loads it into the model two as initial imperfections. In this model the load-displacement graph is extracted and the maximum critical force is determined.

3.2.1 Shell FE model

3.2.1.1 Geometry and section assignment

To prevent any mistakes in the constraints of different parts, the whole frame was modeled as one part using the extrude function. All open sections were assigned shells of thickness based on the cross-section thickness from the common library as it is the standard in steel beams production nowadays. For HE300B $b = 300$ mm, $h = 300$ mm, $t_f = 19$ mm, $t_w = 11$ mm, where t_f is the flange thickness and t_w is the web thickness,and for HE550A $b = 300$ mm, $h = 540$ mm, $t_f = 24$ mm, $t_w = 12.5$ mm. The radius of the standard rolled open sections in reality was neglected in the model and the shells were overlapping in the connection of the flange and the web.

The first model for obtaining the eigenvalue of the structure was assigned elastic material based on the properties of the material. For carbon steel, the modulus of elasticity was $E = 210$ GPa and for all stainless steels, the modulus of elasticity $E = 200$ GPa. The Poisson's ratio was assigned $\nu = 0.3$. Boundary conditions were specified as encastre - rotation and displacement disabled in all directions - in points a, b and loading was applied following the Figure 3.4a.

In the second model as described earlier, initial imperfections from defined buckle step were imported with an amplifier as discussed in Section 3.2.2. Material properties were changed to calculated non-linear materials as stated in Section 3.2.3. For obtaining the critical force acting in point e general static step was chosen as a more robust solution than a Riks method which was not converging in a majority of cases. That was done by defining a specific displacement in a mentioned point and the resulting force was therefore extracted as a reaction force - displacement controlled.

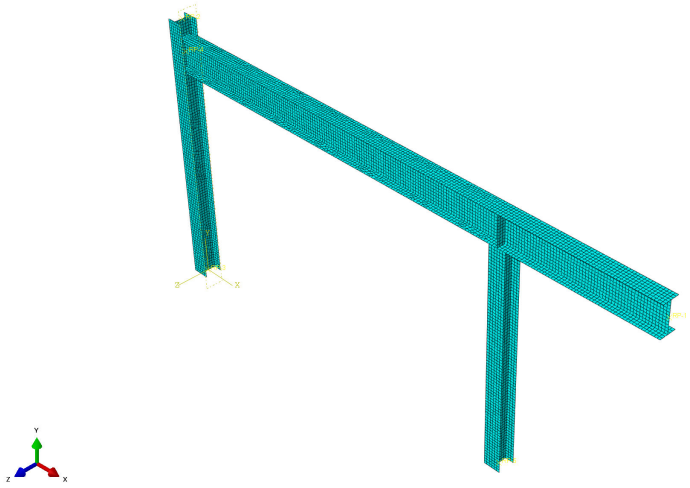

Figure 3.7: Geometry and mesh of the model

3.2.1.2 Mesh type and element size

There exist many types of shell elements used for the calculations and by following [8] for most analysis the standard large-strain shell elements are appropriate which include S3R, S4R, S8R. In this case study, eight noded shell elements with reduced integration were chosen to save time and by using S4R we would need finer mesh to obtain the same results.

The most time dependent entity was the size of the mesh seeds. To obtain the most suitable mesh seed size, Python and MATLAB scripts to test each mesh type were developed with varying mesh seed size from 25 mm up to 1200 mm for one of the austenitic stainless steel materials. The variable was increasing every 5 mm up to 200 mm, every 10 mm up to 500 mm, every 25 mm up to 1000 mm and every 50 mm up to 1200 mm.

3.2.2 Imperfections

For global imperfections, the displacement of one of the eigenvalues from the first linear elastic buckling analysis was loaded into the model number two. Its keywords were edited and amplified by a value calculated using Equation (3.16), where $\overline{\lambda}$ is the relative slenderness of the structure, α is the imperfection factor, χ is the reduction factor, M_{Rk} is the characteristic moments resistance and N_{Rk} is the characteristic resistance to normal force. The imperfection amplification value was calculated for beam and column members with the most critical values. In this study case, the column member was playing the major

role.

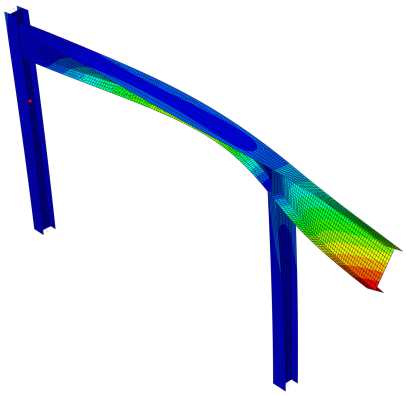

(a) Global - 3D view

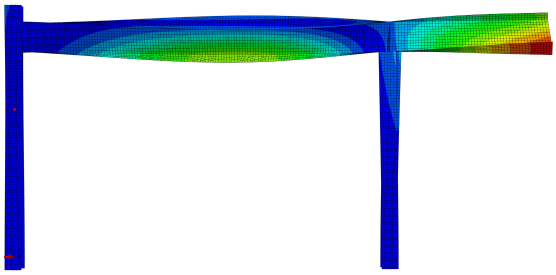

(b) Global - side view

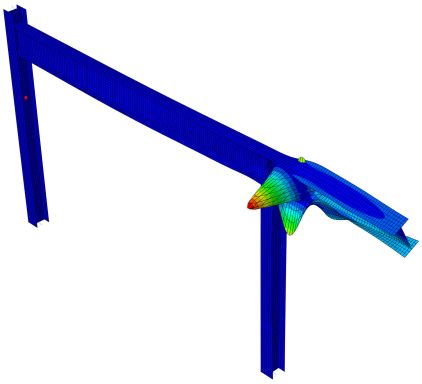

(c) Local - 3D view

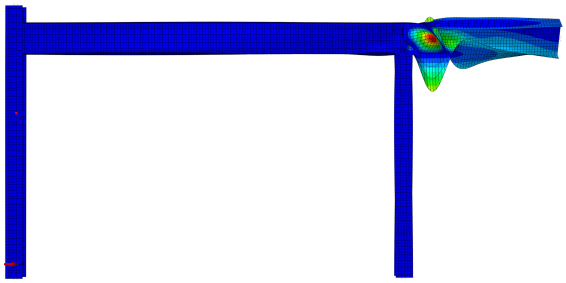

(d) Local - side view

Figure 3.8: Eigen modes used for global and local imperfections

$$e_0 = \alpha(\overline{\lambda} - 0.2)\frac{M_{Rk}}{N_{Rk}}\frac{1 - \frac{\chi\overline{\lambda}^2}{\gamma_{M1}}}{1 - \chi\overline{\lambda}^2} \tag{3.16}$$

In case of local imperfections, a different elastic buckling eigen mode was selected which was amplified by a value $e_0 = b/200$, where b is the web width.

3.2.3 Non-linear material modelling

As explained in Section 2.2 the non-linear material behaviour was modelled using the two-stage modified Ramberg-Osgood model using Equation (2.2), where n given by Equation 2.3 is the strain hardening coefficient, which basically defines the degree of non-linearity of the stress-strain curve. This is the same for the strain hardening coefficient m given by Equation 3.18. E_y (Equation 3.17) is the tangent modulus of the stress strain curve at the yield strength, f_y is the yield stress, f_u is the ultimate stress and ϵ_u is the ultimate strain. The input parameters used for the calculation of the material curve are stated in Table 3.1.

Table 3.1: Material input properties

	Type of stainless steel	Grade	Modulus of Elasticity E (GPa)	Yield Strength f_y (MPa)	Ultimate Tensile Strength f_u (MPa)
1	Austenitic	1.4306	200	200	520
2		1.4301		210	520
3		1.4401		220	530
4		1.4432		220	550
5		1.4311		270	550
6		1.4406		280	580
7		1.4318		330	650
8	Austenitic -ferritic	1.4362	200	400	600
9		1.4462		460	660

$$E_y = \frac{E}{1 + 0.002n\frac{E}{f_y}} \tag{3.17}$$

$$m = 1 + 3.5\frac{f_y}{f_u} \tag{3.18}$$

$$\epsilon_u = 1 - \frac{f_y}{f_u} \tag{3.19}$$

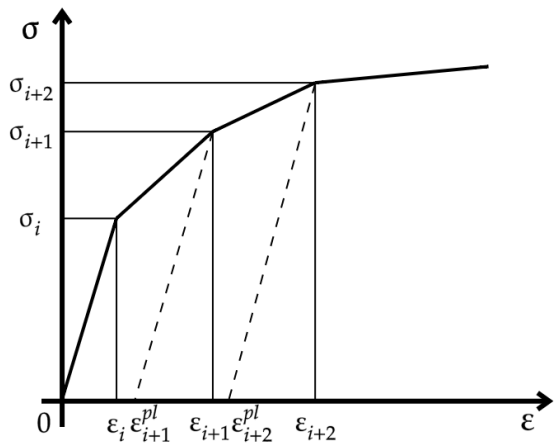

Figure 3.9: Multi linear plastic model

For the material description in the software a multi-linear plastic model was used (Figure 3.9). The stress-strain curve was defined in the starting point where $\sigma = 0$ MPa and $\epsilon = 0$. The definition of the plasticity in the Abaqus is done by inputting tabular

data of stress values and plastic strain values. These plastic strain values were calculated using results of the total strain values from Equation 2.2 minus the elastic strain values calculated using Hooke's law (Equation 3.20).

$$\epsilon_i^{pl} = \epsilon_i - \frac{\sigma_i}{E} \tag{3.20}$$

The difference of elastic and plastic parts of the strain can be seen in Figure 3.10 as seen in [7]. Examples of calculated stress-strain diagrams for all tested stainless steel grades are in Figure 3.11.

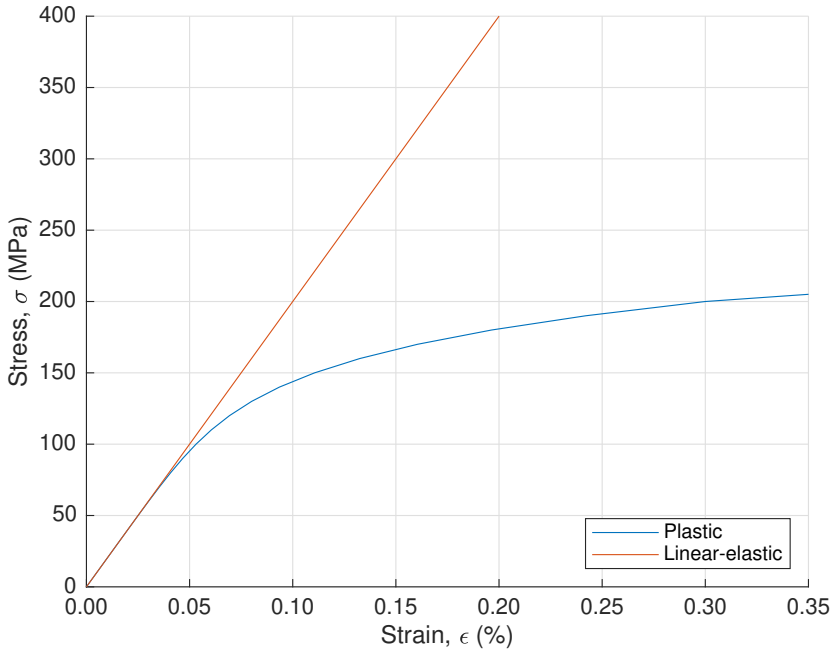

Figure 3.10: Divergence of linear-elastic and plastic stress-strain

3.2.4 Parametric FE study

The definition of the used models and calculation is generated using a Python script executed by a MATLAB program. This program calculates different material properties and changes them for every iteration. Load-displacement graph values are then saved into separate files and processed in MATLAB. Examples of code used for computation and result processing can be found in Appendix C.

As stated before, the study was done for nine grades of stainless steel, covering austenitic and austenitic-ferritic types of stainless steel specified in Table 3.1. A brief explanation of the parametric process can be seen in Figure 3.12.

The first case was the calculation of the ultimate force which the structure is able to bear. All cross-sections were classified as Class 1 and the materials were defined according

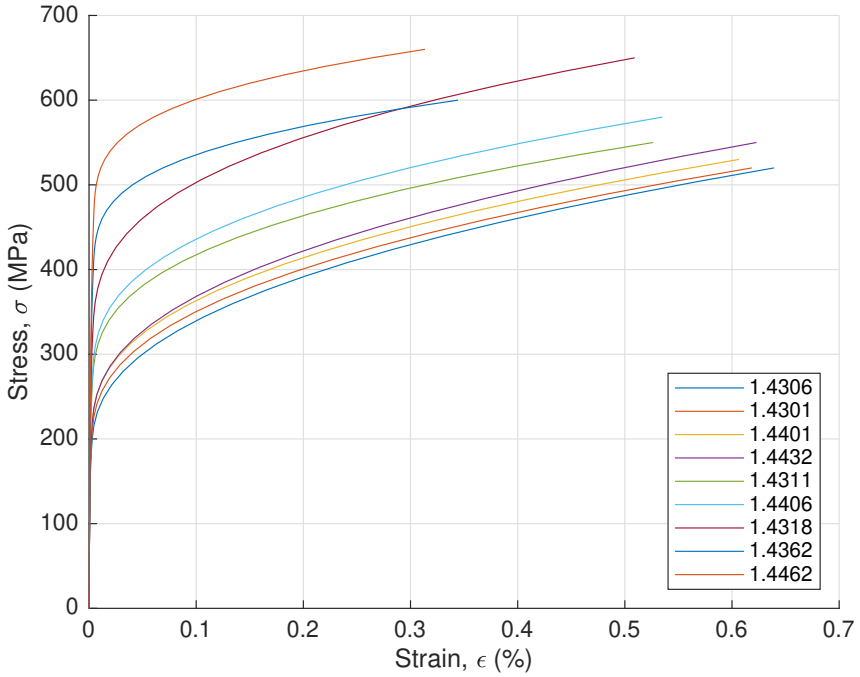

Figure 3.11: Generated stress-strain diagrams for selected stainless steels

to Section 3.2.3. Each global and local imperfections were defined by one eigen mode.

The next case was carried out with different cross-section shell thicknesses to achieve cross-section Class 4 and to study the influence of local buckling. For HE300B $b = 300$ mm, $h = 300$ mm, $t_f = 12$ mm, $t_w = 6$ mm, where t_f is the flange thickness and t_w is the web thickness,and for HE550A $b = 300$ mm, $h = 540$ mm, $t_f = 12$ mm, $t_w = 5$ mm. Initial imperfections were assumed with the first eigen mode only.

The influence of various amounts of eigen modes for initial imperfections were studied - in case of the Class 1 cross-section, three eigen modes were combined with the amplification factor distributed among them based on the percentage values seen in Table 3.2. A same study was done in the case of Class 4 cross-sections.

Table 3.2: Combinations of eigen modes for both cross-section classes

Amp.	Combination no.				
factor	1.	2.	3.	4.	5.
100%	1	-	-	-	-
70%	-	1	-	1	1
50%	-	-	1	-	-
30%	-	-	2	2	3
20%	-	2	3	-	-
10%	-	3	-	-	-

All cases of different modes were analyzed as well with 20% and 40% increase and

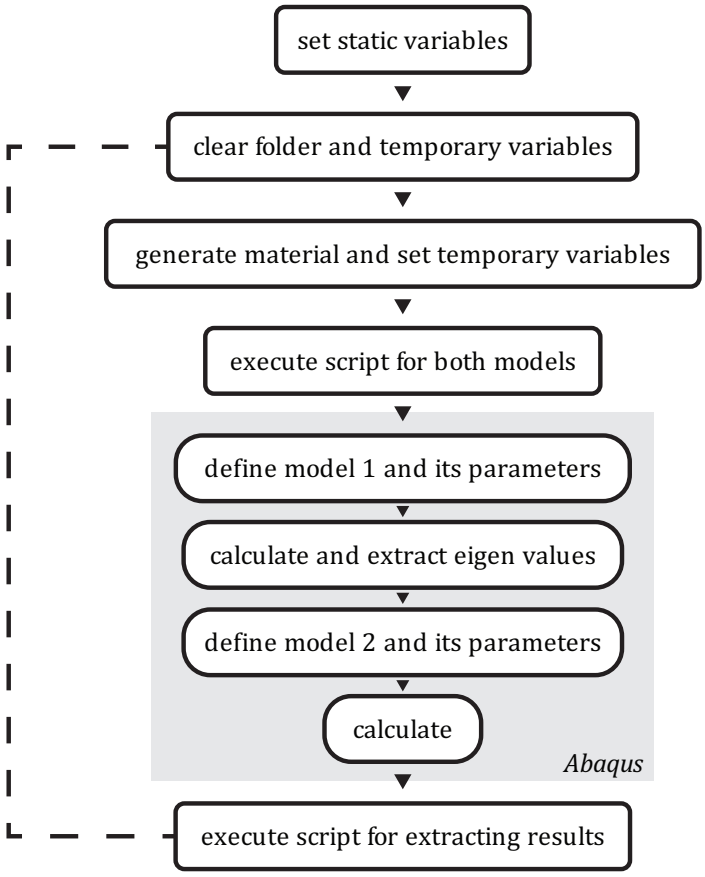

Figure 3.12: Diagram of parametric approach in finite element analysis

decrease of initial imperfections to study the influence of the different amplification factor.

Chapter 4

Results

4.1 Carbon steel and stainless steel EC based check

The assessment of the original structure gave the usage of 60% at total, the highest in the cantilever part. The most critical point of the construction would be the joint of all three members, cantilever (member no. 4), column (member no. 3) and beam (member no. 2).

The critical moment used in the buckling resistance check during member bending as explained in Section 3.1.2.2 was calculated by hand following the approach stated in Annex I of EN 1999-1-1 [14] for cantilever and for beams. Both members have same cross-section properties, in Class 1 case $I_t = 3.515 \cdot 10^6\ mm^4$ $I_z = 1.082 \cdot 10^8\ mm^4$, in Class 4 case $I_t = 3.58 \cdot 10^6\ mm^4$ $I_z = 5.401 \cdot 10^7\ mm^4$, the Young's modulus of elasticity is $E = 210$ GPa for the carbon steel and $E = 200$ GPa for the stainless steel. The shear modulus is calculated from Equation 3.10. The relative non-dimensional critical moment in carbon steel Class 1 cross-section is for member no. 2 $\mu_{cr} = 3.21$ and for member no. 4 $\mu_{cr} = 4.36$. In Class 4, it is $\mu_{cr} = 5.71$ for member no. 2 and $\mu_{cr} = 8.59$ for member no. 4.

In case of stainless steel, the values are the same up to two decimal points. The same members were then modelled in LTBeamN to see differences in the results. In examining the tables with results of the critical moment (Table 4.1, Table 4.2) as well as the results

Table 4.1: Elastic critical moments for different moments - carbon steel

Member no.	M_{cr} (kNm)			
	Class 1		Class 4	
	By hand	By LTBeamN	By hand	By LTBeamN
2	3751	3374	1506	1363
4	12582	12641	5587	5656

Table 4.2: Elastic critical moments for different moments - stainless steel

Member no.	M_{cr} (kNm)			
	Class 1		Class 4	
	By hand	By LTBeamN	By hand	By LTBeamN
2	3571	3213	1434	1298
4	11983	12039	5321	5378

of the code based check (Table 4.3 and Table 4.4), the differences are very small. Thus, the values of the critical bending moments for the upcoming iterations were calculated using the software.

Little nuances in the results of the elastic critical moments could be caused by the definition of the coordinate z of the load acting on the structure. In the calculation by hand, acting forces were assumed in the shear center of the member meanwhile in software it was assumed on the top edge of the beam. Furthermore, slightly different values of torsion, warping constants and second moments of inertia were used for each calculation.

Table 4.3: Critical force value acting in point e for carbon steel grades

Grade	f_y (MPa)	F_{cr} (kN)			
		Class 1		Class 4	
		By hand	By software	By hand	By software
S235	235	407	407	183	183
S275	275	472	472	212	212
S355	355	600	600	269	270

The ultimate critical force acting in point e was calculated according to the code by hand and by software for the three grades of carbon steel (Table 4.3) and then for nine grades of stainless steel (Table 4.4) in both examined cross-section classes. Concerning the carbon steel, there are nearly no differences in the results with the most critical member being no. 4. In the case of stainless steel, the results were varying slightly and even though member no. 4 was reaching the design capacity, member no. 2 was playing the role in this case.

4.2 Mesh convergence and type of the mesh

As explained in section Section 3.2.1.2 the convergence study was performed to choose the appropriate value of mesh seed size. In the following graphs it is possible to see that the critical force does not have any significant differences after reaching a value of 400

Table 4.4: Critical force value acting in point e for stainless steel grades

Grade	f_y (MPa)	F_{cr} (kN)			
		Class 1		Class 4	
		By hand	By software	By hand	By software
1.4306	200	265	288	120	128
1.4301	210	277	298	124	134
1.4401	220	289	308	129	139
1.4432	220	289	308	129	139
1.4311	270	349	358	148	158
1.4406	280	360	365	151	162
1.4318	330	415	410	168	166
1.4362	400	484	468	188	179
1.4462	460	515	505	202	190

elements per square meter. Therefore it would be pointless choosing finer mesh since the computation time would increase exponentially.

Therefore, eight noded shell elements mesh type with reduced integration was the best choice for the sake of the time required for computation when compared to a four noded shell element mesh type which would have to be two times finer.

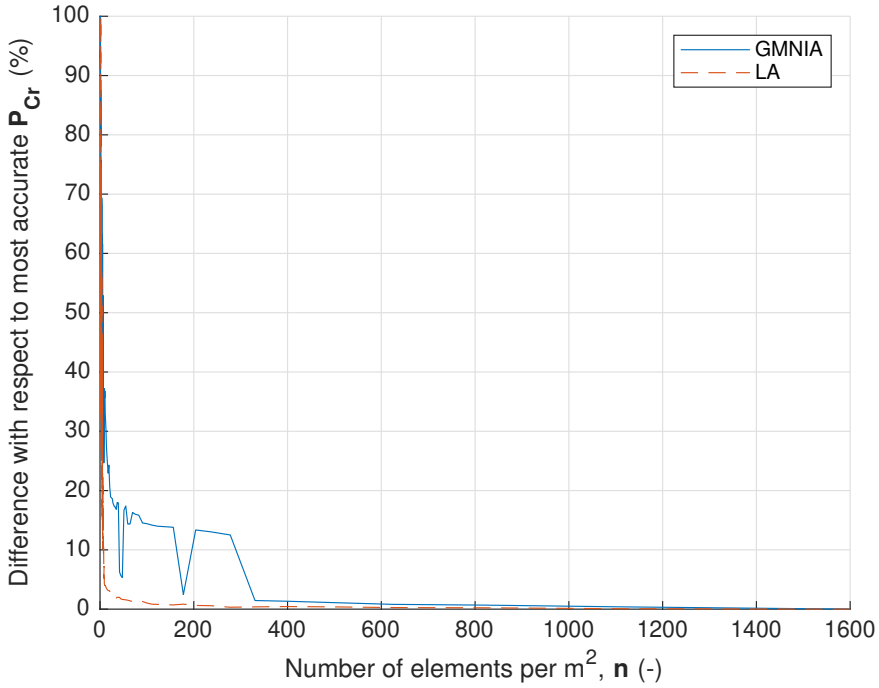

Figure 4.1: Convergence of critical force for S4 mesh type

Higher spikes and inconsistencies mainly in GMNIA (seen in Figure 4.1 and Figure 4.2) could be caused by having mesh seed size large enough that it is not possible to obtain the results correctly.

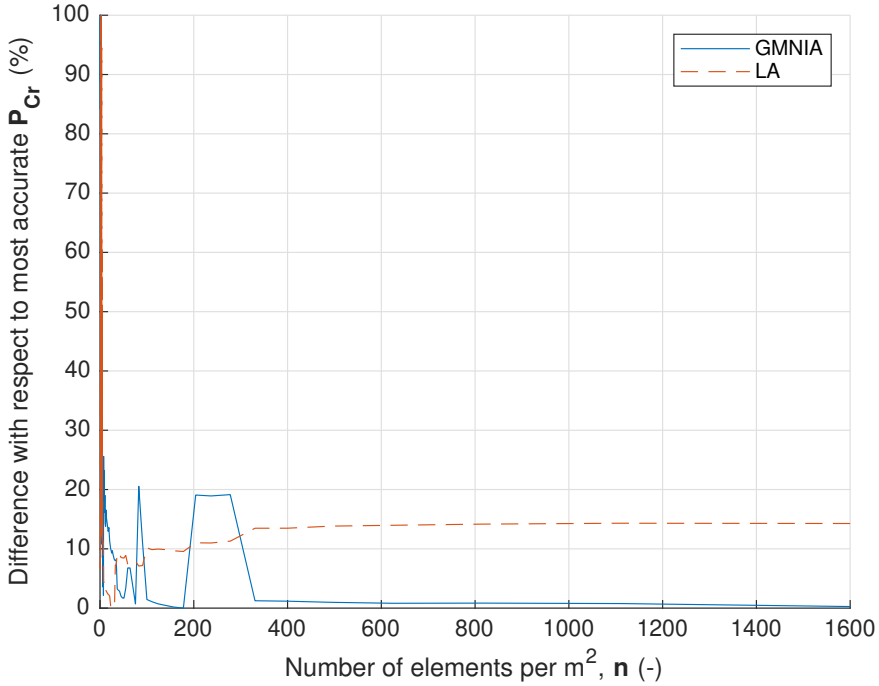

Figure 4.2: Convergence of critical force for S4R mesh type

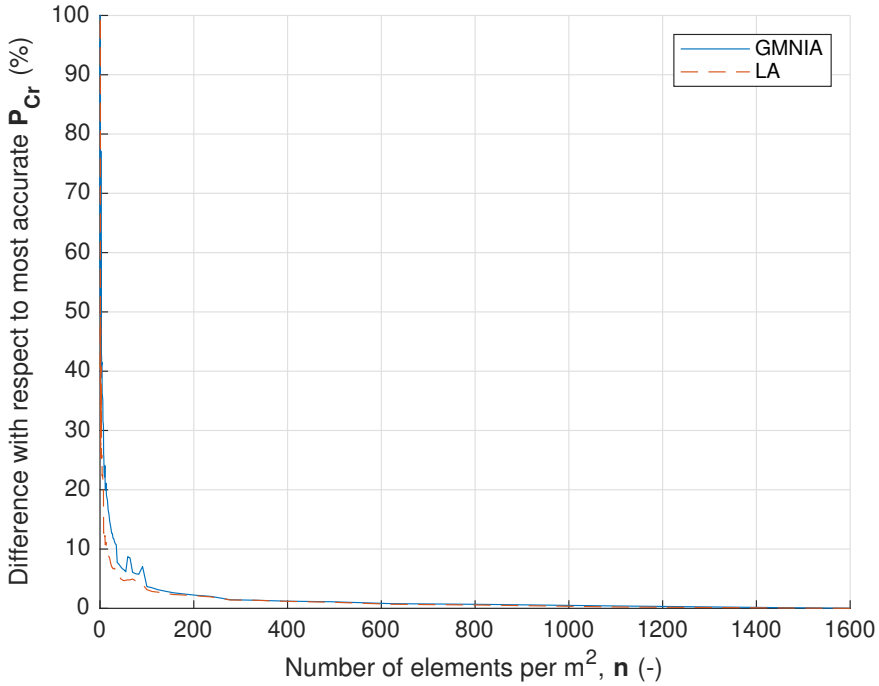

Figure 4.3: Convergence of critical force for S8R mesh type

4.3 Load-displacement graphs for different steels

Load-displacement graphs were used to determine the critical in-plane vertical force in point e with an imperfection amplifier as explained in Section 3.2.2.

The load-displacement graph for three common carbon steel grades - S235, S275 and S355 can be seen in Figure 4.4. In Figure 4.5, Figure 4.6 the load-displacement graph for nine studied stainless steel grades of Class 1 and Class 4 cross-sections can be seen.

It is evident that carbon steel is a material with a defined yield point because when it reaches it, the load-displacement curve undergoes short strain hardening and approaches the maximum force before necking and a loss of stiffness could be observed in the material. Compared to the stainless steel with no defined yield point, strain hardening starts earlier than in the first case, increasing slowly, leading to the ultimate strength of the material. Due to this, the behaviour of the stainless steel curve is then much more gradual before reaching the capacity of the material. In the case of cross-section Class 4, the curve has a similar shape however the slope is higher. Studied stainless steels also show that there is a larger ductile limit before a strength loss.

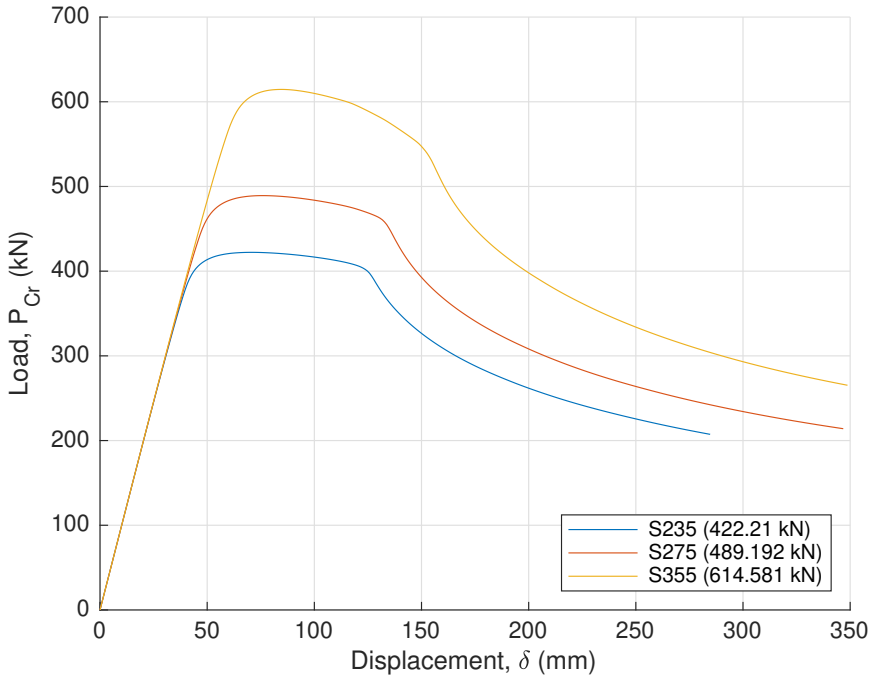

Figure 4.4: Load-displacement graph of carbon steel

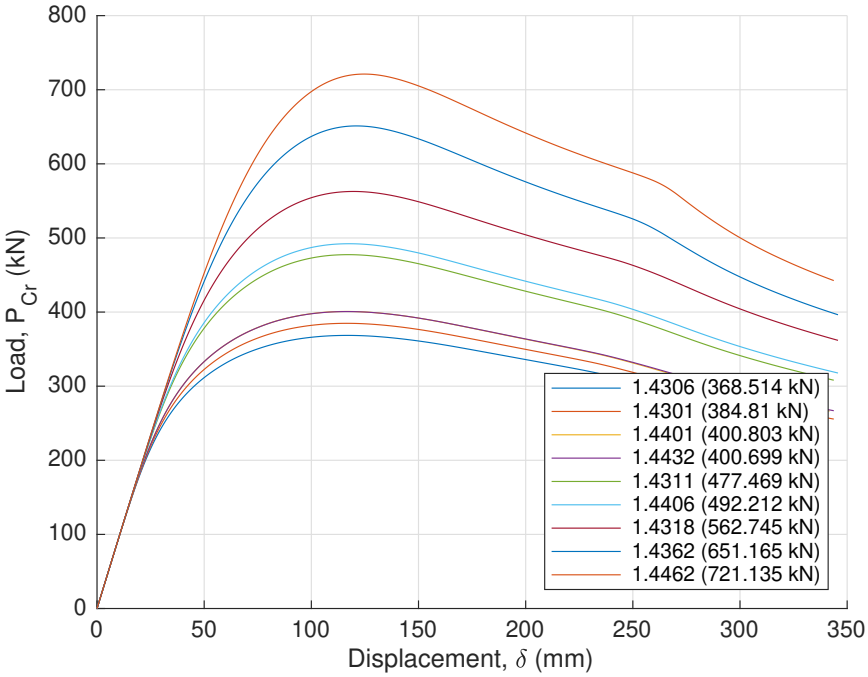

Figure 4.5: Load-displacement graph of stainless steel - Class 1

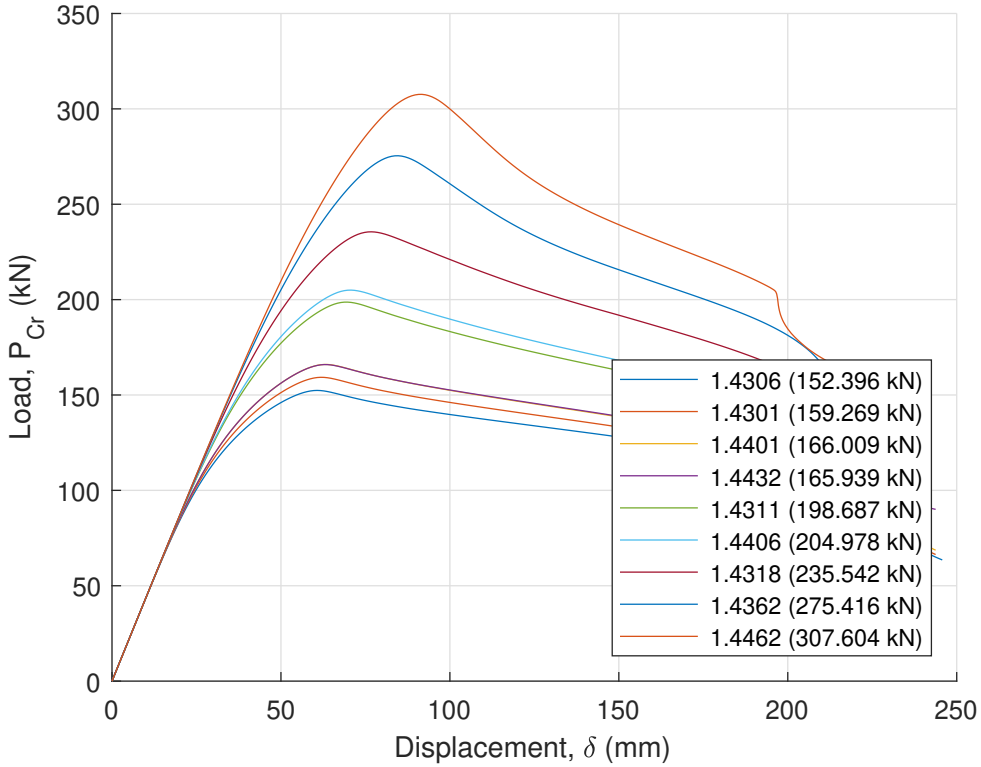

Figure 4.6: Load-displacement graph of stainless steel - Class 4

4.4 Comparison of GMNIA and EC approach

Resulting forces calculated using the code approach were compared with the forces determined by GMNIA. These forces were extracted as a maximum of a load-displacement graph of the material. Carbon steel differences can be seen in Table 4.5, stainless steel in Table 4.6 and Table 4.7.

Table 4.5: Difference of critical force values between code and GMNIA approach for carbon steel grades

Grade	f_y (MPa)	F_{cr} (kN)		Relative difference
		Code	GMNIA	
S235	235	406	422	+3.79 %
S275	275	471	489	+3.68 %
S355	355	598	614	+2.61 %

Table 4.6: Difference of critical force values between code and GMNIA approach for stainless steel grades - Class 1

Grade	f_y (MPa)	F_{cr} (kN)		Relative difference
		Code	GMNIA	
1.4306	200	288	368	+21.73 %
1.4301	210	298	384	+22.39 %
1.4401	220	308	400	+23.00 %
1.4432	220	308	400	+23.00 %
1.4311	270	358	477	+24.94 %
1.4406	280	365	492	+25.83 %
1.4318	330	410	562	+27.04 %
1.4362	400	468	651	+28.11 %
1.4462	460	505	721	+29.95 %

In Table 4.8 it can be observed that the variation of the forces from both types of analysis is quite stable and more accurate in the carbon steel case.

The increased value of critical force in a geometrically and materially non-linear analysis with initial imperfections is observed in the case of stainless steel which is due to the behaviour of the material's non-linearity. The smaller increase in carbon steel is due to modelled plastic bi-linear behaviour which is similar to the real behaviour when considering small strains.

Table 4.7: Difference of critical force values between code and GMNIA approach for stainless steel grades - Class 4

Grade	f_y (MPa)	F_{cr} (kN)		Relative difference
		Code	GMNIA	
1.4306	200	128	152	+15.78 %
1.4301	210	134	159	+15.72 %
1.4401	220	139	166	+16.26 %
1.4432	220	139	165	+15.75 %
1.4311	270	158	198	+20.20 %
1.4406	280	162	204	+20.58 %
1.4318	330	166	235	+29.36 %
1.4362	400	179	275	+34.90 %
1.4462	460	190	307	+38.11 %

Table 4.8: Increase in critical loading for both types of steel

	No. of samples	F_{GMNIA}/F_{code}		
		Mean	COV	Increase
Carbon steel	3	1.035	0.007	3.47 %
Stainless steel - class 1	9	1.337	0.038	33.70 %
Stainless steel - class 4	9	1.315	0.126	31.50 %

4.5 Imperfection and mode sensitiveness in GMNIA

4.5.1 Initial imperfections amplification

To determine how large role the error in imperfection determination could play, a study in imperfection sensitiveness was performed together with a study when a local buckling mode is assumed in the analysis and when it is neglected. The global imperfections amplifier was increased and decreased by 20% and 40% and all these five cases were calculated with and without applying a local buckling mode.

As it was expected, decrease of the imperfection amplifier leads to a larger critical force and vice-versa.

The difference in local buckling is negligible for the present case - Class 1 cross-section - as seen in Table 4.9. The only observable difference is from the thousandths place and it does not play any role in the final comparison.

Class 4 cross-sections are by definition cross-sections where local buckling will appear before the attainment of yield stress. To study the influence of imperfection amplification, the first eigen mode was applied as an initial imperfection and increased and decreased by the same percentage as it was in the case before.

Comparing Table 4.9 and Table 4.10, amplification of the factor leads to higher critical

Table 4.9: Influence of local buckling and imperfection amplification - Class 1

Initial imperfections amplifier	F_{GMNIA}/F_{code}					
	w/ local buckling			w/o local buckling		
	Mean	COV	Increase	Mean	COV	Increase
-40% decrease	1.3867	0.042	38.6652%	1.3866	0.042	38.6644%
-20% decrease	1.3617	0.0398	36.1717%	1.3617	0.0398	36.1708%
no increase	1.3337	0.0385	33.7066%	1.3337	0.0385	33.7060%
+20% increase	1.3168	0.0363	31.6769%	1.3168	0.0363	31.6760%
+40% increase	1.2960	0.0349	29.5995%	1.2960	0.0349	29.5986%

force ratio increase in Class 4 cross-section.

Table 4.10: Influence of imperfection amplification - Class 4

Initial imperfections amplifier	F_{GMNIA}/F_{code}		
	Mean	COV	Increase
-40% decrease	1.3901	0.1197	39.0074%
-20% decrease	1.3516	0.1229	35.1558%
no increase	1.3185	0.1257	31.8514%
+20% increase	1.2897	0.1279	28.9664%
+40% increase	1.2640	0.1296	26.3984%

4.5.2 Mode combination

The influence of different eigen modes for initial imperfections, defined in Section 3.2.4, was studied for both stainless steel cross-section classes. Results of both cross-sections classes are shown in Figure 4.7 and in Table 4.11 and Table 4.12.

4.5.2.1 Class 1

The critical forces were the lowest when only one eigen mode was applied. The combinations of the first, the second and the third mode, where the first mode amplification distribution is 70%; the first and the second mode and the first and the third mode are close to each other with minor differences. The highest increase was observed in the last eigen mode combination of the first, the second and the third mode with the amplifier distribution 50% for the first mode, 30% for the second mode and 20% for the third mode. Therefore the evaluated structure showed the highest sensitivity to the amplifier distribution of the first eigen mode. Furthermore the higher the imperfection amplification is, the larger the difference between the load capacities.

4.5.2.2 Class 4

Analogous to Class 1, the lowest critical force was found when only one eigen mode was applied and the highest critical force was found in the combination of the three modes with the same amplifier distribution. However the results of all combinations are more equally distributed compared to the previous case. The main difference was observed between the combination of the first and the second mode and the combination of the first and the third mode, where the second combination resulted in a smaller critical force. Moreover this cross-section class is more sensitive to the imperfection amplification as seen in Figure 4.7 where the structure's stiffness is declining at a higher rate.

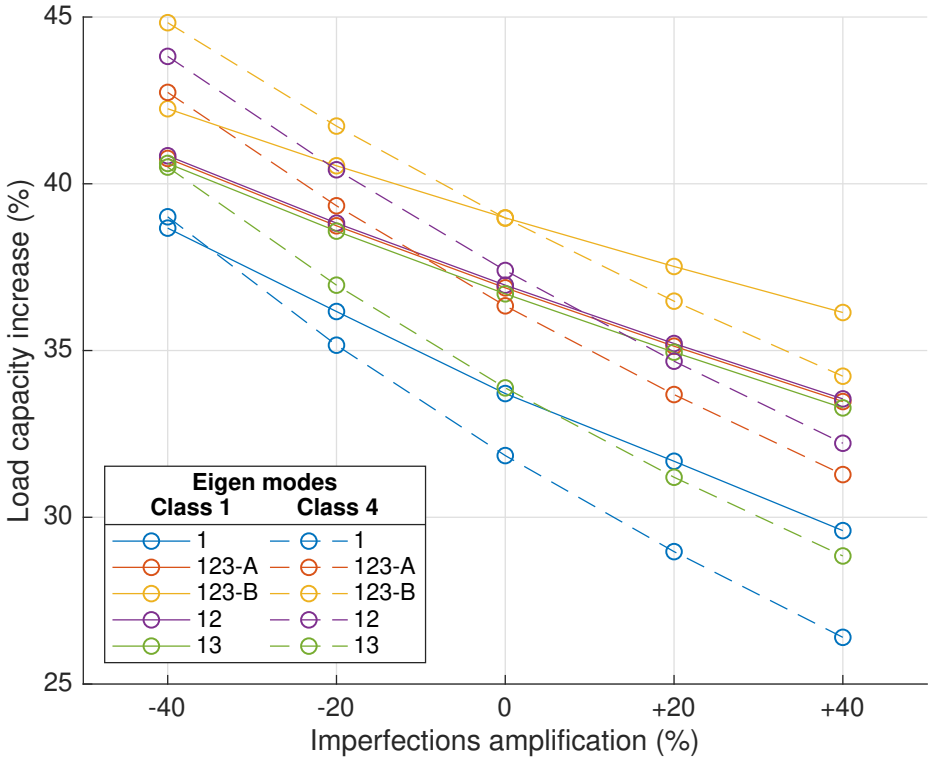

Figure 4.7: Response to the different modes

Table 4.11: The influence of the different modes - Class 1

F_{GMNIA}/F_{code}															
Mode comb.	1			123 - A[1]			123 - B[2]			12			13		
Imp. amp.	Mean	COV	Increase	Mean	COV	Increase	Mean	COV	Increase	Mean	COV	Increase	Mean	COV	Increase
-40%	1.387	0.042	38.665%	1.408	0.045	40.764%	1.423	0.047	42.248%	1.408	0.045	40.837%	1.406	0.045	40.614%
-20%	1.362	0.040	36.172%	1.387	0.043	38.739%	1.405	0.045	40.539%	1.388	0.043	38.817%	1.386	0.043	38.575%
0%	1.337	0.039	33.707%	1.369	0.041	36.878%	1.390	0.044	38.976%	1.370	0.041	36.957%	1.367	0.042	36.702%
+20%	1.317	0.036	31.677%	1.351	0.040	35.129%	1.375	0.043	37.516%	1.352	0.040	35.210%	1.350	0.040	34.946%
+40%	1.296	0.035	29.600%	1.335	0.039	33.469%	1.361	0.042	36.136%	1.336	0.038	33.549%	1.333	0.039	33.276%

Table 4.12: The influence of the different modes - Class 4

F_{GMNIA}/F_{code}															
Mode comb.	1			123 - A[1]			123 - B[2]			12			13		
Imp. amp.	Mean	COV	Increase	Mean	COV	Increase	Mean	COV	Increase	Mean	COV	Increase	Mean	COV	Increase
-40%	1.390	0.120	39.007%	1.427	0.117	42.744%	1.448	0.116	44.825%	1.438	0.117	43.815%	1.405	0.118	40.497%
-20%	1.352	0.123	35.156%	1.393	0.120	39.340%	1.417	0.118	41.734%	1.404	0.119	40.424%	1.370	0.121	36.955%
0%	1.319	0.126	31.851%	1.363	0.122	36.343%	1.390	0.120	38.966%	1.374	0.122	37.395%	1.339	0.124	33.881%
+20%	1.290	0.128	28.966%	1.337	0.124	33.677%	1.365	0.122	36.478%	1.347	0.124	34.680%	1.312	0.126	31.204%
+40%	1.264	0.130	26.398%	1.313	0.126	31.280%	1.342	0.124	34.231%	1.322	0.125	32.219%	1.288	0.128	28.838%

[1]Distribution of amplifier - 70%, 20%, 10%
[2]Distribution of amplifier - 50%, 30%, 20%

Chapter 5

Conclusion and suggestions for further research

5.1 Conclusion

Since the current Eurocode design methods for stainless steel are based on a carbon steel, the behaviour of the stainless steel portal frame in the case study was examined and assessed using these standards for three grades of carbon and nine grades of stainless steel. The results of the code check were compared against another parametric study carried out using a finite element approach and full geometrical and material non-linear analysis with initial imperfections. Both of these approaches were done for two types of cross-section classes, Class 1 and Class 4.

The hypothesis in the beginning which stated how large role material non-linearity plays in the different analysis approaches has been strengthened. The results of the linear-elastic approach given by equations in [4] are over-predicted and conservative due to the strain-hardening missing part of the stress-strain non-linear material behaviour. By neglecting the material non-linearity, safe results will be obtained, but as the study showed, it is much more appropriate to use analysis where possible to include material non-linearity. The triggering of local buckling showed similar results as the cross-sections which were resistant to it. Nevertheless, the results in this study are not the same in general for all types of portal frames. In other cases, the depedency on a critical load factor would have to be considered.

Assuming the initial imperfections, parametric study with different amplification factors was carried out to point out and verify how large mistakes could be in defining the imperfections amplifier incorrectly. In the studied case, the amplifier decrease and increase (by twenty and forty percent) changed the results slightly, roughly by two and a half percent when the amplifier decreased and by two percent when the amplifier increased

for cross-section Class 1. Cross-section Class 4 showed similarity in both directions, three and a half percent when the amplifier decreased and three percent when the amplifier increased. The influence of the local buckling in cross-section Class 1 was negligible in the present case.

The study of the influence of different modes showed importance of the first eigen mode only and its amplification factor, because the lowest structure stiffness was found in this case. Furthermore when the first mode was used in more combinations with other modes, the value of the amplification factor was the same in the first mode. These results showed nearly no differences in cross-section Class 1 compared to Class 4. In addition to cross-section Class 4, the study also showed the differences and lower stiffness in the combination of the first and the third modes compared to the combination of the first and the second modes.

5.2 Suggestions for further research

It is important to design stainless steel structures as efficient as possible due to their cost. Therefore obtaining the accurate design capacity of the frame is necessary and that is possible using full geometrically and materially non-linear analysis with initial imperfections.

Based on studies carried out with hollow and boxed sections, residual stresses were not incorporated in this study. However carrying a study aimed to effects of residual stresses in open sections and including them in the study could slightly change the results.

The flanges and the webs modelled using the shells of the open cross-sections in the studied FE model were overlapping in their connection. More detailed FE models could be developed together with incorporating constraints among the structure members to achieve joint behaviour closer to the reality.

Bibliography

[1] Steel Construction Institute (Great Britain), *Design manual for structural stainless steel*. English. 2017, OCLC: 1043371844, ISBN: 978-1-85942-226-7.

[2] *Design Manual for Structural Stainless Steel - Commentary*, 4th. Ascot, Berkshire, UK: Steel Construction Institute, 2018.

[3] *EN 1993-1-1, Eurocode 3 - Design of Steel Structures - Part 1-1: General Rules and Rules for Buildings*. Brussels: European Committee for Standardisation (CEN), 2005.

[4] *EN 1993-1-4, Eurocode 3 - Design of Steel Structures - Part 1-4: General Rules - Supplementary Rules for Stainless Steel*. Brussels: European Committee for Standardisation (CEN), 2006.

[5] I. Arrayago, E. Real, and L. Gardner, "Description of stress–strain curves for stainless steel alloys", en, *Materials & Design*, vol. 87, pp. 540–552, Dec. 2015, ISSN: 02641275. DOI: 10.1016/j.matdes.2015.08.001.

[6] M. Jandera, D. Syamsuddin, and B. Zidlicky, "Stainless Steel Beam-Columns Behaviour", en, *The Open Civil Engineering Journal*, vol. 11, no. Suppl-1, M5, pp. 358–368, Jun. 2017, ISSN: 1874-1495. DOI: 10.2174/1874149501711010358.

[7] F. Walport, L. Gardner, E. Real, I. Arrayago, and D. Nethercot, "Effects of material nonlinearity on the global analysis and stability of stainless steel frames", en, *Journal of Constructional Steel Research*, vol. 152, pp. 173–182, Jan. 2019, ISSN: 0143974X. DOI: 10.1016/j.jcsr.2018.04.019.

[8] ABAQUS, *Abaqus CAE User's Manual, Version 6.14*. Pawtucket, RI, USA: Hibbitt, Karlsson & Sorensen, Inc., 2014.

[9] *EN 1990, Eurocode 0 - Basis of Structural Design*. Brussels: European Committee for Standardisation (CEN), 2002.

[10] J. R Henderson, *Design of steel portal frame buildings to Eurocode 3*, English. Ascot: Steel construction Institute, 2015, OCLC: 953781167, ISBN: 978-1-85942-214-4.

[11] *EN 1991-1-1, Eurocode 1: Actions on Structures - Part 1-1: General Actions - Densities, Self-weight, Imposed Loads for Buildings*. Brussels: European Committee for Standardisation (CEN), 2002.

[12] *EN 1991-1-3, Eurocode 1: Actions on Structures - Part 1-3: General Actions - Snow Loads*. Brussels: European Committee for Standardisation (CEN), 2003.

[13] *EN 1991-1-4, Eurocode 1: Actions on Structures - Part 1-4: General Actions - Wind Loads*. Brussels: European Committee for Standardisation (CEN), 2004.

[14] *EN 1999-1-1, Eurocode 9: Design of Aluminium Structures - Part 1-1: General Structural Rules*. Brussels: European Committee for Standardisation (CEN), 2007.

[15] Y. Bu and L. Gardner, "Finite element modelling and design of welded stainless steel I-section columns", en, *Journal of Constructional Steel Research*, vol. 152, pp. 57–67, Jan. 2019, ISSN: 0143974X. DOI: 10.1016/j.jcsr.2018.03.026.

Appendix A

Load-displacement graphs

The load-displacement graphs from Section 4.5 are attached here. From Figure A.1 to Figure A.8 there are graphs of Class 1 cross-section when local buckling was assumed, secondly for the cases without local buckling. Figure A.9 shows the results of the analysis with base value of an imperfection amplifier just without local buckling. From Figure A.1 to Figure A.8 there are graphs of Class 4 cross-section, where local buckling was triggered in all cases.

Figure A.10 to Figure A.29 displays the resulting graphs of Class 1 cross-section when more eigen modes were loaded into the analysis and Figure A.30 to Figure A.53 of Class 4 cross-section.

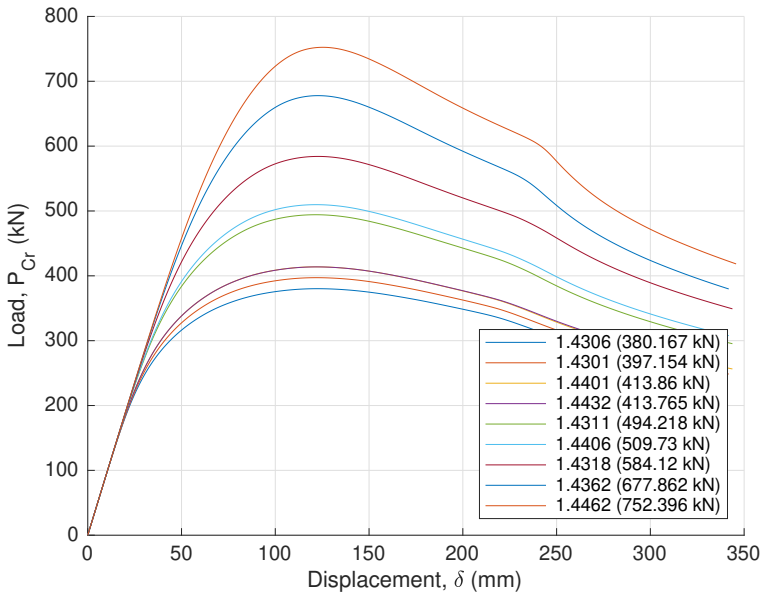

Figure A.1: Global imperfections decreased 40% (with local buckling)

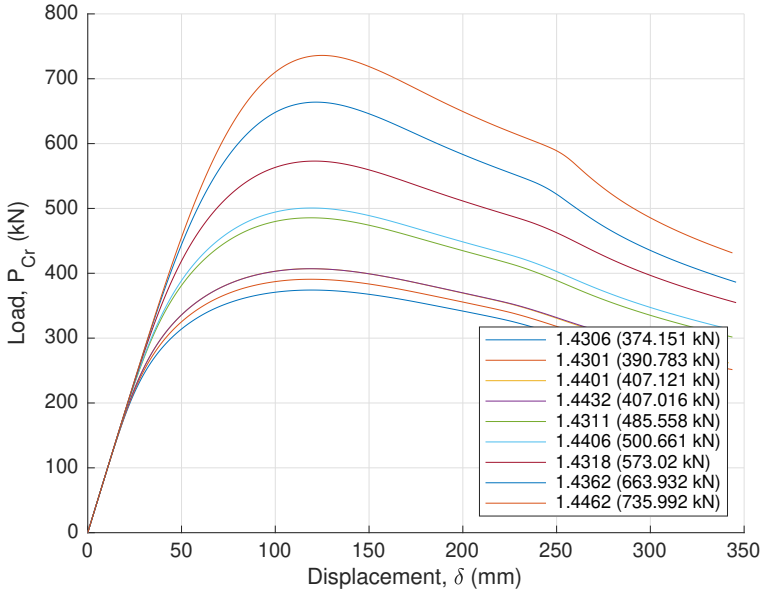

Figure A.2: Global imperfections decreased 20% (with local buckling)

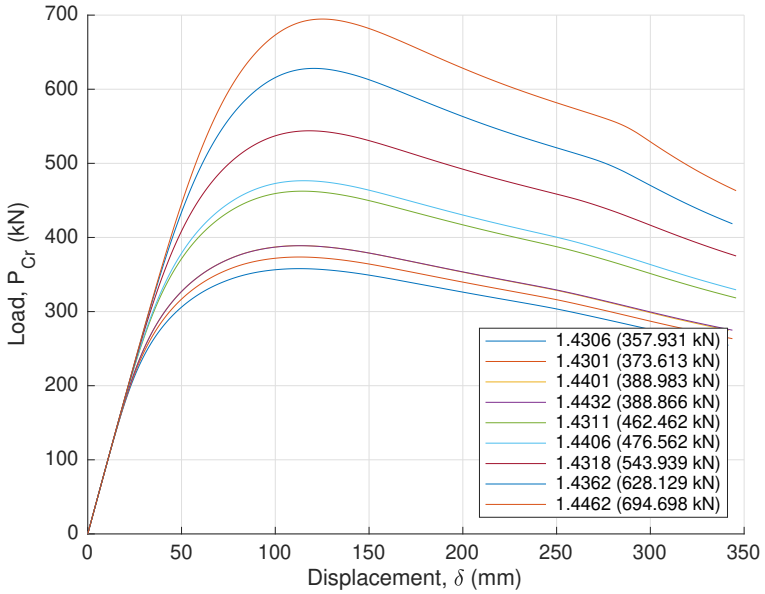

Figure A.3: Global imperfections increased 40% (with local buckling)

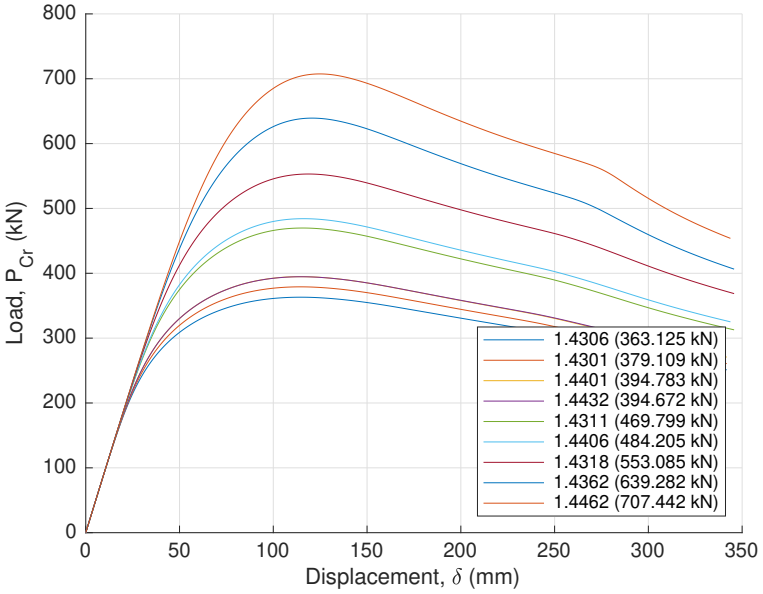

Figure A.4: Global imperfections increased 20% (without local buckling)

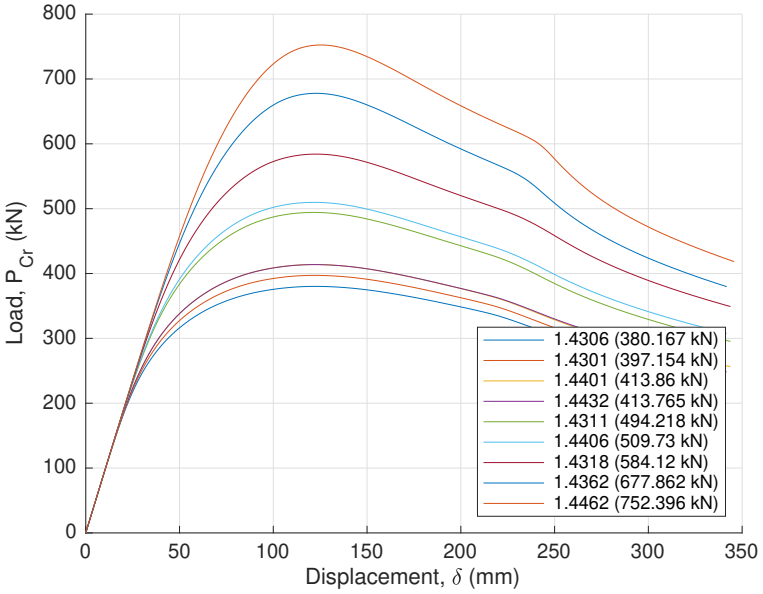

Figure A.5: Global imperfections decreased 40% (without local buckling)

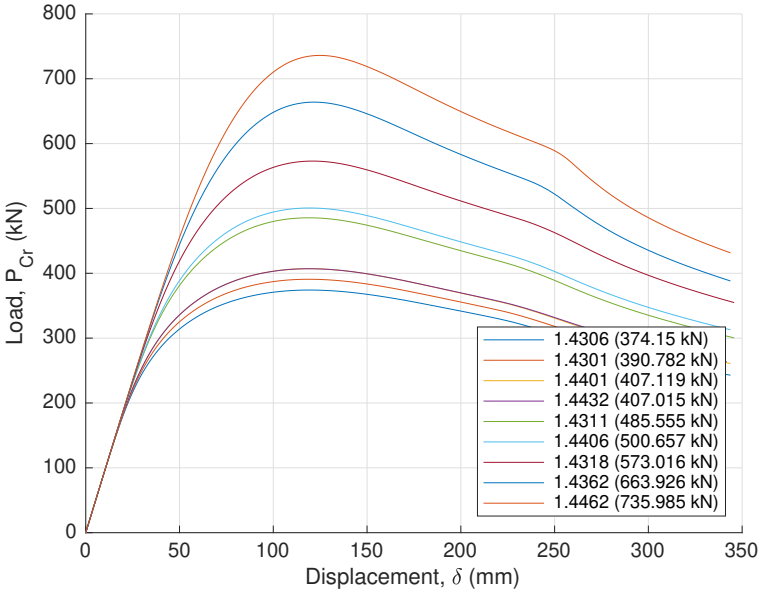

Figure A.6: Global imperfections decreased 20% (without local buckling)

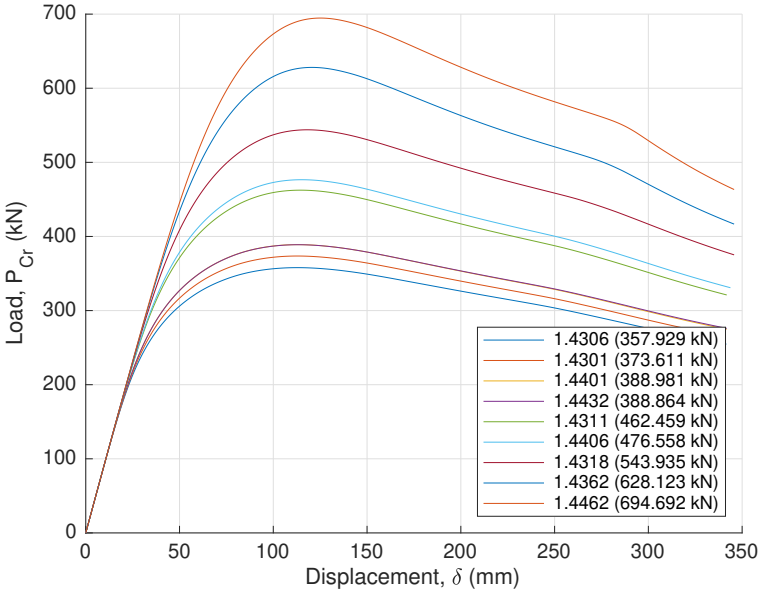

Figure A.7: Global imperfections increased 40% (without local buckling)

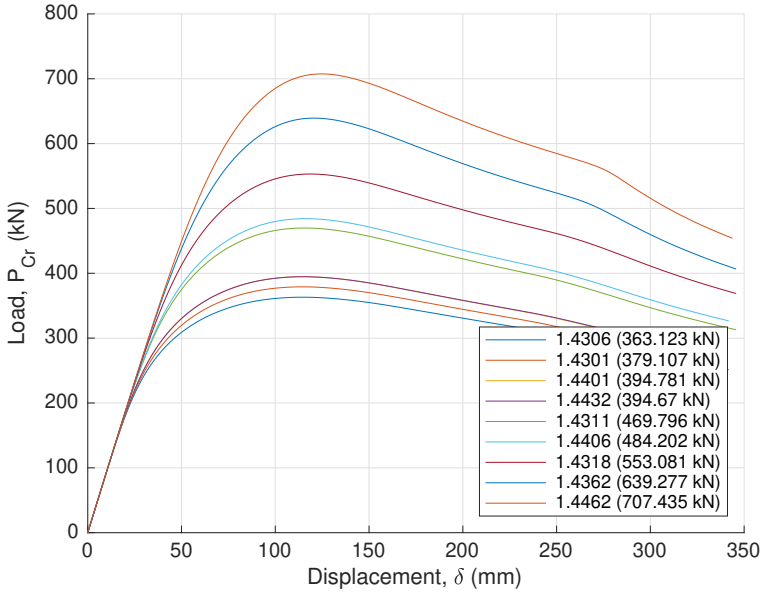

Figure A.8: Global imperfections increased 20% (without local buckling)

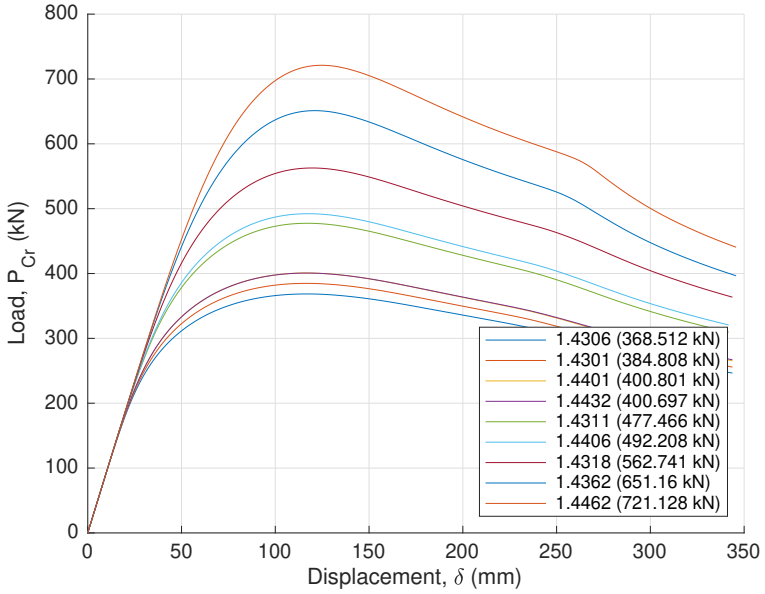

Figure A.9: Global imperfections (without local buckling)

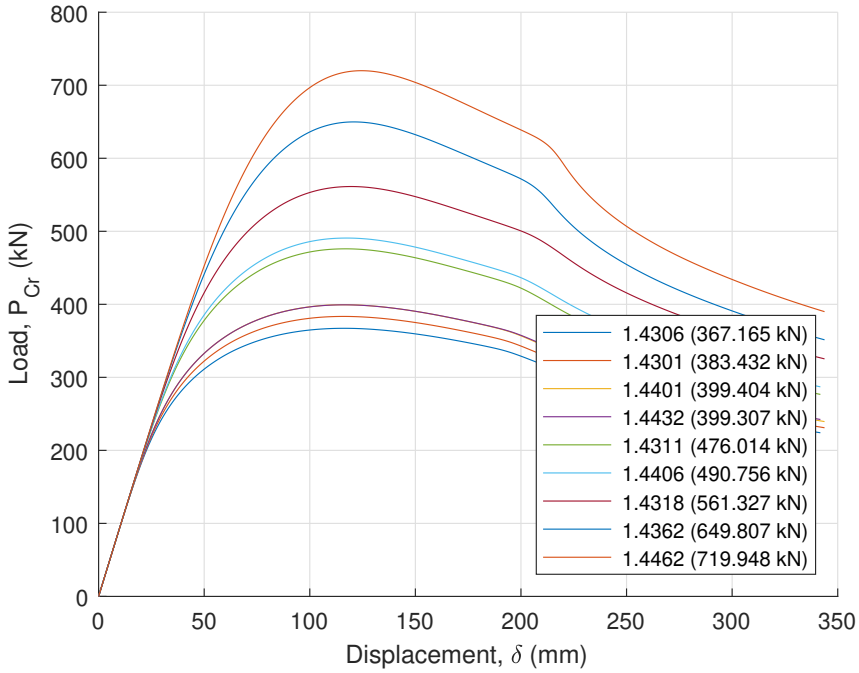

Figure A.10: Three modes - 123A - imperfections increased +40%

.

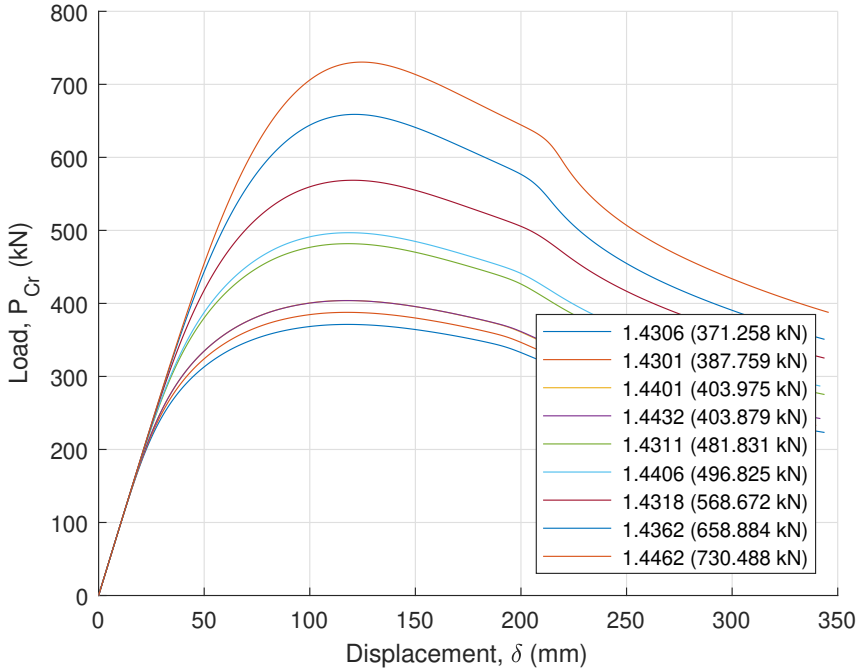

Figure A.11: Three modes - 123A - imperfections increased +20%

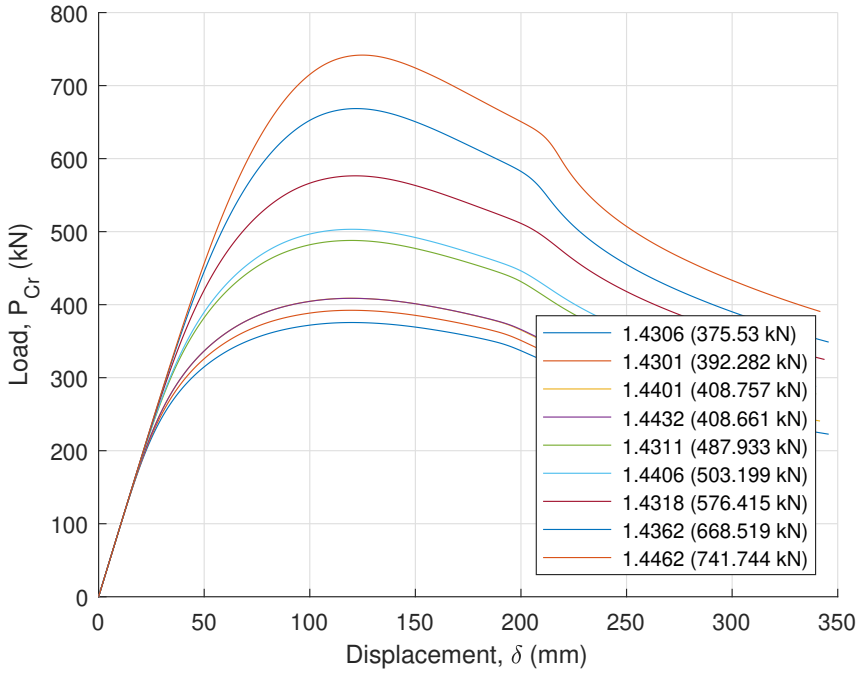

Figure A.12: Three modes - 123A - no imperfections amplification

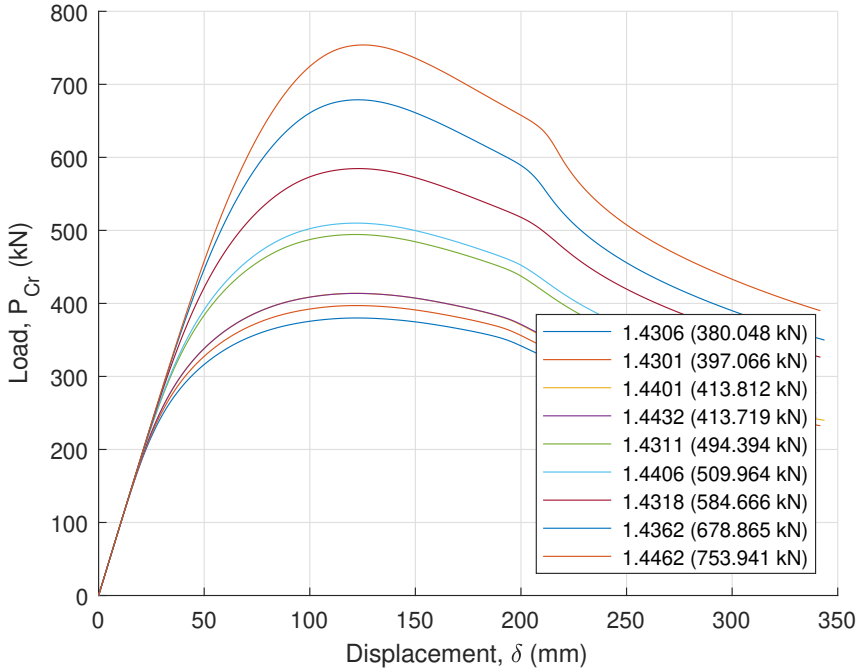

Figure A.13: Three modes - 123A - imperfections decreased -20%

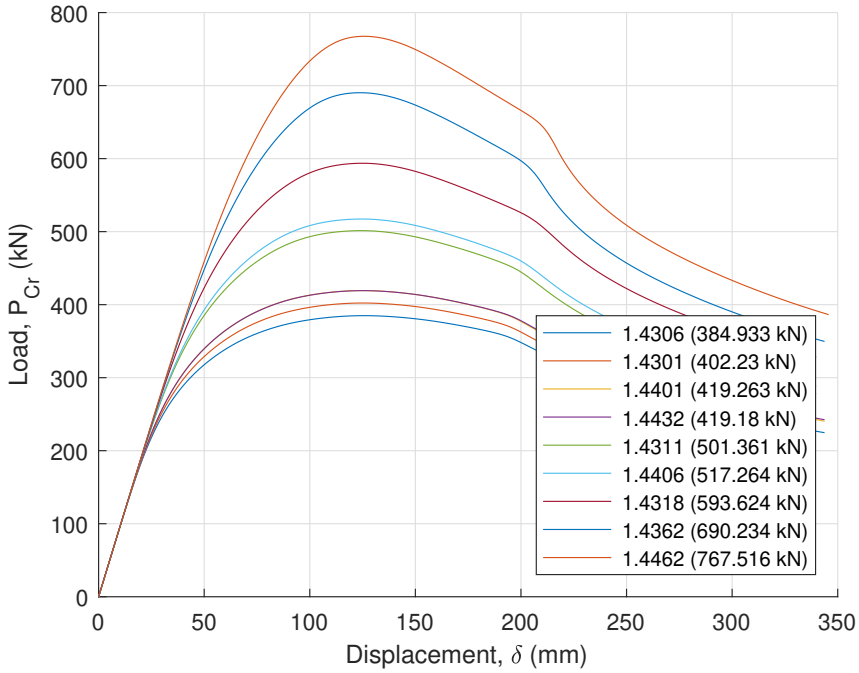

Figure A.14: Three modes - 123A - imperfections decreased -40%

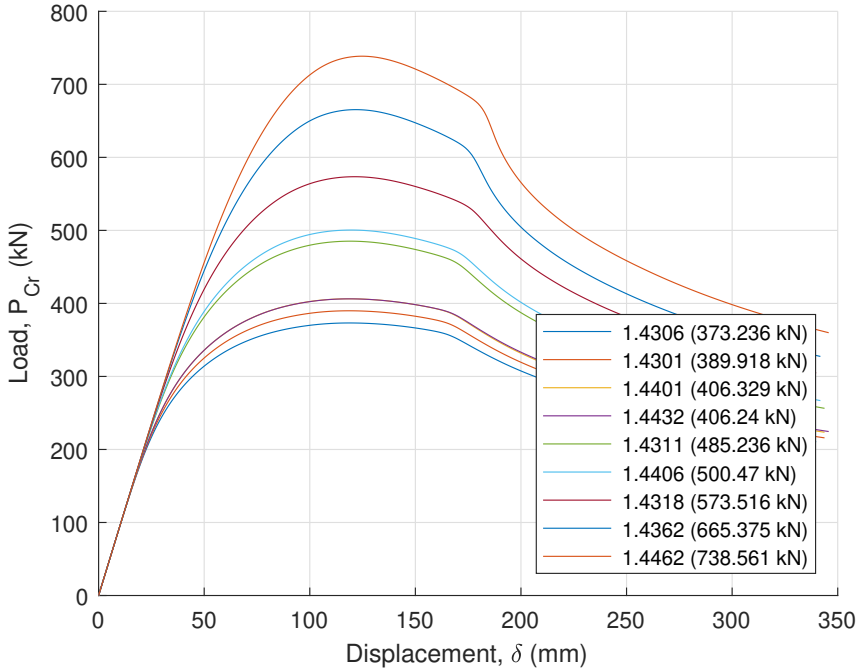

Figure A.15: Three modes - 123B - imperfections increased +40%

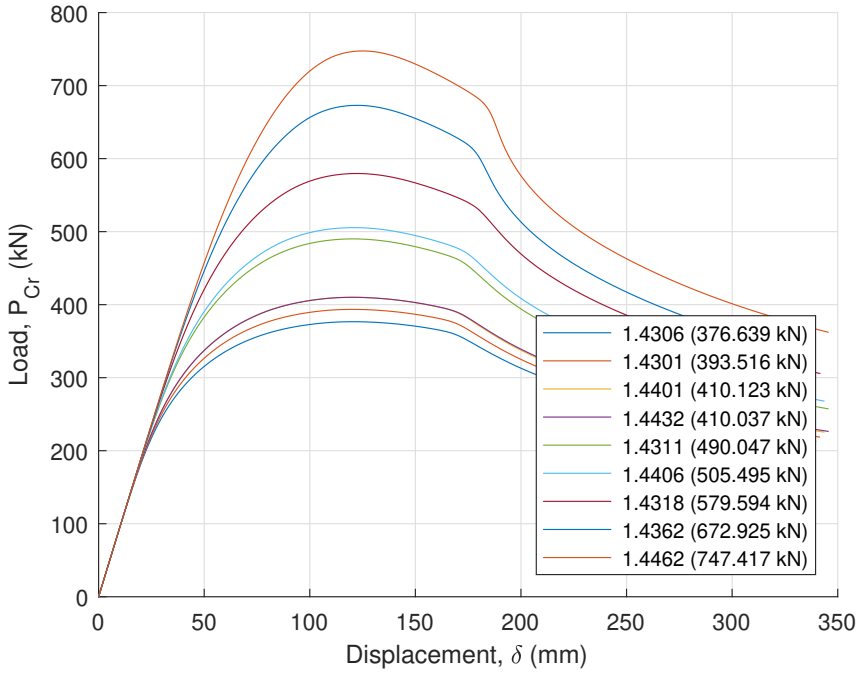

Figure A.16: Three modes - 123B - imperfections increased +20%

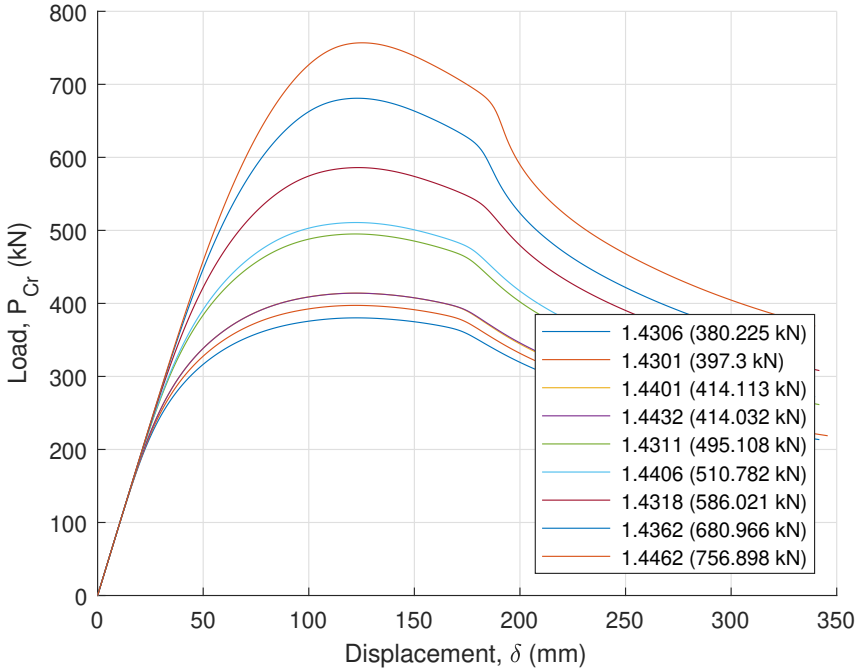

Figure A.17: Three modes - 123B - no imperfections amplification

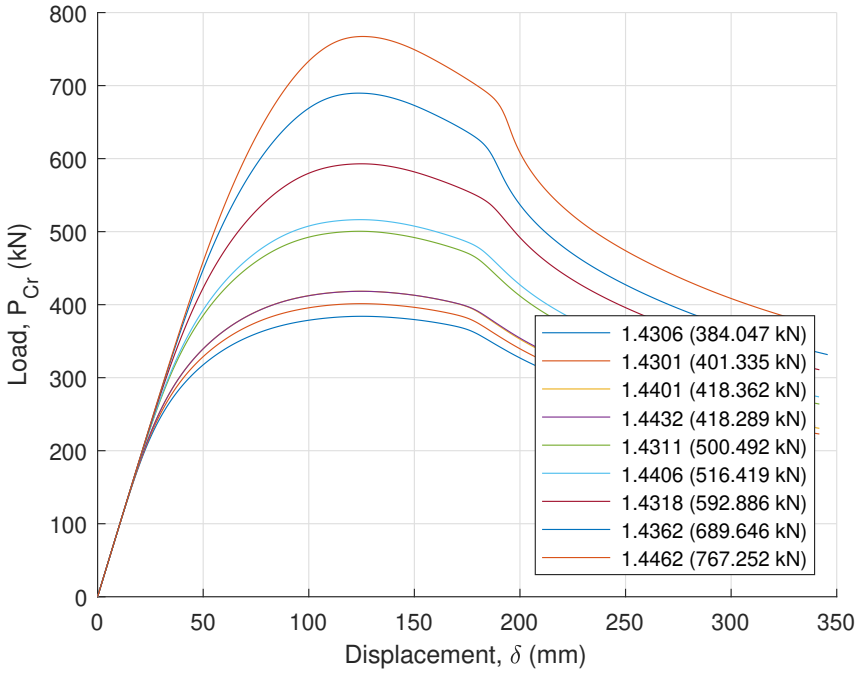

Figure A.18: Three modes - 123B - imperfections decreased -20%

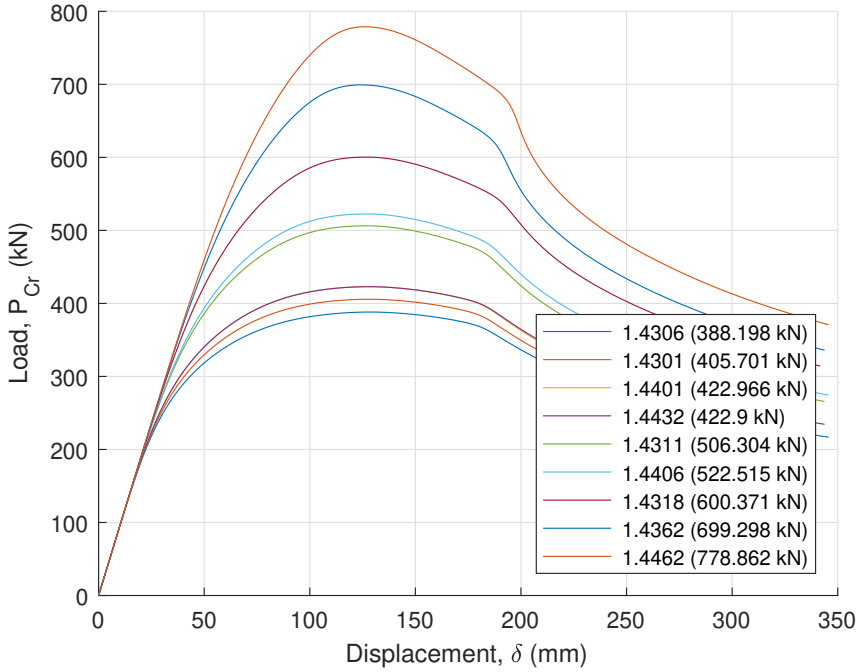

Figure A.19: Three modes - 123B - imperfections decreased -40%

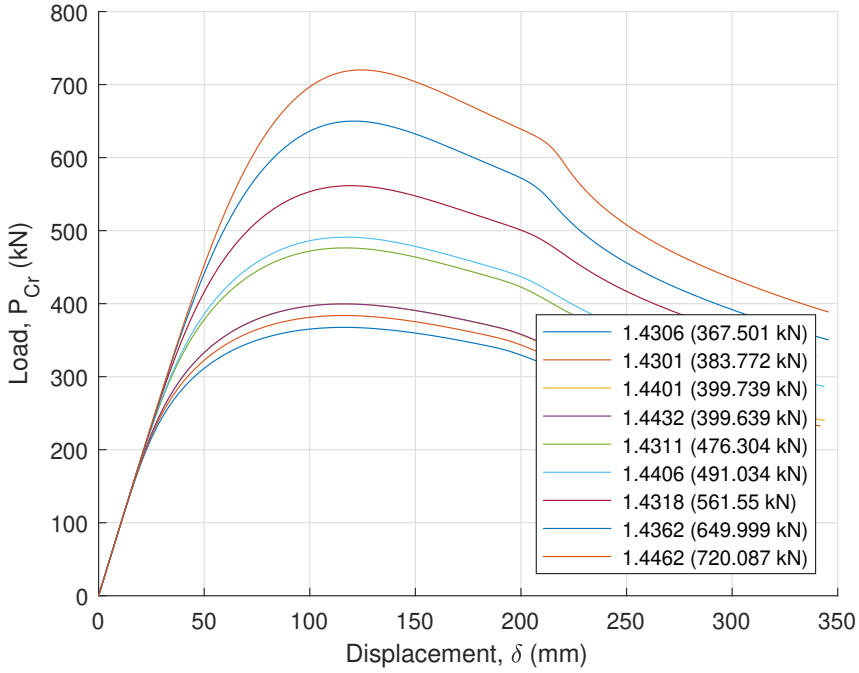

Figure A.20: Two modes - 12 - imperfections increased +40%

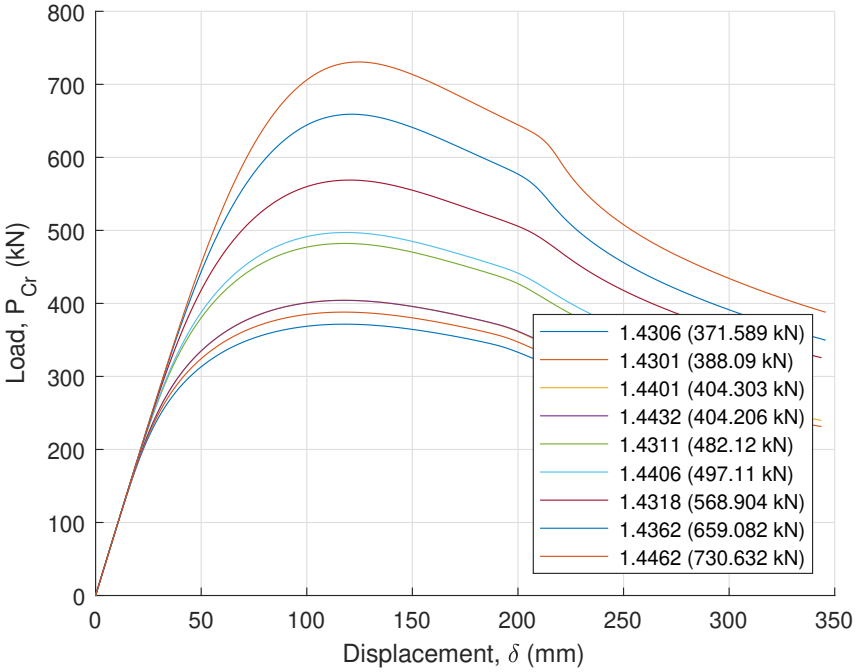

Figure A.21: Two modes - 12 - imperfections increased +20%

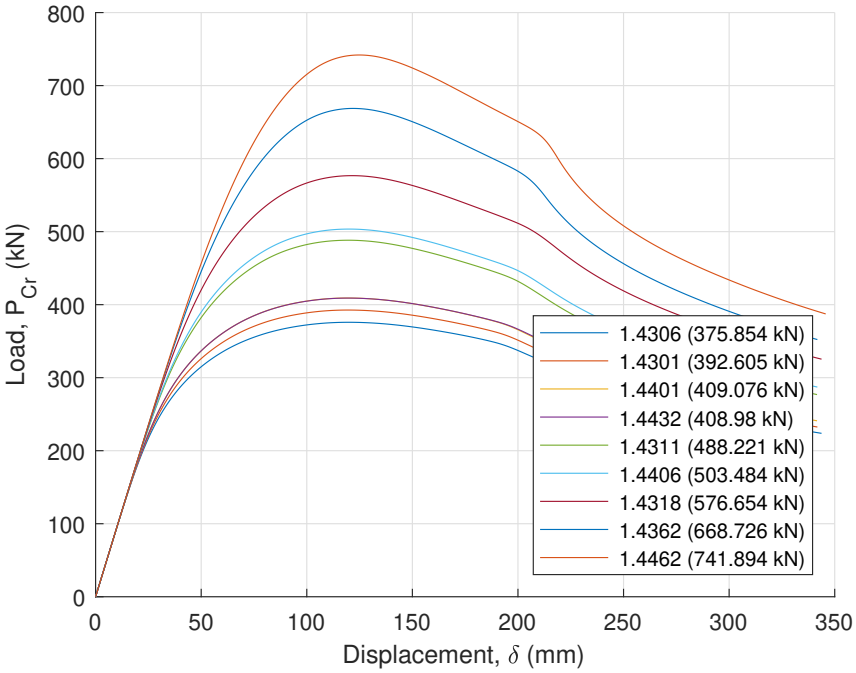

Figure A.22: Two modes - 12 - no imperfections amplification

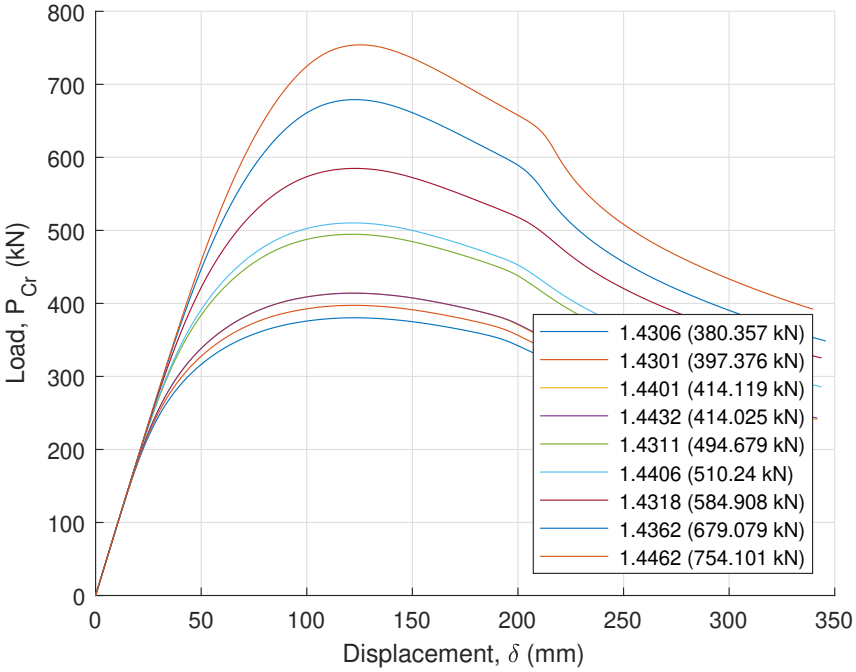

Figure A.23: Two modes - 12 - imperfections decreased -20%

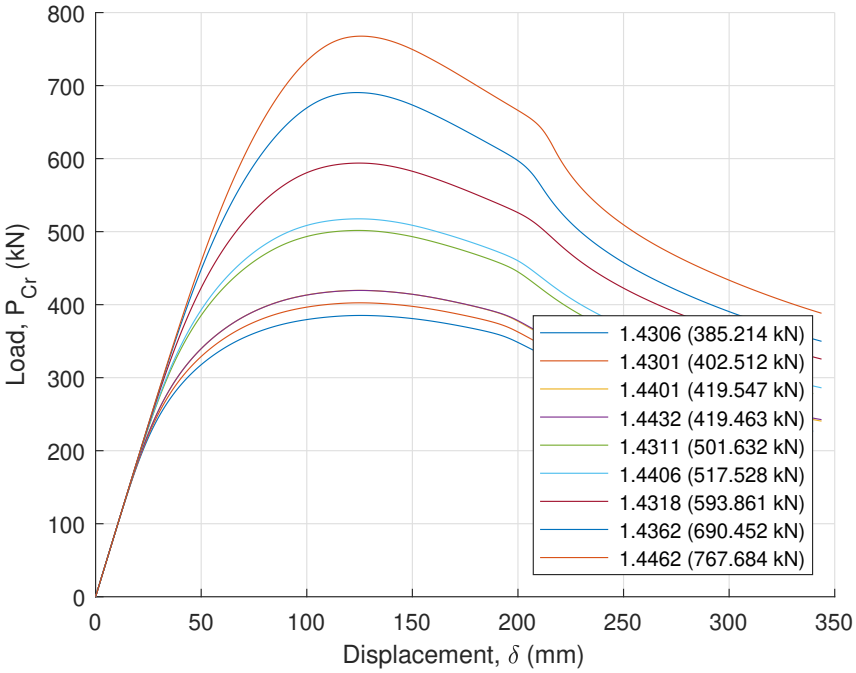

Figure A.24: Two modes - 12 - imperfections decreased -40%

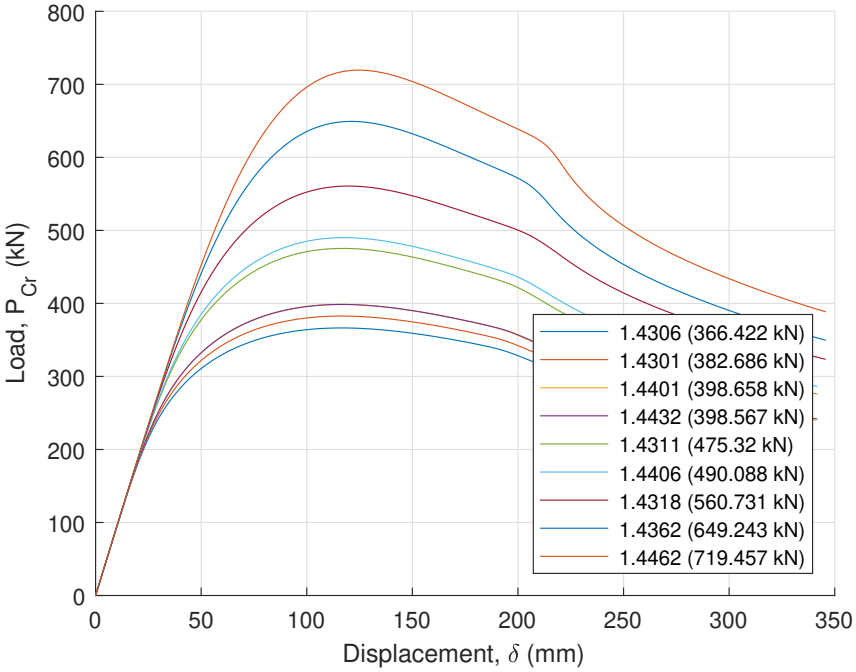

Figure A.25: Two modes - 13 - imperfections increased +40%

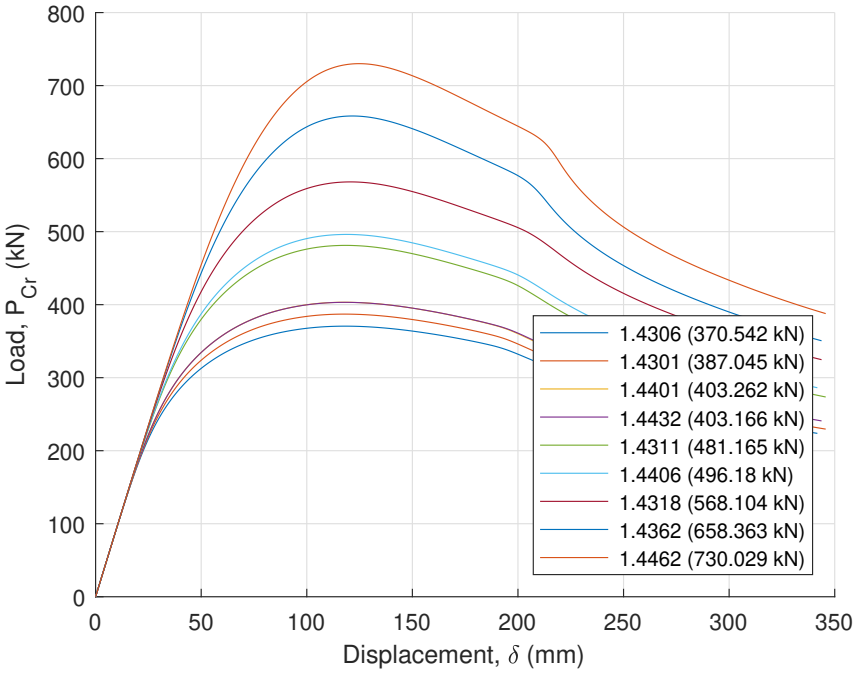

Figure A.26: Two modes - 13 - imperfections increased +20%

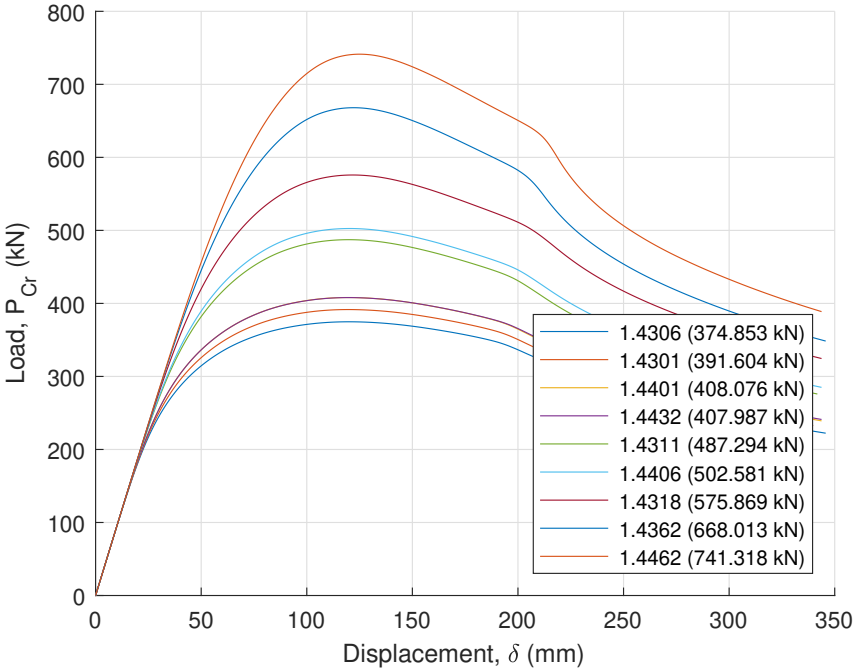

Figure A.27: Two modes - 13 - no imperfections amplification

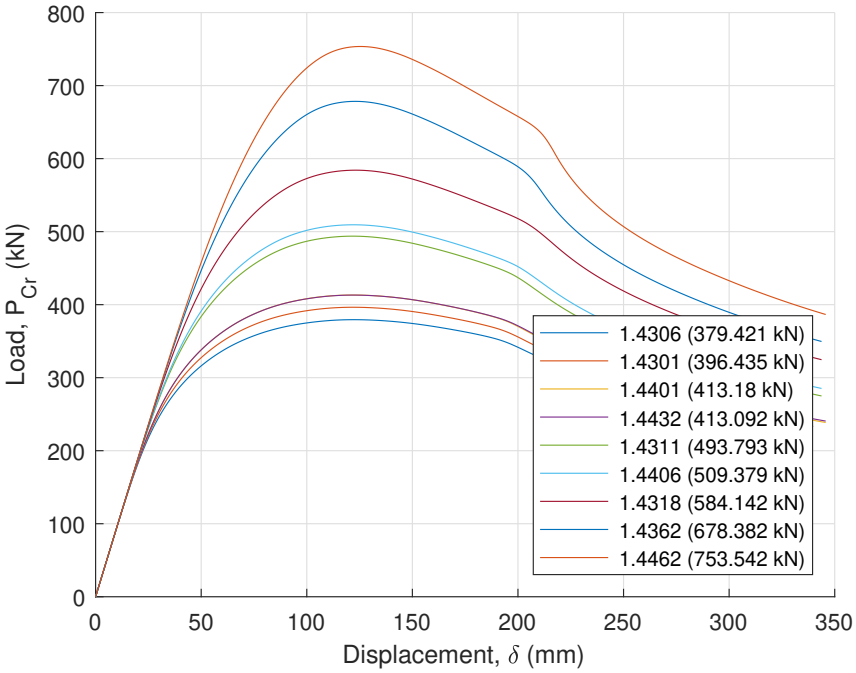

Figure A.28: Two modes - 13 - imperfections decreased -20%

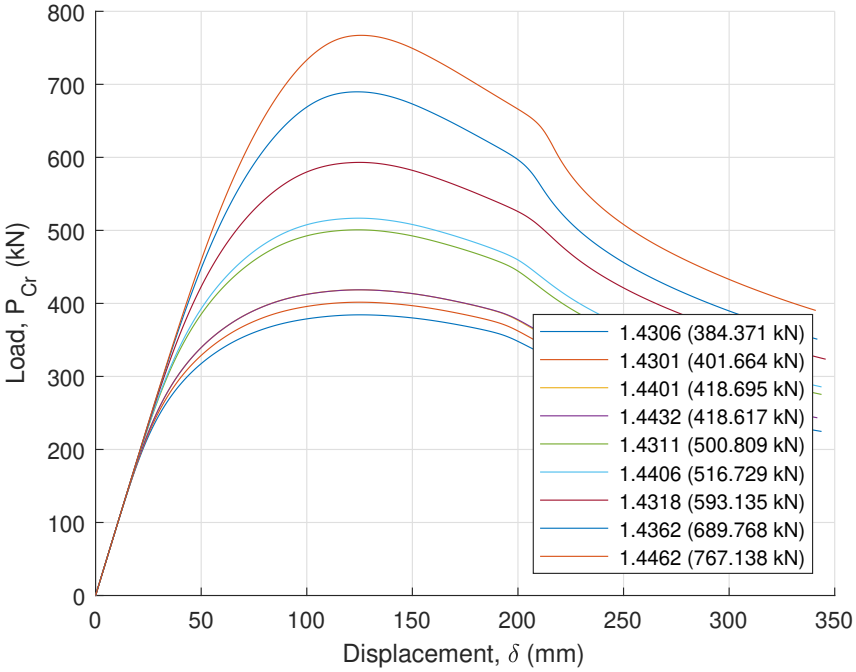

Figure A.29: Two modes - 13 - imperfections decreased -40%

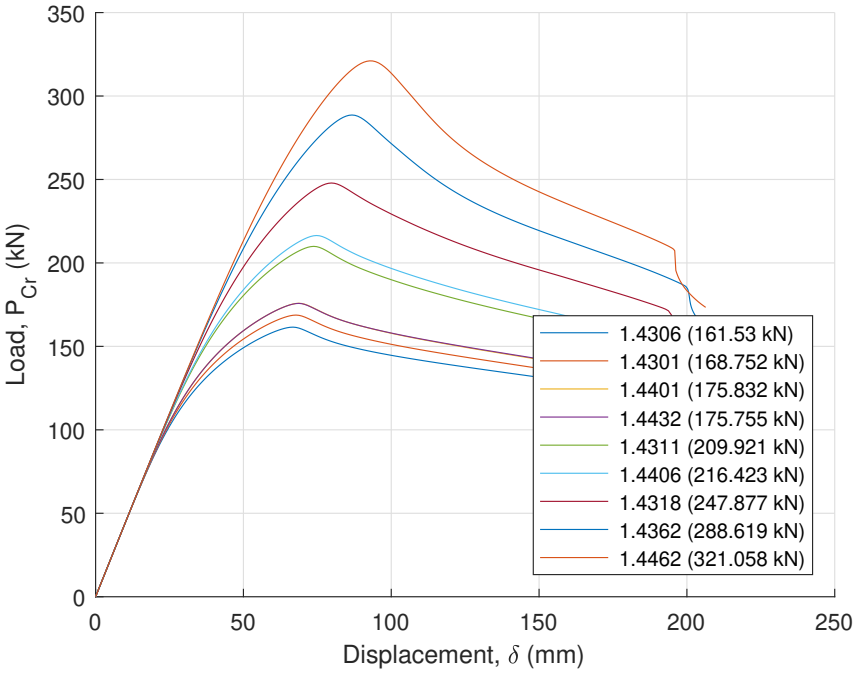

Figure A.30: One mode - 1 - imperfections decreased -40%

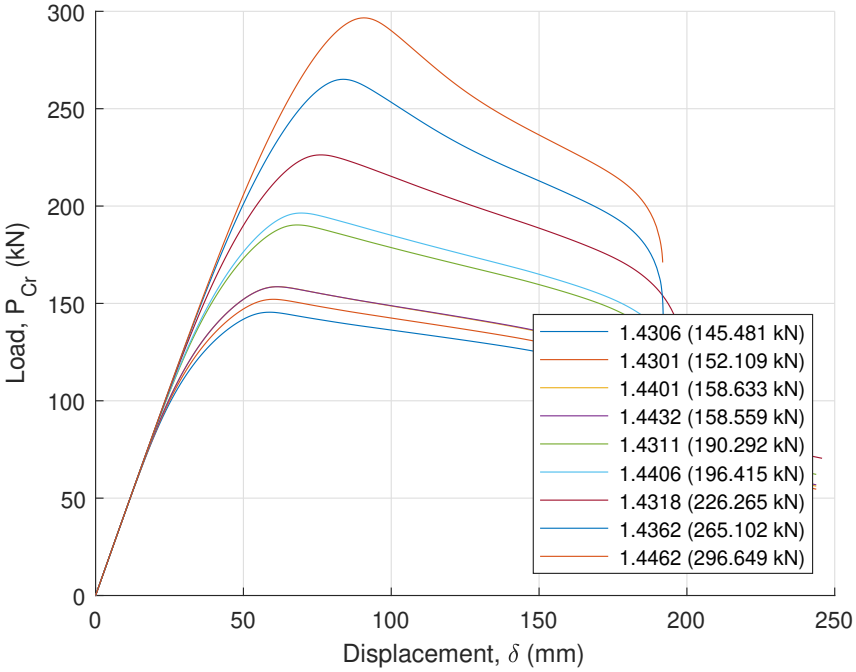

Figure A.31: One mode - 1 - imperfections increased +40%

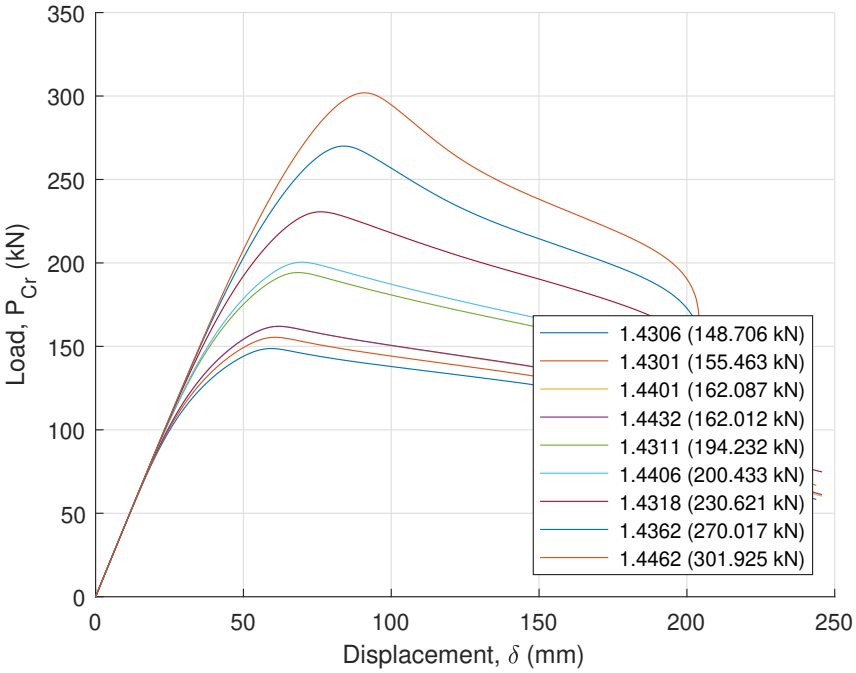

Figure A.32: One mode - 1 - imperfections increased +20%

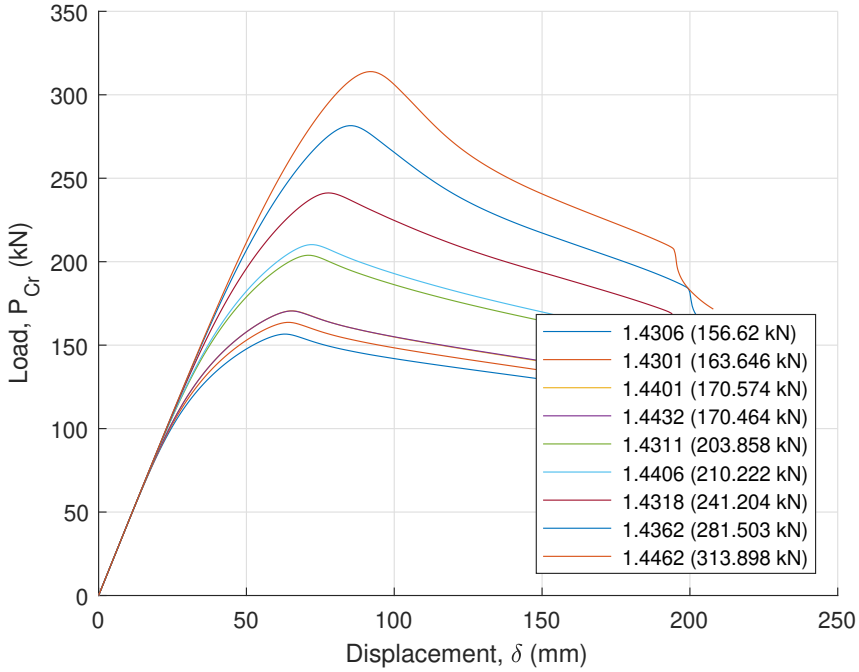

Figure A.33: One mode - 1 - imperfections decreased -20%

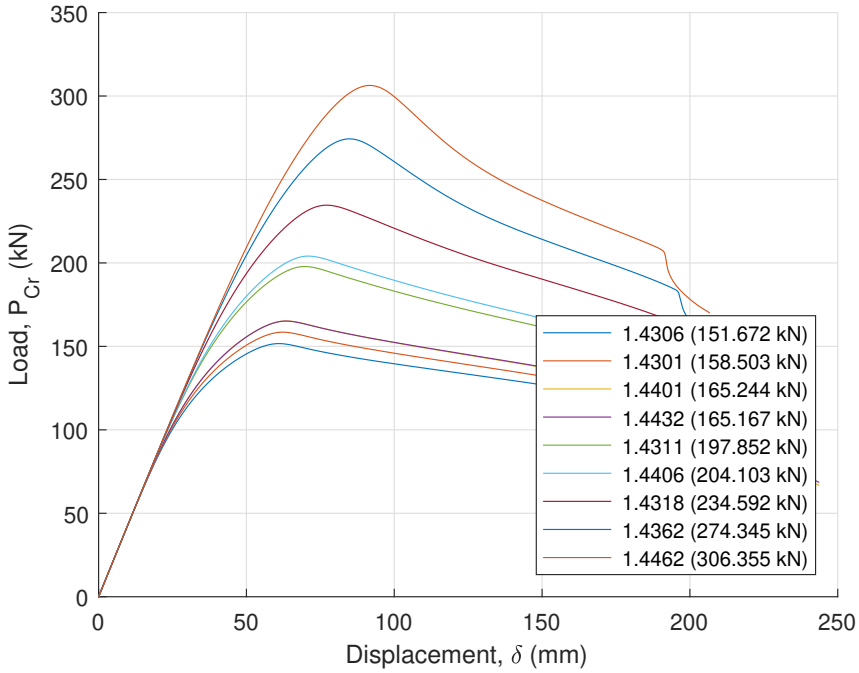

Figure A.34: Three modes - 123A - imperfections increased +40%

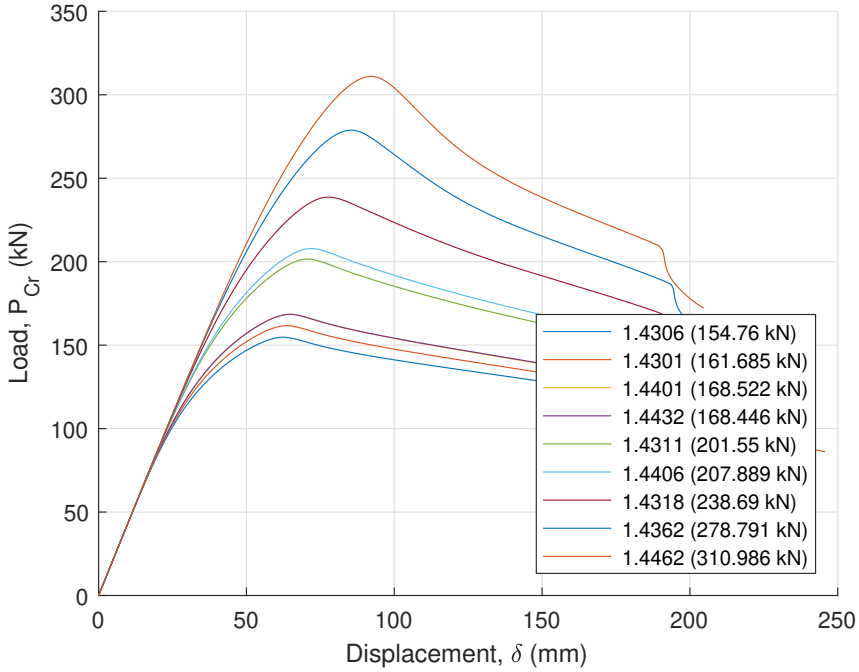

Figure A.35: Three modes - 123A - imperfections increased +20%

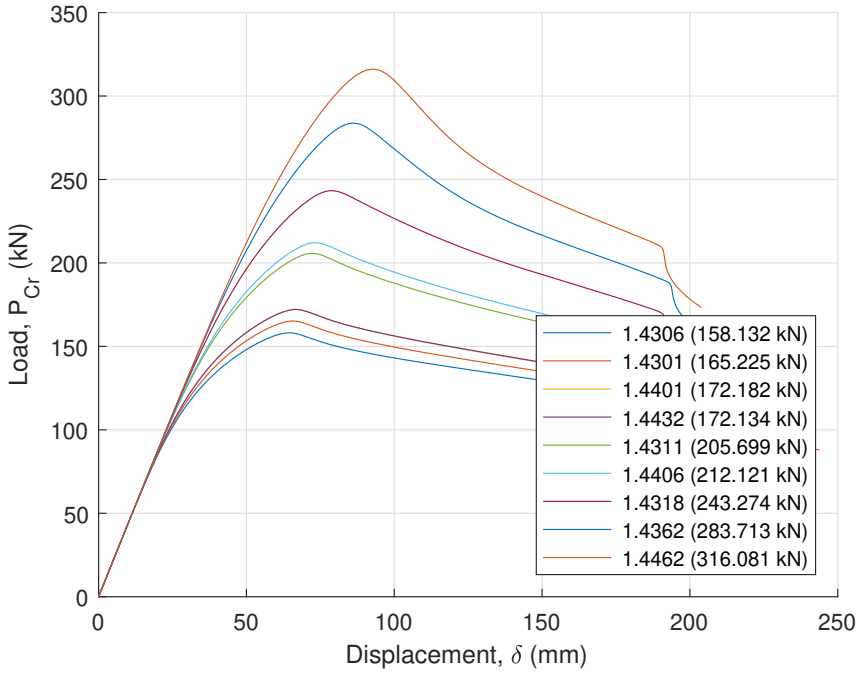

Figure A.36: Three modes - 123A - no imperfections amplification

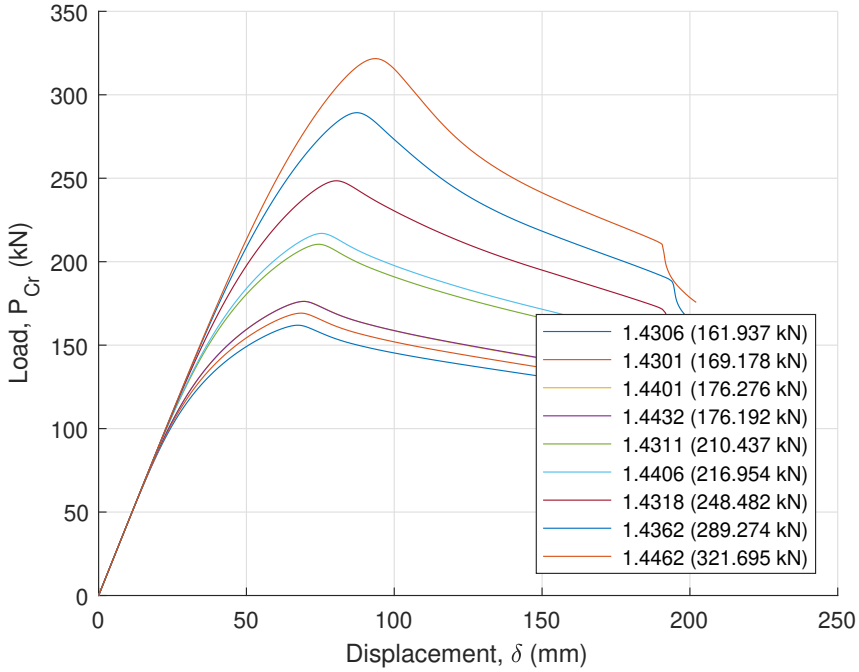

Figure A.37: Three modes - 123A - imperfections decreased -20%

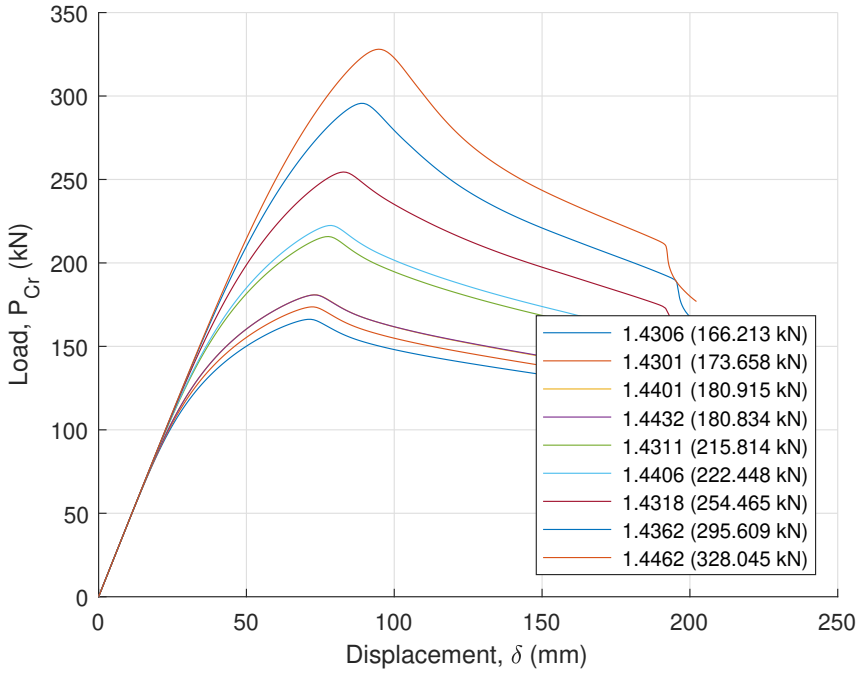

Figure A.38: Three modes - 123A - imperfections decreased -40%

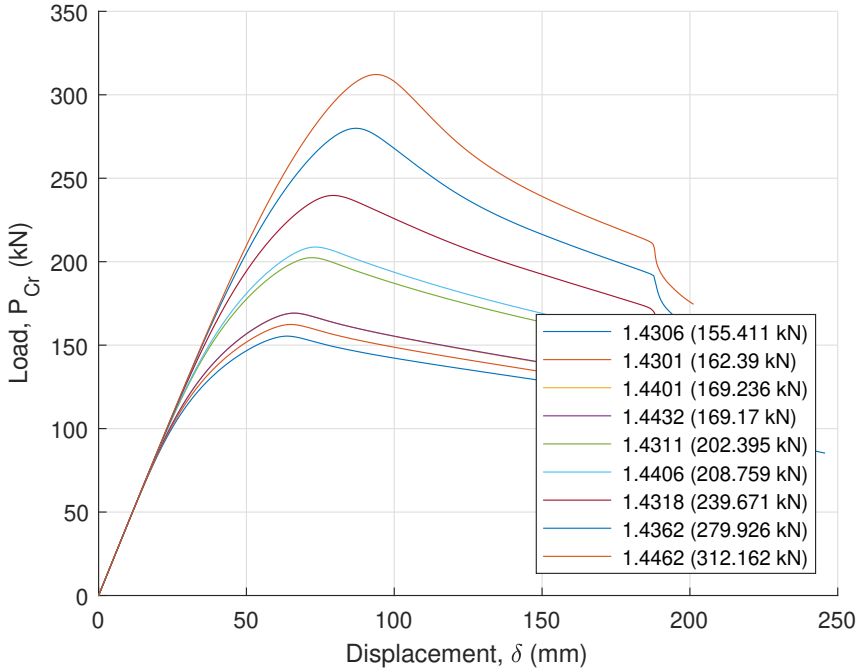

Figure A.39: Three modes - 123B - imperfections increased +40%

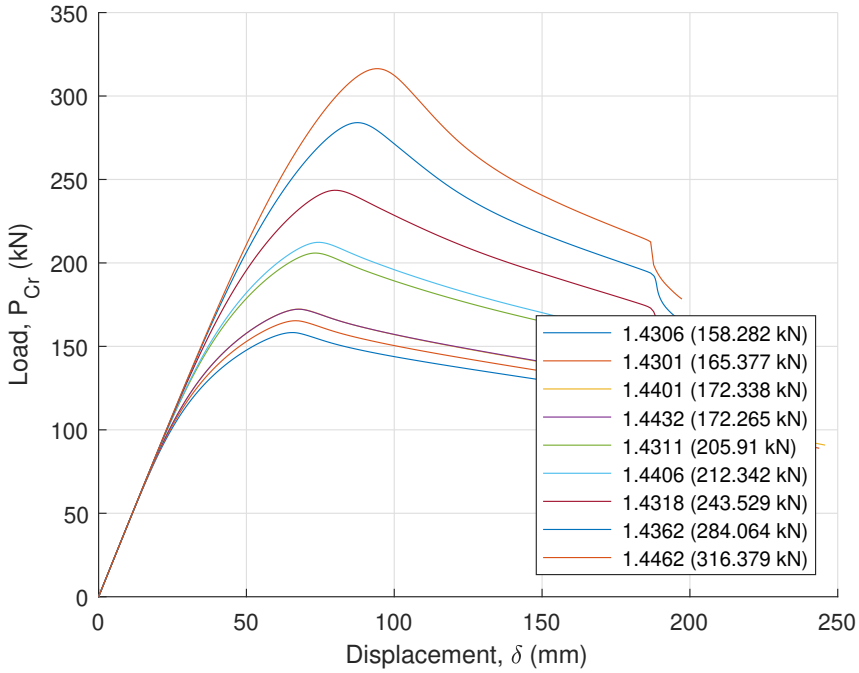

Figure A.40: Three modes - 123B - imperfections increased +20%

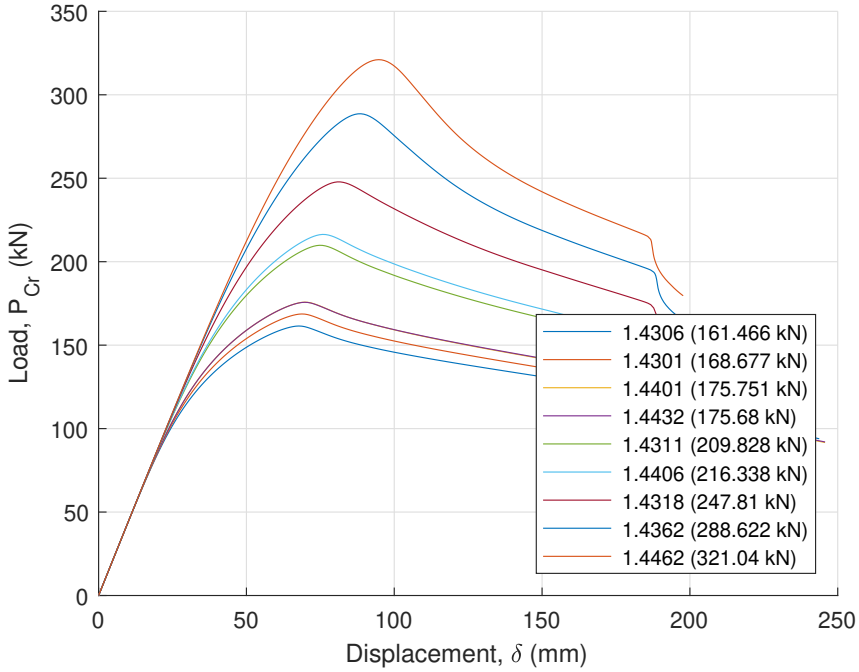

Figure A.41: Three modes - 123B - no imperfections amplification

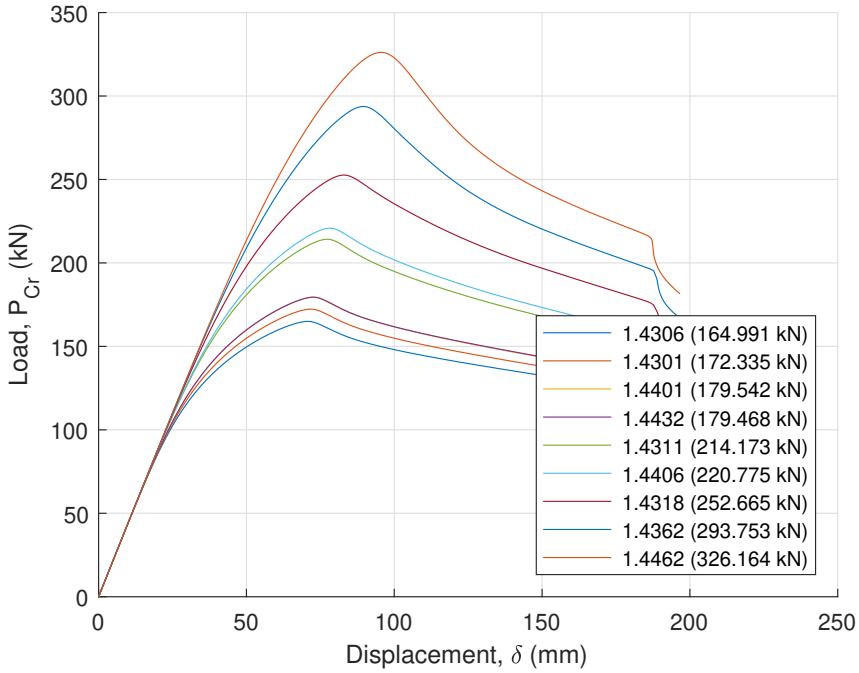

Figure A.42: Three modes - 123B - imperfections decreased -20%

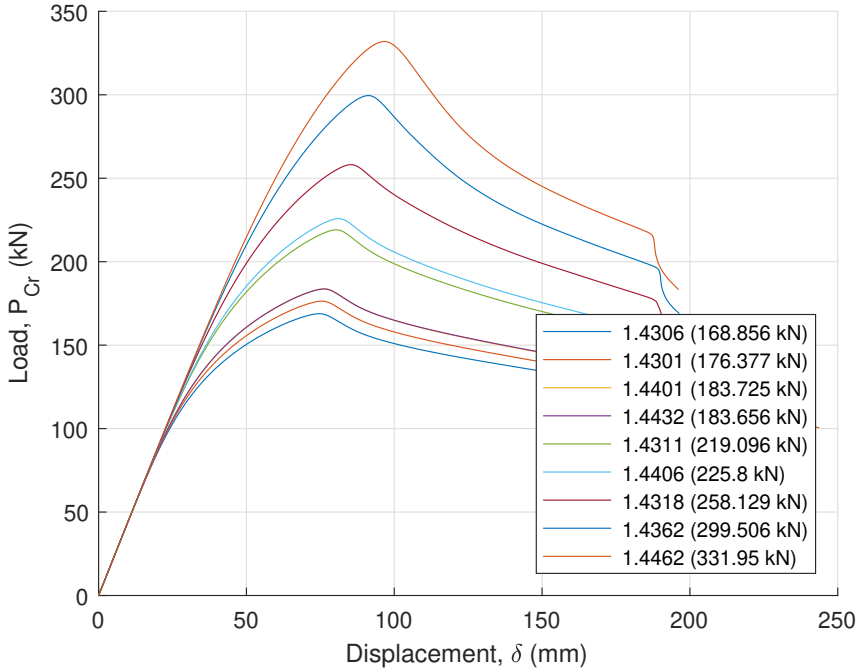

Figure A.43: Three modes - 123B - imperfections decreased -40%

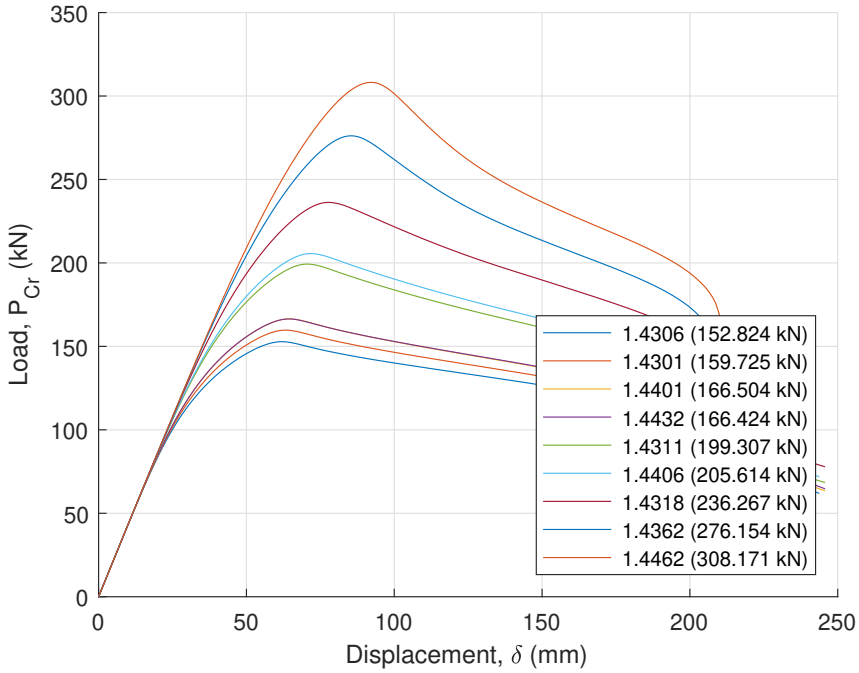

Figure A.44: Two modes - 12 - imperfections increased +40%

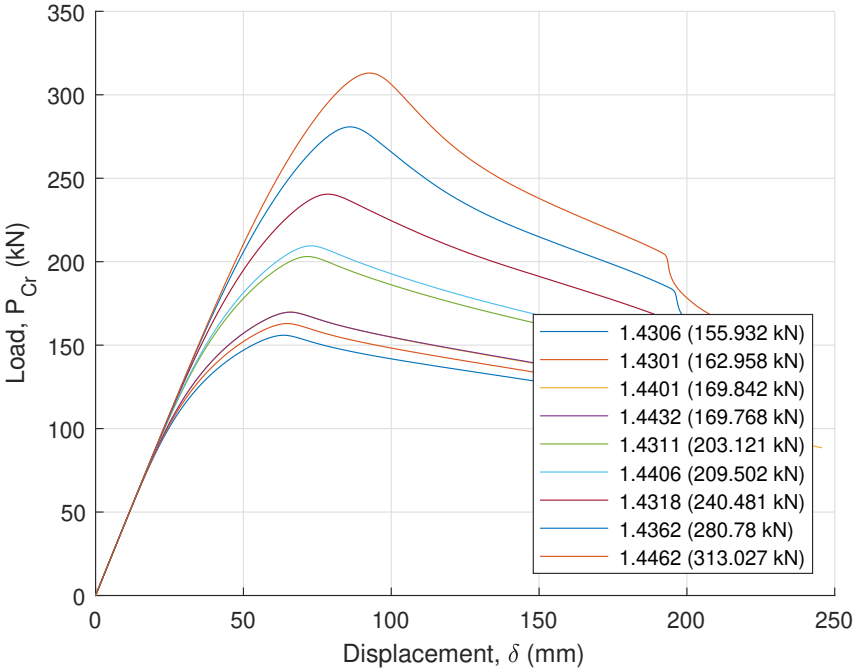

Figure A.45: Two modes - 12 - imperfections increased +20%

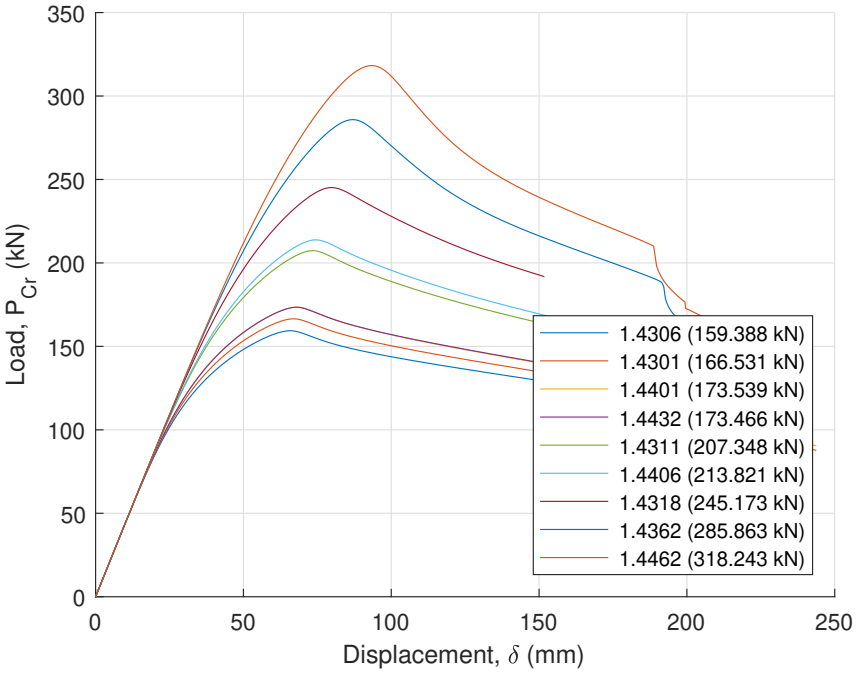

Figure A.46: Two modes - 12 - no imperfections amplification

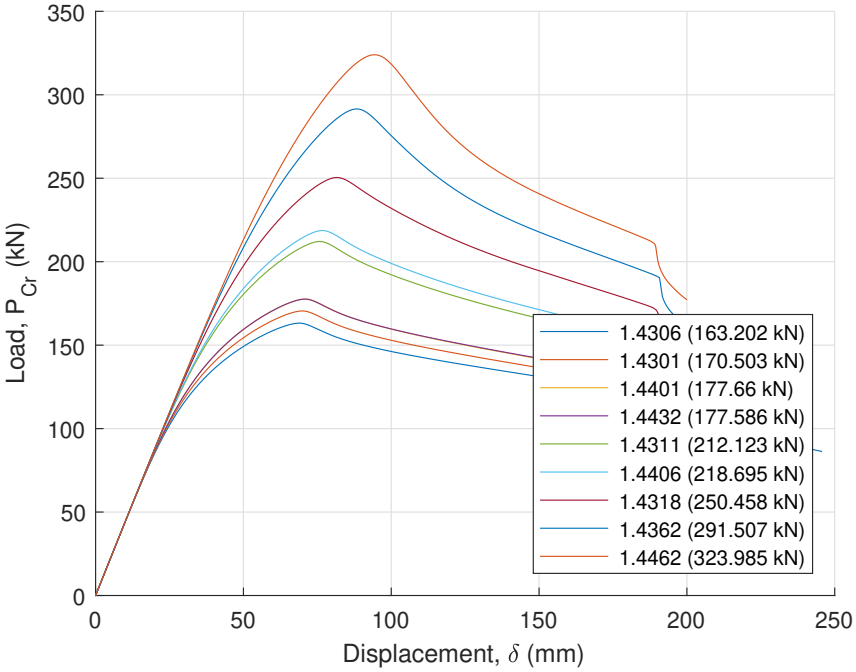

Figure A.47: Two modes - 12 - imperfections decreased -20%

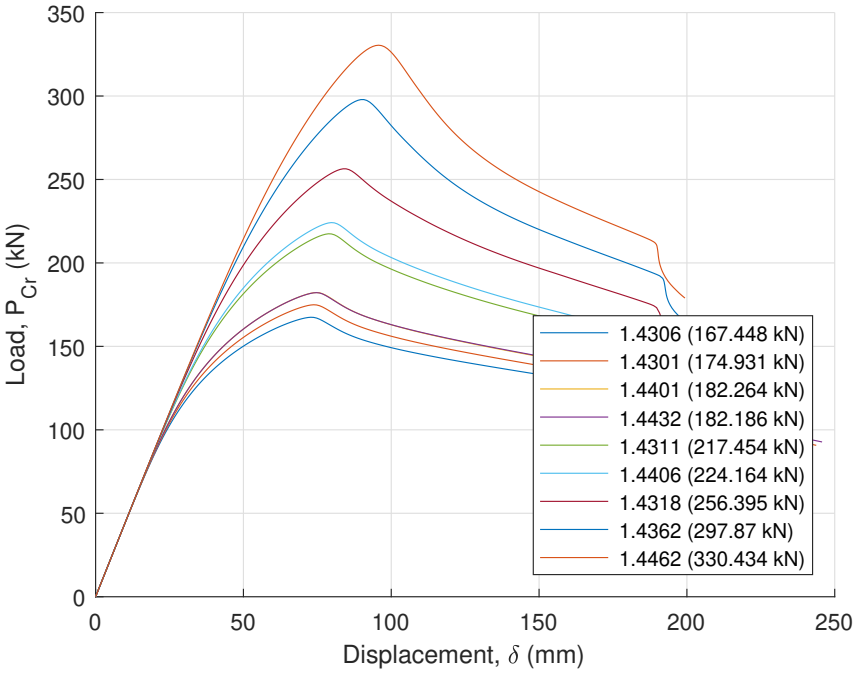

Figure A.48: Two modes - 12 - imperfections decreased -40%

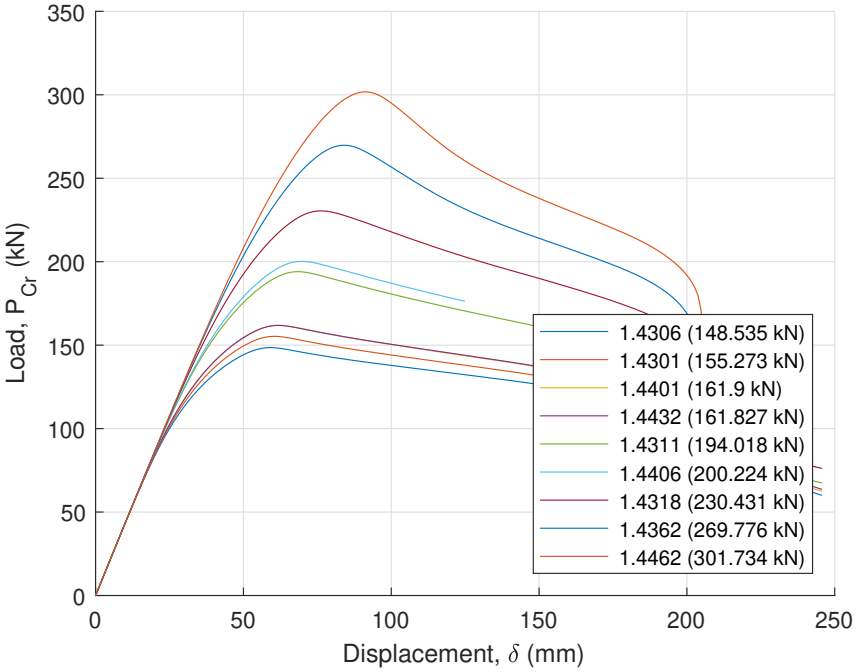

Figure A.49: Two modes - 13 - imperfections increased +40%

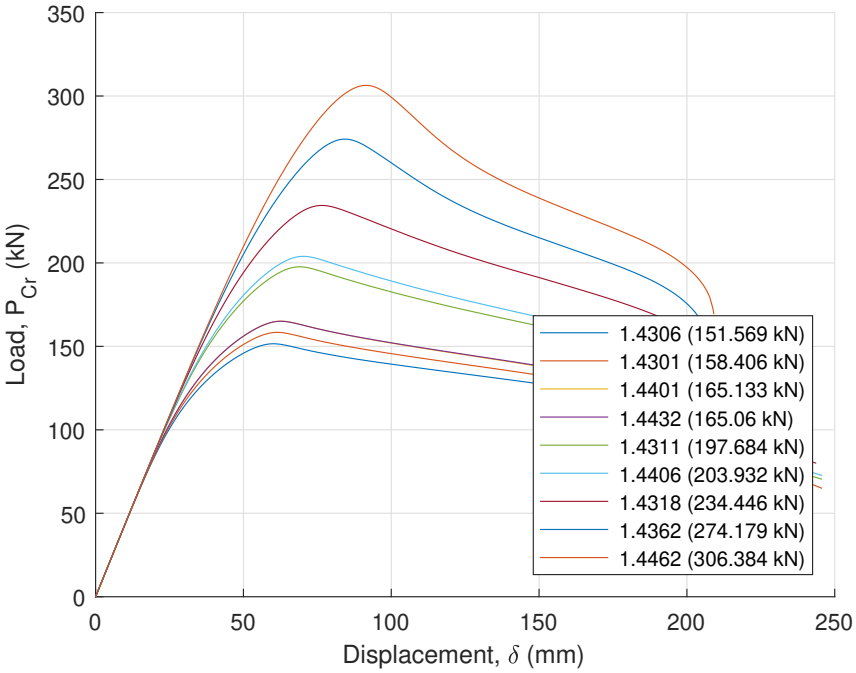

Figure A.50: Two modes - 13 - imperfections increased +20%

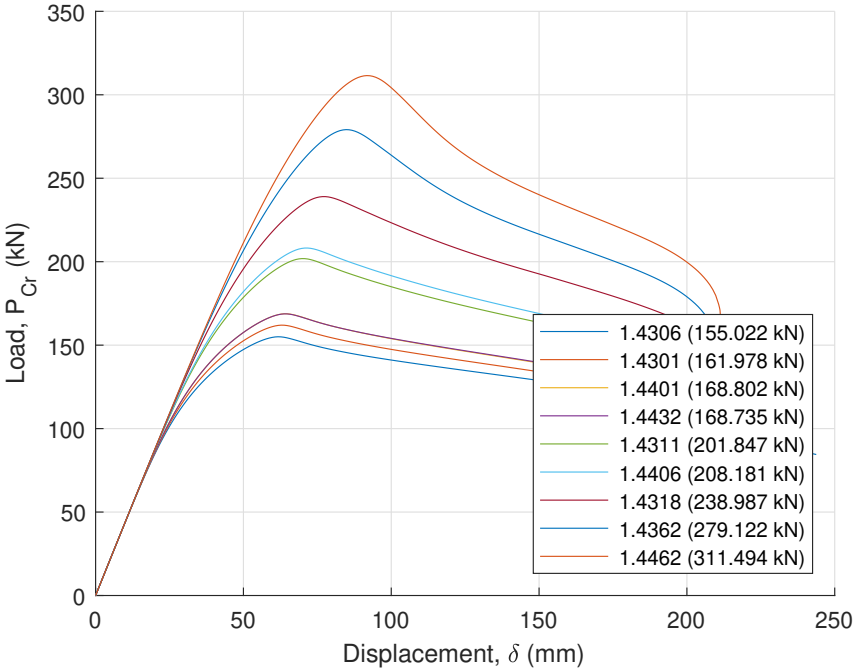

Figure A.51: Two modes - 13 - no imperfections amplification

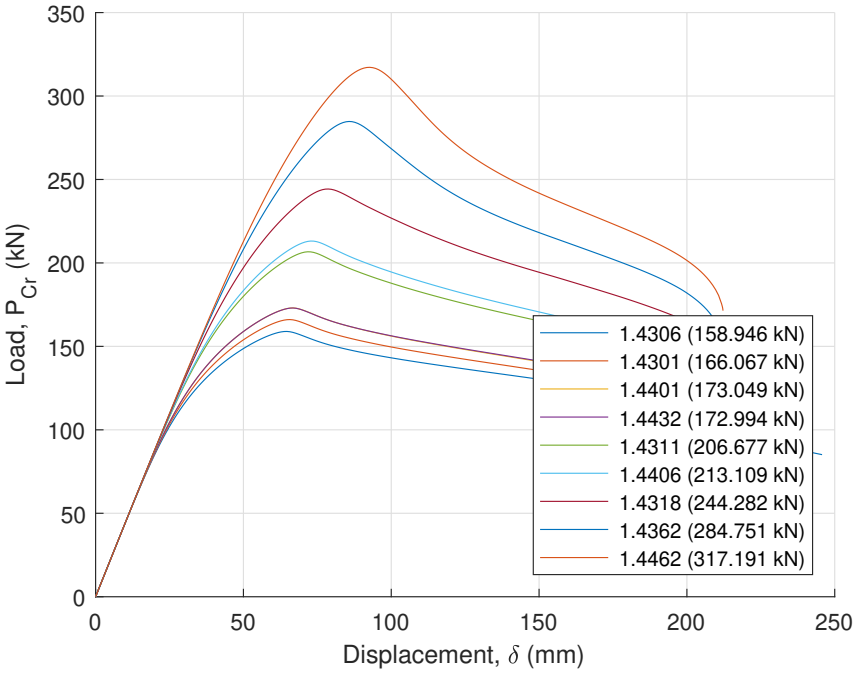

Figure A.52: Two modes - 13 - imperfections decreased -20%

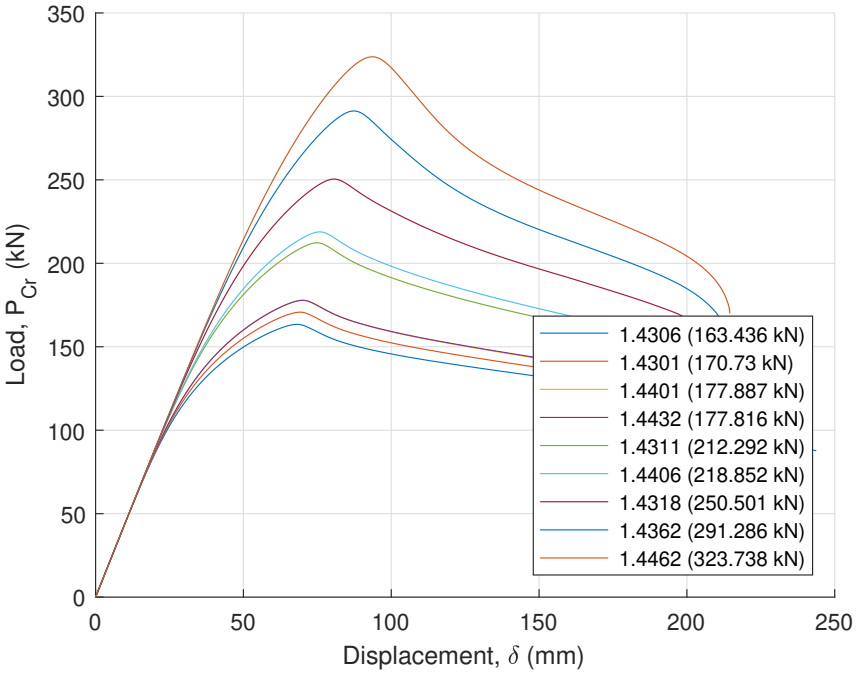

Figure A.53: Two modes - 13 - imperfections decreased -40%

Appendix B

Checks done by hand

EC BASED CHECK

BASE GEOMETRY

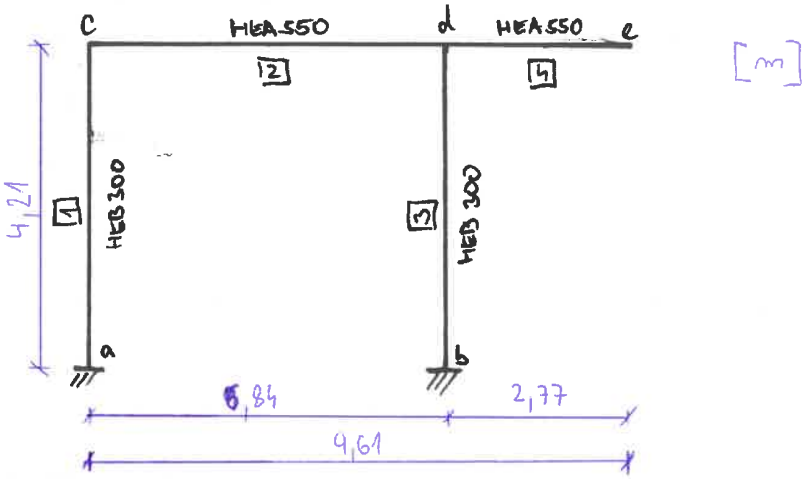

ACTING LOADS

FROM A ROOF BEAM

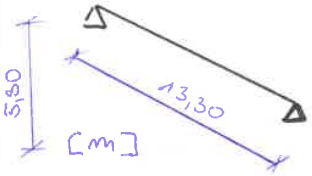

l_w.. loading width

$\rho_c = 2500\ kg/m^3$

$l_w = 3,36\ m$

$t = 0,5\ m$

$g = 10\ m/s^2$

↓ ROOF WEIGHT g_{k1}

- concrete slab C30/37

$$g \cdot l_w \cdot t \cdot \rho_c = 3,36 \cdot 0,5 \cdot 2500 \cdot 10 \cdot 10^{-3} = 42\ kN/m$$

↓ SNOW LOAD $s_{k,1}$

- for Stockholm $s_k = 2,0\ kN/m^2$

$$l_w \cdot s_k = 6,72\ kN/m$$

↓ BEAM SELFWEIGHT $g_{k,2}$

- weight in model $m = 1700\ kg$

$l = 13,30\ m$

$g_s = 1700/13,3 = 127,8\ kg/m$

$\rho_s = 7850\ kg/m^3$

$$g \cdot g_s = 10 \cdot 127,8 = 1,278\ kN/m$$

↓ LIVE LOAD $q_{k,1}$

- technology $0,7\ kN/m^2$

$$q \cdot l_w = 0,7 \cdot 3,36 = 2,352\ kN/m$$

LOADS TOTAL

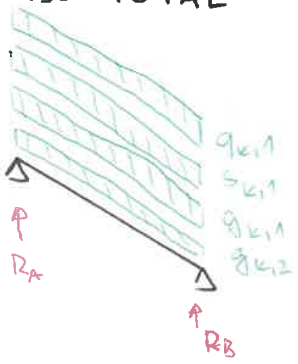

$R_B = 349\ kN$

R_A is anchored into the wall

FROM A CORRIDOR BEAM

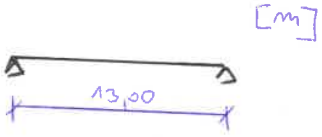

↓ SLAB FLOOR $g_{k,1}$

- concrete slab C25/30

$\rho_c = 2500\ kg/m^3$
$g = 10\ m/s^2$
$t = 0,25\ m$
$l_w = 1,175\ m$

$$t \cdot g \cdot \rho_c \cdot l_w = 0,25 \cdot 10 \cdot 2500 \cdot 10^{-3} = 7,34\ kN/m$$

↓ BEAM SELF WEIGHT $g_{k,2}$

- weight in model $m = 4,6\ t$

$g_b = 4600/13 = \doteq 353,8\ kg/m$

$$g \cdot g_b = 10 \cdot 353,8 \cdot 10^{-3} = 3,538\ kN/m$$

↓ LIVE LOAD $q_{k,1}$

- office building $q = 2,0\ kN/m^2$

$$q \cdot l_w = 2,0 \cdot 1,175 = 2,35\ kN/m$$

LOADS TOTAL

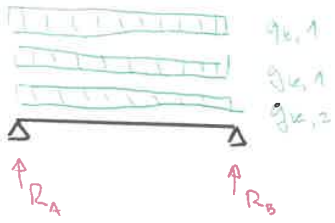

$R_A = 86,1$ kN

R_B is anchored to another beam

SWAY IMPERFECTIONS

Eq. (5.5)

$h = 4,21$ m

$m = 2$

$$\phi = \phi_0 \cdot \alpha_h \cdot \alpha_m$$

$$\phi_0 = \frac{1}{200}$$

$$\alpha_h = \frac{2}{\sqrt{h}} = \frac{2}{\sqrt{4,21}} = 0,97$$

$$\alpha_m = \sqrt{0,5\left(1+\frac{1}{m}\right)} = \sqrt{0,5\left(1+\frac{1}{2}\right)} = 0,86$$

$$\phi = \frac{1}{200} \cdot 0,97 \cdot 0,86 = 0,0042$$

$$H = \phi \cdot \Sigma V = 0,0042 \cdot (349 + 86,1) = 1,96 \text{ kN}$$

INTERNAL FORCES

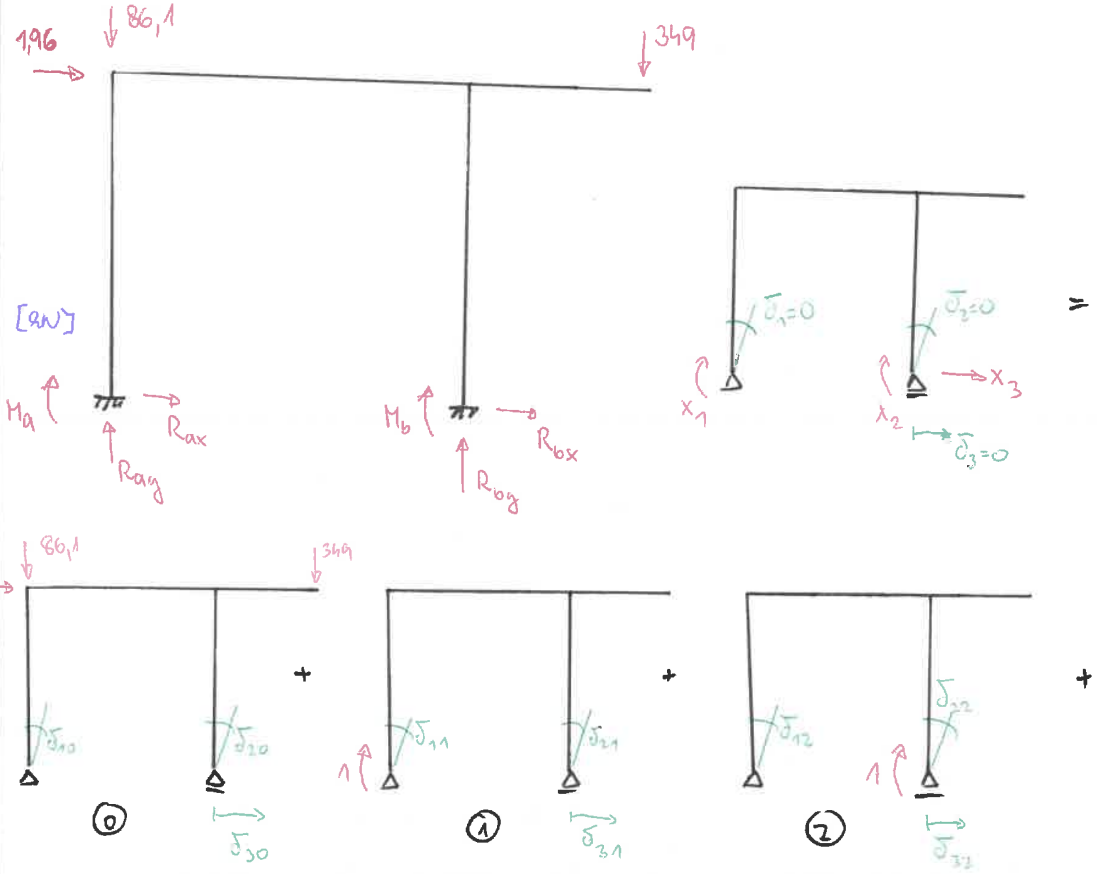

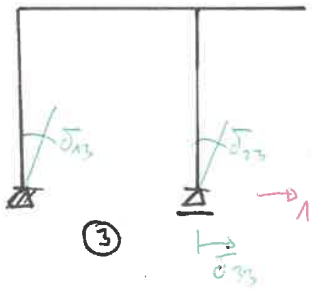

$$\delta_1 = 0 \qquad \delta_{10} + \delta_{11} X_1 + \delta_{12} X_2 + \delta_{13} X_3 = 0$$

$$\delta_2 = 0 \qquad \delta_{20} + \delta_{21} X_1 + \delta_{22} X_2 + \delta_{23} X_3 = 0$$

$$\delta_3 = 0 \qquad \delta_{30} + \delta_{31} X_1 + \delta_{32} X_2 + \delta_{33} X_3 = 0$$

MOMENT DIAGRAMS

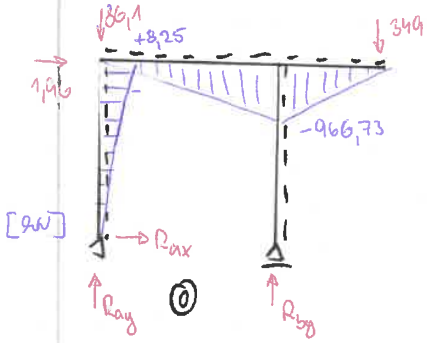

$$\sum F_{ix} = 0 \qquad 1{,}96 + R_{ax} = 0 \qquad R_{ax} = -1{,}96 \text{ kN}$$

$$\sum F_{iy} = 0 \qquad 86{,}1 + 349 - R_{ay} - R_{by} = 0$$

$$\sum M_a = 0 \qquad 349 \cdot 9{,}61 - R_{by} \cdot 6{,}84 = 0$$

$$R_{by} = 490{,}33 \text{ kN}$$

$$R_{ay} = -55{,}23 \text{ kN}$$

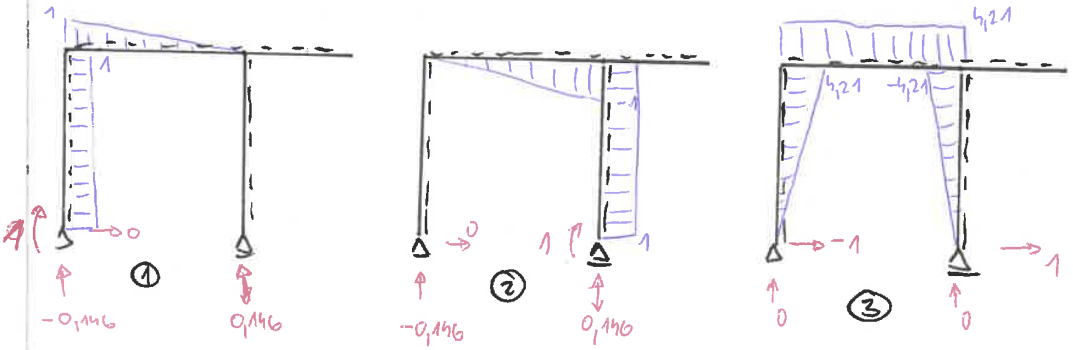

$$\delta_{11} = \frac{1}{EI_c}\left(1 \cdot 1 \cdot 4{,}21\right) + \frac{1}{EI_b}\left(\frac{6{,}84 \cdot 1}{2} \cdot \frac{2}{3}\right) = \frac{4{,}21}{EI_c} + \frac{2{,}28}{EI_b}$$

$$\delta_{12} = \frac{1}{EI_b}\left(-\frac{1}{3} \cdot \frac{1 \cdot 6{,}84}{2}\right) = -\frac{1{,}14}{EI_b}$$

$$\delta_{13} = \frac{1}{EI_c}\left(4{,}21 \cdot 1 \cdot \frac{1}{2} \cdot (4{,}21)\right) + \frac{1}{EI_b}\left(\frac{1 \cdot 6{,}84}{2} \cdot 4{,}21\right) = \frac{8{,}86}{EI_c} + \frac{14{,}398}{EI_b}$$

$$\delta_{22} = \frac{1}{EI_b}\left(-1 \cdot \frac{6{,}84}{2} \cdot \frac{2}{3}\right) + \frac{1}{EI_b}\left(1 \cdot 4{,}21\right) = \frac{2{,}28}{EI_b} + \frac{4{,}21}{EI_c}$$

$$\delta_{23} = \frac{1}{EI_b}\left(-\frac{1 \cdot 6{,}84}{2} \cdot 4{,}21\right) + \frac{1}{EI_c}\left(4{,}21 \cdot \frac{1}{2} \cdot (-4{,}21)\right) = -\frac{14{,}398}{EI_b} - \frac{8{,}86}{EI_c}$$

$$\delta_{33} = \frac{1}{EI_c}\left[\frac{(-4{,}21)\cdot 4{,}21}{2}\cdot\frac{2}{3}\cdot 2\cdot(-4{,}21)\right] + \frac{1}{EI_b}\left(4{,}21\cdot 6{,}84\cdot 4{,}21\right) =$$

$$= \frac{49{,}74}{EI_c} + \frac{121{,}23}{EI_b}$$

$$\delta_{10} = \frac{1}{EI_c}\left(\frac{8{,}25\cdot 4{,}21}{2}\cdot 1\right) + \frac{1}{EI_b}\left[\frac{(-966{,}73)\cdot 6{,}84}{2}\cdot\frac{1}{3}\right] = \frac{17{,}36}{EI_c} - \frac{1102}{EI_b}$$

$$\delta_{20} = \frac{1}{EI_b}\left[\frac{(-966{,}73)\cdot 6{,}84}{2}\cdot\left(-\frac{2}{3}\right)\right. = \frac{2204}{EI_b}$$

$$\delta_{30} = \frac{1}{EI_c}\left(\frac{8{,}25\cdot 4{,}21}{2}\cdot\frac{2}{3}\cdot 4{,}21\right) + \frac{1}{EI_b}\left(\frac{-966{,}73\cdot 6{,}84}{2}\cdot 4{,}21\right) =$$

$$= \frac{48{,}74}{EI_c} - \frac{13919}{EI_b}$$

$E = 210\ GPa$

$I_b = 1{,}11\cdot 10^{-3}\ m^4$

$I_c = 8{,}56\cdot 10^{-5}\ m^4$

$$\begin{bmatrix} \frac{4{,}21}{EI_c}+\frac{2{,}28}{EI_b} & -\frac{1{,}14}{EI_b} & \frac{8{,}86}{EI_c}+\frac{14{,}398}{EI_b} \\ -\frac{1{,}14}{EI_b} & \frac{2{,}28}{EI_b}+\frac{4{,}21}{EI_c} & -\frac{14{,}398}{EI_b}-\frac{8{,}86}{EI_c} \\ \frac{8{,}86}{EI_c}+\frac{14{,}398}{EI_b} & -\frac{14{,}398}{EI_b}-\frac{8{,}86}{EI_c} & \frac{49{,}74}{EI_c}+\frac{121{,}23}{EI_b} \end{bmatrix}\begin{bmatrix} X_1 \\ X_2 \\ X_3 \end{bmatrix} = \begin{bmatrix} \frac{17{,}36}{EI_c}-\frac{1102}{EI_b} \\ \frac{2204}{EI_b} \\ \frac{48{,}74}{EI_c}-\frac{13919}{EI_b} \end{bmatrix}$$

$$X = \begin{bmatrix} -60{,}6419 \\ 36{,}8470 \\ 33{,}7774 \end{bmatrix}$$

$$R_{ax} = -1{,}96 + X_1\cdot 0 + X_2\cdot 0 + X_3\cdot(-1) = -35{,}734\ kN$$

$$R_{ay} = -55{,}23 + X_1\cdot 0{,}146 + X_2\cdot 0{,}146 + X_3\cdot 0 = -51{,}7559\ kN$$

$$R_{by} = 490{,}33 + X_1\cdot(-0{,}146) + X_2\cdot(-0{,}146) + X_3\cdot 0 = 486{,}85\ kN$$

$$R_{bx} = 0 + X_1\cdot 0 + X_2\cdot 0 + X_3\cdot 1 = 33{,}7774\ kN$$

$$M_a = 0 + X_1\cdot 1 + X_2\cdot 0 + X_3\cdot 0 = -60{,}6419\ kNm$$

$$M_b = 0 + X_1\cdot 0 + X_2\cdot 1 + X_3\cdot 0 = 36{,}8470\ kNm$$

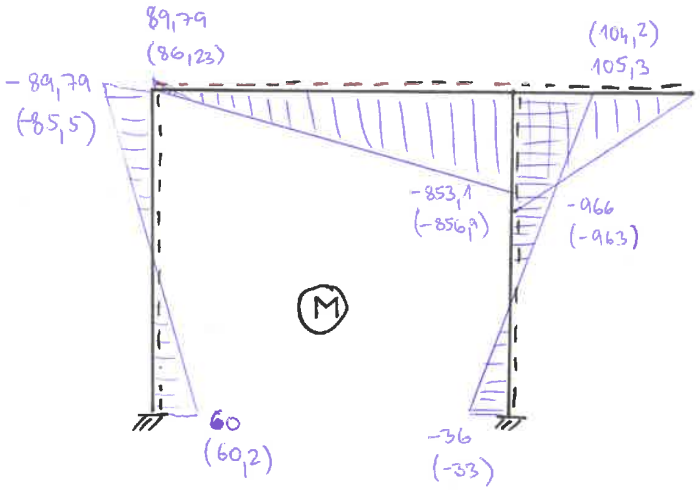

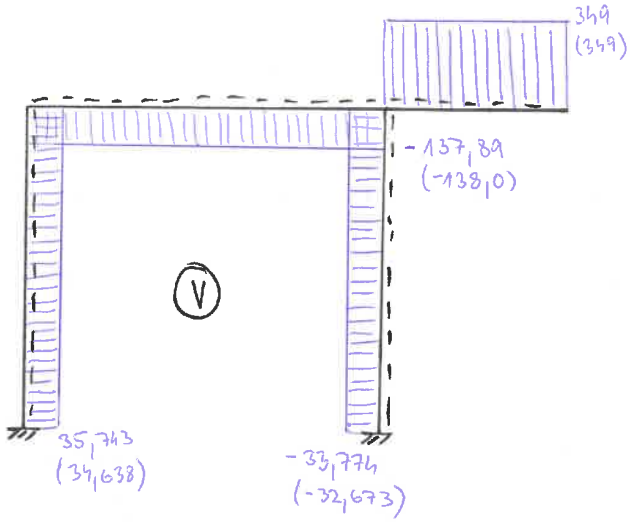

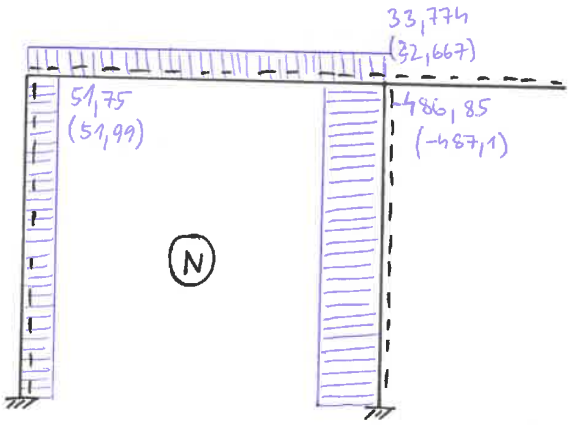

- note: values in braces are obtained from commercial software for structural analysis DLUBAL RFEM

MATERIAL AND CROSS-SECTION CHARACTERISTICS

Table (3.1)

S355

$f_y = 355$ MPa

$f_u = 490$ MPa

$E = 210$ GPa

$G = 81\,000$ MPa

$\nu = 0,3$

HEB 300

$I_y = 2\,517\,000\,00$ mm^4

$I_z = 8\,563\,0000$ mm^4

$A = 14910$ mm^2

$I_t = 1\,850\,000$ mm^4

$I_\omega = 1,688 \cdot 10^{+12}$ mm^6

$W_{pl,y} = 1\,869000$ mm^3

$W_{pl,z} = 870100$ mm^3

$W_{el,y} = 1\,678000$ mm^3

$W_{el,z} = 570\,900$ mm^3

$t_f = 19$ mm $\quad c_f = 117,5$ mm

$t_w = 11$ mm

$h = 300$ mm

$b = 300$ mm

$c_w = 208$ mm

HEA 550

$I_y = 1\,119\,000\,0$ mm^4

$I_z = 108200\,000$ mm^4

$A = 21\,180$ mm^2

$I_t = 3515000$ mm^4

$I_\omega = 7,189 \cdot 10^{12}$ mm^6

$W_{pl,y} = 4\,622000$ mm^3

$W_{pl,z} = 1\,107\,000$ mm^3

$W_{el,y} = 4146\,000$ mm^3

$W_{el,z} = 721\,300$ mm^3

$t_f = 24$ mm $\quad c_f = 116,75$ mm

$t_w = 12,5$ mm

$h = 540$ mm

$b = 300$ mm

$c_w = 438$ mm

CROSSECTION CLASSIFICATION

Table (5.2)

HEB 300

$\varepsilon = 0,81$

$c/t_w = \frac{208}{11} = 18,9$

web

$18,9 \leq 72 \cdot 0,81 = 58$ (bending)

$18,9 \leq 33 \cdot 0,81 = 26$ (compression) ①

flange

$c/t_f = \frac{117,5}{19} = 6,18$

$6,18 \leq 9 \cdot 0,81 = 7,29$ (compression) ①

→ class 1

HEA 550

$\varepsilon = 0{,}81$

web

$c/t = \frac{438}{12{,}5} = 35{,}04$

$35{,}04 \leq 0{,}81 \cdot 72 = 58$ (bending)

→ ①

flange

$c/t = \frac{116{,}75}{24} = 4{,}86$

$4{,}86 \leq 0{,}81 \cdot 9 = 7{,}29$

→ ①

→ class 1

RESISTANCE OF CROSS-SECTIONS

MEMBER NO. 1

Cl. 6.2.3

TENSION

$N_{Ed} = 51{,}75$ kN

$\gamma_{M0} = 1$ Eq. (6.7)

$N_{Rd} = \frac{A \cdot f_y}{\gamma_{M0}} = \frac{14910 \cdot 355}{1} = 5293$ kN

$\frac{51{,}75}{5293} = 9{,}7 \cdot 10^{-3} \leq 1$

Cl. 6.2.6

SHEAR

$V_{Ed} = 35{,}74$ kN

Eq. (6.18)

$A_{v,pl} = 11810\,mm^2$

$V_{Rd} = \frac{A_v (f_y/\sqrt{3})}{\gamma_{M0}} = \frac{11810\,(355/\sqrt{3})}{1} = 2420$ kN

$\frac{35{,}74}{2420} = 0{,}01 \leq 1$

Cl. 6.2.9.1

BENDING AND AXIAL FORCE

$M_{Ed} = 89{,}79$ kNm

Eq (6.13)

$M_{Rd} = M_{N,z,Rd} = \frac{W_{pl,z} \cdot f_y}{\gamma_{M0}}$

Eq. (6.33; 6.34)

$= 308{,}8$ kNm

$N_{pl,Rd} = 5293$ kN

$N_{Ed} = 51{,}75$ kN

$51{,}75 \leq 0{,}25 \cdot 5293 = 1323$ kN

$51{,}75 \leq \frac{0{,}5 \cdot 300 \cdot 11 \cdot 10^{-3} \cdot 355}{1} = 1171{,}5$ kN

Eq. (6.12)

$$\frac{89,8}{308,8} = 0,29 \leq 1$$

MEMBER NO. 3

Cl. 6.2.4

COMPRESSION

$N_{Ed} = 486,85\ kN$

$N_{c,Rd} = \frac{A \cdot f_y}{\gamma_{M0}} = 5293\ kN$

$$\frac{486,85}{5293} = 0,09 \leq 1$$

Cl. 6.2.6

SHEAR

$V_{Ed} = 33,774\ kN$

$V_{c,Rd} = V_{pl,Rd} = 2420\ kN$

$$\frac{33,774}{2420} = 0,01 \leq 1$$

Cl. 6.2.9.1

BENDING AND AXIAL FORCE

$M_{Ed} = 105,3\ kNm$

$M_{pl,Rd} = 308,8\ kNm$

Eq (6.13)

Eq (6.33; 6.34)

$N_{Ed} = 486,85\ kN$

$486,85 \leq 1323$

$486,85 \geq 1171,5$

$$\frac{105,3}{308,8} = 0,34 \leq 1$$

MEMBER NO. 2

Cl. 6.2.3

TENSION

$N_{Ed} = 33,74\ kN$

$N_{t,Rd} = \frac{A \cdot f_y}{\gamma_{M0}} = \frac{21180 \cdot 355}{\gamma_{M0}} = 7518\ kN$

$$\frac{33,74}{7518} = 4,48 \cdot 10^{-3} \leq 1$$

Cl. 6.2.6

SHEAR

$V_{Ed} = 137$ kN

Eq (6.18)

$A_{v,pl} = 8376$ mm²

$$V_{c,Rd} = V_{pl,Rd} = \frac{A_{v,pl}\,(f_y/\sqrt{3})}{\gamma_{M0}} = \frac{8376\,(355/\sqrt{3})}{\gamma_{M0}=1} = 1716 \text{ kN}$$

$$\frac{137}{1716} = 0{,}08 \leq 1$$

Cl. 6.2.9.1.

BENDING AND AXIAL FORCE

$N_{Ed} = 33{,}74$ kN $\quad N_{pl,Rd} = 7518$ kN

Eq (6.33, 6.34)

$M_{Ed} = 853{,}1$ kNm

$33{,}74 \leq 0{,}25 \cdot 7518 = 1879{,}5$ kN

Eq (6.13)

$$M_{Rd} = M_{pl,Rd} = \frac{W_{pl,y}\cdot f_y}{\gamma_{M0}} \qquad 33{,}74 \leq \frac{0{,}5\cdot 438\cdot 12{,}5\cdot 355\cdot 10^{-3}}{1} = 971{,}8 \text{ kN}$$

$$= \frac{4\,622\,000\cdot 355}{1} = 1640{,}8 \text{ kNm}$$

$$\frac{853{,}1}{1640{,}8} = 0{,}52 \leq 1$$

MEMBER NO. 4

Cl. 6.2.5.

BENDING

$M_{Ed} = 966{,}73$ kNm

Eq (6.13)

$M_{c,Rd} = M_{pl,Rd} = 1640{,}8$ kNm

$$\frac{966{,}73}{1640{,}8} = 0{,}58 \leq 1$$

Cl. 6.2.6

SHEAR

$V_{Ed} = 349$ kN

Eq. (6.18)

$V_{c,Rd} = 1716$ kN $\qquad \frac{349}{1716} = 0{,}20 \leq 1$

Cl. 6.2.8

BENDING AND SHEAR

$M_{Ed} = 966{,}73$ kNm
$M_{pl,Rd} = M_{pl,Rd} = 1640{,}8$ kNm
$V_{Ed} = 349$ kN
$V_{c,Rd,pl} = 1716$ kN

if $V_{Ed} \leq 0{,}5 \cdot V_{c,Rd,pl}$ can be omitted

$349 \leq 0{,}5 \cdot 1716 = 858$

$$\frac{966{,}73}{1640{,}8} = 0{,}58 \leq 1$$

BUCKLING RESISTANCE OF MEMBERS

MEMBER NO. 2

Cl. 6.3.2.1

BENDING

$M_{Ed} = 853,1$ kNm

$M_{b,Rd} = \chi_{LT} \cdot W_y \cdot \frac{f_y}{\gamma_{M1}}$

$\gamma_{M1} = 1$

$W_y = W_{pl,y}$

Cl. 6.3.2.3

$$\chi_{LT} = \frac{1}{\phi_{LT} + \sqrt{\phi_{LT}^2 - \beta \bar{\lambda}_{LT}^2}} \qquad \chi_{LT} \leq 1 \qquad \chi_{LT} \leq \frac{1}{\bar{\lambda}_{LT}^2}$$

$$\phi_{LT} = 0,5 \left[1 + \alpha_{LT} (\bar{\lambda}_{LT} - \bar{\lambda}_{LT,0}) + \beta \bar{\lambda}_{LT}^2 \right]$$

$$\bar{\lambda}_{LT} = \sqrt{\frac{W_y f_y}{M_{cr}}}$$

$\beta = 0,75$

$\bar{\lambda}_{LT,0} = 0,4$

$h/b = 1,8 \rightarrow b$

$\alpha_{LT} = 0,34$

$L = 6,84$ m

CRITICAL MOMENT

$$M_{cr} = \mu_{cr} \cdot \frac{\pi \cdot \sqrt{E I_z \cdot G I_t}}{L}$$

$\psi = -0,1$

$$M_{cr} = \mu_{cr} \frac{\pi \cdot \sqrt{210 \cdot 10^9 \cdot 3,515 \cdot 10^{-6} \cdot 81000 \cdot 10^3 \cdot 1,082 \cdot 10^{-4}}}{6,84} = 1168,2 \, \mu_{cr}$$

$k_w = 1$; $k_y = 1$; $z_j = 0$; $z_g = 0$

$$k_{wt} = \frac{\pi}{k_w \cdot L} \sqrt{\frac{E \cdot I_w}{G \cdot I_t}} = \frac{\pi}{1 \cdot 6,84} \sqrt{\frac{210 \cdot 10^9 \cdot 7,189}{3,515 \cdot 10^{-6} \cdot 81 \cdot 10^6}} = 1,057$$

$k_z = 0,7 L$

$C_1 = 3,322$

$C_3 = 1,55$

$$\mu_{cr} = \frac{C_1}{k_z} \sqrt{(1 + k_{wt}^2} = \frac{3,322}{0,7} \sqrt{1 + 1,057^2}$$

$$\mu_{cr} = 4,833$$

$M_{cr} = 4,833 \cdot 1168,2 = 5645$ kNm

$$\bar{\lambda}_{LT} = \sqrt{\frac{4622000 \cdot 355}{5645 \cdot 10^6}} = 0,53 \rightarrow \chi_{LT} = 0,87$$

$M_{b,Rd} = 0,87 \cdot 4622000 \cdot 355 = 1427,5$

$$\frac{853,1}{1427,5} = 0,59 \leq 1$$

MEMBER NO. 4

Cl. 6.3.2.1

BENDING

$M_{Ed} = 966$ kNm

$M_{b,Rd} = \chi_{LT} W_y \cdot \frac{f_y}{\gamma_{M1}}$

CRITICAL MOMENT

for cantilever $k_y = k_z = k_w = 2$

$z_j = 0 \quad z_g = 0$

$$k_{wt} = \frac{\pi}{k_w L}\sqrt{\frac{EI_w}{GI_t}} = \sqrt{\frac{210\cdot 10^3 \cdot 7,189\cdot 10^{12}}{81000 \cdot 3515000}} \cdot \frac{\pi}{2\cdot 2770} = 1,35$$

$$k_{wt,0} = k_{wt} \cdot k_w = 1,35 \cdot 2 = 2,71$$

for $k_{wt,0} \leq 8$ and $z_j = 0 \; ; z_g = 0$

$$\mu_{cr} = 1,27 + 1,14 \cdot k_{wt,0} + 0,017\, k_{wt,0}^2 = 1,27 + 1,14 \cdot 2,71 + 0,017 \cdot 2,71^2 = 4,484$$

$$M_{cr} = \mu_{cr} \cdot \frac{\pi\sqrt{E \cdot I_z \cdot G \cdot I_t}}{L} = 4,484 \cdot \frac{\pi\sqrt{210\cdot 10^3 \cdot 1,082\cdot 10^8 \cdot 81000 \cdot 351500}}{2770}$$

$M_{cr} = 12762,1$ kNm

$$\bar{\lambda}_{LT} = \sqrt{\frac{4622000 \cdot 355}{12762,1 \cdot 10^6}} = 0,35 \quad \rightarrow \quad \chi_{LT} = 0,98$$

$M_{b,Rd} = 0,98 \cdot 4622000 \cdot 355 = 1607,9$ kNm

$$\frac{966}{1607,9} = 0,60 \leq 1$$

MEMBER NO. 3

Cl. 6.3.3.

BENDING AND AXIAL COMPRESSION

Eq (6.61)

omitting M_y since the cross section is 90° rotated

$$\frac{N_{Ed}}{\frac{\chi_y N_{Rk}}{\gamma_{M1}}} + k_{yz} \frac{M_{z,Ed} + \Delta M_{z,Ed}}{\frac{M_{z,Rk}}{\gamma_{M1}}} \leq 1$$

Eq (6.62)

$$\frac{N_{Ed}}{\frac{\chi_z N_{Rk}}{\gamma_{M1}}} + k_{zz} \frac{M_{z,Ed} + \Delta M_{z,Ed}}{\frac{M_{z,Rk}}{\gamma_{M1}}} \leq 1$$

$N_{Ed} = 486,85$ kN

$N_{Rk} = f_y \cdot A = 355 \cdot 14910 = 5293$ kN

$M_{Rk,z} = f_y \cdot W_{pl,z} = \overset{870\ 100}{1407000} \cdot 355 = \overset{308,9}{392,985}$ kNm

$\Delta M_{z,Ed} = 0$ $\quad M_{z,Ed} = 105,3$ kNm

$L_{cr} = 4,21$ m

$i_y = 129,9$ mm

$i_z = 75,8$ mm

$\alpha_y = 0,34$

$\alpha_z = 0,49$

$$\bar{\lambda}_y = \sqrt{\frac{A \cdot f_y}{N_{cr,y}}} = \frac{L_{cr} \cdot 1}{i_y \cdot \lambda_1}$$

$$\lambda_1 = 93,9 \sqrt{\frac{E}{f_y}} = 93,9 \sqrt{\frac{210000}{355}}$$

$$\lambda_1 = 76,37$$

$$\bar{\lambda}_y = \frac{4210 \cdot 1}{129,9 \cdot 76,37} = 0,424$$

$$\bar{\lambda}_z = \frac{4210 \cdot 1}{75,8 \cdot 76,37} = 0,727$$

$$\phi_y = 0,5 \cdot \left[1 + \alpha_y (\bar{\lambda}_y - 0,2) + \bar{\lambda}_y^2\right] = 0,5 \cdot \left[1 + 0,34 (0,424 - 0,2) + 0,424^2\right]$$

$$\phi_y = 0,628$$

$$\phi_z = 0,5 \cdot \left[1 + \alpha_z (\bar{\lambda}_z - 0,2) + \bar{\lambda}_z^2\right] = 0,5 \cdot \left[1 + 0,49 (0,727 - 0,2) + 0,727^2\right]$$

$$\phi_z = 0,893$$

$$\chi_y = \left(\phi_y + \sqrt{(\phi_y^2 - \bar{\lambda}_y^2)}\right)^{-1} = \left(0,628 + \sqrt{0,628^2 - 0,424^2}\right)^{-1} = 0,916$$

$$\chi_z = \left(\phi_z + \sqrt{(\phi_z^2 - \bar{\lambda}_z^2)}\right)^{-1} = \left(0,893 + \sqrt{0,893^2 - 0,727^2}\right)^{-1} = 0,708$$

Table B.1

Table B.3

choose of $k_{yy}, k_{yz}, k_{zy}, k_{zz}$

C_{mz}

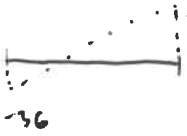

$\psi = -0,34$

$0,6 + 0,4 \cdot 0,34 \cdot (-1) = 0,464$

$C_{mz} = 0,464$

$$k_{zz,1} = C_{mz}\left(1 + (2\cdot\bar{\lambda}_z - 0,6)\frac{N_{Ed}}{\chi_z \cdot \frac{N_{Rk}}{\gamma_{M1}}}\right)$$

$$= 0,464\left(1 + (2\cdot 0,727 - 0,6)\frac{486,85}{0,708\cdot 5293}\right) = 0,515$$

$$k_{zz,2} = C_{mz}\left(1 + 1,4\frac{N_{Ed}}{\chi_z N_{Rk}}\right) = 0,464\left(1 + 1,4\frac{486,85}{0,708\cdot 5293}\right) = 0,548$$

$k_{yz} = 0,6 \cdot k_{zz,1} = 0,309$

Eq (6.61)

$$\frac{486,85}{0,946\cdot 5293} + 0,309\frac{105,3}{308,9} = 0,20 \leq 1$$

$$\frac{486,85}{0,727\cdot 5293} + 0,515\frac{105,3}{308,9} = 0,30 \leq 1$$

Appendix C

Developed codes

Developed codes were splitted into two types. Codes written in Python for Abaqus modelling, definition of the properties and extracting the results, and codes writen in MATLAB for executing the whole process of computations and proccesing the results.

Attached there are only two Python scripts for calculating the critical force (LBA and GMNIA - Listing C.1) and for results extracting (Listing C.2). Code developed for the mesh convergence is slightly different in manner of mesh seed size variable. First of the matlab codes is material properties generator according to Annex C of [4] (Listing C.3), next code is showing the execution of the whole script (Listing C.4) and last attached code was written to process the results of the current iterations (Listing C.5).

The rest of the codes can be found visiting the hyperlink provided by the QR code together with the text files containing the outputs.

Figure C.1: QR code with hyperlink to the developed codes

Listing C.1: Example of the code developed for calculating the critical force

```
### General Information
# Developed script for Diploma thesis calculations
# Author: Martin Kapoun
# Contact: martin.kapoun@gmail.com
# Home university: CTU in Prague
# Date: 12/2018
# Developed during ERASMUS exchange program at KTH Royal
# Technical University in Stockholm
###

### Description of the code
# Python script for modelling and defining the properties of the
# analyzed structure. Two models are created with variables of material
# executed from different file. Model one is linear buckling
# analysis, extracting two eigen modes and loading them as an initial
# imperfections into model two, model two is nonlinear buckling
# analysis with output for load-displacement graph
###

from part import *
from material import *
from section import *
from assembly import *
from step import *
from interaction import *
from load import *
from mesh import *
from optimization import *
from job import *
from sketch import *
from visualization import *
from connectorBehavior import *

import os

os.chdir('C:/_thesis')

execfile('C:/_thesis/s07var.py')
execfile('C:/_thesis/s07material.py')

Me = str(Me)
Ma = str(Ma)
```

```
load1 = -86100
load2 = 1960
load3 = -349000


### Model-1 ###
mdb.models['Model-1'].ConstrainedSketch(name='__sweep__', sheetSize=1000.0)
mdb.models['Model-1'].sketches['__sweep__'].Line(point1=(-160.0, -100.0),
    point2=(-160.0, 60.0))
mdb.models['Model-1'].sketches['__sweep__'].geometry.findAt((-160.0, -20.0))
mdb.models['Model-1'].sketches['__sweep__'].VerticalConstraint(addUndoState=
    False, entity=mdb.models['Model-1'].sketches['__sweep__'].geometry.findAt((
    -160.0, -20.0), ))
mdb.models['Model-1'].sketches['__sweep__'].Line(point1=(-160.0, 60.0), point2=
    (120.0, 60.0))
mdb.models['Model-1'].sketches['__sweep__'].geometry.findAt((-20.0, 60.0))
mdb.models['Model-1'].sketches['__sweep__'].HorizontalConstraint(addUndoState=
    False, entity=mdb.models['Model-1'].sketches['__sweep__'].geometry.findAt((
    -20.0, 60.0), ))

... modelling part of the code is largely omitted ...

mdb.models['Model-1'].parts['Part-1'].ShellExtrude(depth=540.0,
    flipExtrudeDirection=OFF, sketch=
    mdb.models['Model-1'].sketches['__profile__'], sketchOrientation=LEFT,
    sketchPlane=mdb.models['Model-1'].parts['Part-1'].faces.findAt((6910.0,
    3960.0, 109.779876), (0.0, 1.0, 0.0)), sketchPlaneSide=SIDE1, sketchUpEdge=
    mdb.models['Model-1'].parts['Part-1'].edges.findAt((7662.5, 3960.0,
    159.779875), ))
del mdb.models['Model-1'].sketches['__profile__']

### Material ###
mdb.models['Model-1'].Material(name='stainless-'+Ma+'-linear')
mdb.models['Model-1'].materials['stainless-'+Ma+'-linear'].Elastic(table=((
    200000.0, 0.3), ))


### Sections ###
mdb.models['Model-1'].HomogeneousShellSection(idealization=NO_IDEALIZATION,
    integrationRule=SIMPSON, material='stainless-'+Ma+'-linear', name='HEA550-tf'
    , numIntPts=5, poissonDefinition=DEFAULT, preIntegrate=OFF, temperature=
    GRADIENT, thickness=24.0, thicknessField='', thicknessModulus=None,
    thicknessType=UNIFORM, useDensity=OFF)
mdb.models['Model-1'].HomogeneousShellSection(idealization=NO_IDEALIZATION,
```

```
    integrationRule=SIMPSON, material='stainless-'+Ma+'-linear', name='HEA550-tw'
    , numIntPts=5, poissonDefinition=DEFAULT, preIntegrate=OFF, temperature=
    GRADIENT, thickness=12.5, thicknessField='', thicknessModulus=None,
    thicknessType=UNIFORM, useDensity=OFF)
mdb.models['Model-1'].HomogeneousShellSection(idealization=NO_IDEALIZATION,
    integrationRule=SIMPSON, material='stainless-'+Ma+'-linear', name='HEB300',
    numIntPts=5, poissonDefinition=DEFAULT, preIntegrate=OFF, temperature=
    GRADIENT, thickness=19.0, thicknessField='', thicknessModulus=None,
    thicknessType=UNIFORM, useDensity=OFF)
mdb.models['Model-1'].sections.changeKey(fromName='HEB300', toName='HEB300-tf')
mdb.models['Model-1'].HomogeneousShellSection(idealization=NO_IDEALIZATION,
    integrationRule=SIMPSON, material='stainless-'+Ma+'-linear', name='HEB300-tw'
    , numIntPts=5, poissonDefinition=DEFAULT, preIntegrate=OFF, temperature=
    GRADIENT, thickness=11.0, thicknessField='', thicknessModulus=None,
    thicknessType=UNIFORM, useDensity=OFF)
mdb.models['Model-1'].HomogeneousShellSection(idealization=NO_IDEALIZATION,
    integrationRule=SIMPSON, material='stainless-'+Ma+'-linear', name='PL10',
    numIntPts=5, poissonDefinition=DEFAULT, preIntegrate=OFF, temperature=
    GRADIENT, thickness=10.0, thicknessField='', thicknessModulus=None,
    thicknessType=UNIFORM, useDensity=OFF)

### Sections Assignment ###
mdb.models['Model-1'].parts['Part-1'].SectionAssignment(offset=0.0,
    offsetField='', offsetType=MIDDLE_SURFACE, region=Region(
    faces=mdb.models['Model-1'].parts['Part-1'].faces.findAt(((6960.0,
    1333.333333, -140.220125), (0.0, 0.0, -1.0)), ((6910.0, 1333.333333,
    159.779875), (0.0, 0.0, 1.0)), ((6760.0, 1333.333333, 159.779875), (0.0,
    0.0, 1.0)), ((6760.0, 1333.333333, -140.220125), (0.0, 0.0, 1.0)), ((100.0,
    3200.0, -140.220125), (0.0, 0.0, 1.0)), ((-50.0, 3200.0, 159.779875), (0.0,
    0.0, 1.0)), ((100.0, 3200.0, 159.779875), (0.0, 0.0, 1.0)), ((-100.0,
    3200.0, -140.220125), (0.0, 0.0, -1.0)), )), sectionName='HEB300-tf',
    thicknessAssignment=FROM_SECTION)
mdb.models['Model-1'].parts['Part-1'].SectionAssignment(offset=0.0,
    offsetField='', offsetType=MIDDLE_SURFACE, region=Region(
    faces=mdb.models['Model-1'].parts['Part-1'].faces.findAt(((6860.0,
    2646.666667, -90.220124), (-1.0, 0.0, 0.0)), ((0.0, 3200.0, 59.779875), (
    1.0, 0.0, 0.0)), )), sectionName='HEB300-tw', thicknessAssignment=
    FROM_SECTION)
mdb.models['Model-1'].parts['Part-1'].SectionAssignment(offset=0.0,
    offsetField='', offsetType=MIDDLE_SURFACE, region=Region(
    faces=mdb.models['Model-1'].parts['Part-1'].faces.findAt(((2386.666667,
    4500.0, 144.779877), (0.0, 1.0, 0.0)), ((7780.0, 4500.0, -90.220124), (0.0,
    1.0, 0.0)), ((6810.0, 3960.0, 109.779876), (0.0, 1.0, 0.0)), ((6910.0,
    3960.0, -90.220124), (0.0, -1.0, 0.0)), ((7780.0, 4500.0, 59.779875), (0.0,
    1.0, 0.0)), ((6810.0, 3960.0, -90.220124), (0.0, -1.0, 0.0)), ((
```

```
    2386.666667, 4500.0, -25.220125), (0.0, 1.0, 0.0)), ((100.0, 4500.0,
    44.779875), (0.0, -1.0, 0.0)), ((6910.0, 3960.0, 109.779876), (0.0, 1.0,
    0.0)), )), sectionName='HEA550-tf', thicknessAssignment=FROM_SECTION)
mdb.models['Model-1'].parts['Part-1'].SectionAssignment(offset=0.0,
    offsetField='', offsetType=MIDDLE_SURFACE, region=Region(
    faces=mdb.models['Model-1'].parts['Part-1'].faces.findAt(((7780.0, 4320.0,
    9.779875), (0.0, 0.0, 1.0)), ((4623.333333, 4140.0, 9.779875), (0.0, 0.0,
    1.0)), )), sectionName='HEA550-tw', thicknessAssignment=FROM_SECTION)
mdb.models['Model-1'].parts['Part-1'].SectionAssignment(offset=0.0,
    offsetField='', offsetType=MIDDLE_SURFACE, region=Region(
    faces=mdb.models['Model-1'].parts['Part-1'].faces.findAt(((6860.0, 4320.0,
    -90.220124), (1.0, 0.0, 0.0)), ((6860.0, 4320.0, 59.779875), (1.0, 0.0,
    0.0)), )), sectionName='PL10', thicknessAssignment=FROM_SECTION)

### Assembly ###
mdb.models['Model-1'].rootAssembly.DatumCsysByDefault(CARTESIAN)
mdb.models['Model-1'].rootAssembly.Instance(dependent=OFF, name='Part-1-1',
    part=mdb.models['Model-1'].parts['Part-1'])

### Step ###
mdb.models['Model-1'].BuckleStep(maxIterations=100, name='Step-1', numEigen=6,
    previous='Initial', vectors=12)

### Reference Points ###
mdb.models['Model-1'].rootAssembly.ReferencePoint(point=
    mdb.models['Model-1'].rootAssembly.instances['Part-1-1'].InterestingPoint(
    mdb.models['Model-1'].rootAssembly.instances['Part-1-1'].edges.findAt((
    9620.0, 4095.0, 9.779875), ), MIDDLE))
mdb.models['Model-1'].rootAssembly.ReferencePoint(point=
    mdb.models['Model-1'].rootAssembly.instances['Part-1-1'].vertices.findAt((
    0.0, 4800.0, 9.779875), ))
mdb.models['Model-1'].rootAssembly.ReferencePoint(point=
    mdb.models['Model-1'].rootAssembly.instances['Part-1-1'].vertices.findAt((
    0.0, 0.0, 9.779875), ))
mdb.models['Model-1'].rootAssembly.ReferencePoint(point=
    mdb.models['Model-1'].rootAssembly.instances['Part-1-1'].InterestingPoint(
    mdb.models['Model-1'].rootAssembly.instances['Part-1-1'].edges.findAt((0.0,
    4095.0, 9.779875), ), MIDDLE))
mdb.models['Model-1'].rootAssembly.ReferencePoint(point=
    mdb.models['Model-1'].rootAssembly.instances['Part-1-1'].InterestingPoint(
    mdb.models['Model-1'].rootAssembly.instances['Part-1-1'].edges.findAt((
    6860.0, 20.0, -65.220125), ), MIDDLE))
mdb.models['Model-1'].RigidBody(name='Constraint-1', pinRegion=Region(
    edges=mdb.models['Model-1'].rootAssembly.instances['Part-1-1'].edges.findAt(
    ((9620.0, 4500.0, -27.720125), ), ((9620.0, 4095.0, 9.779875), ), ((9620.0,
```

```
    3960.0, -102.720125), ), ((9620.0, 4500.0, 122.279875), ), ((9620.0,
    3960.0, 122.279875), ), )), refPointRegion=Region(referencePoints=(
    mdb.models['Model-1'].rootAssembly.referencePoints[4], )))
mdb.models['Model-1'].RigidBody(name='Constraint-2', pinRegion=Region(
    edges=mdb.models['Model-1'].rootAssembly.instances['Part-1-1'].edges.findAt(
    ((112.5, 4800.0, -140.220125), ), ((0.0, 4800.0, 47.279875), ), ((0.0,
    4800.0, -102.720125), ), ((-37.5, 4800.0, 159.779875), ), ((112.5, 4800.0,
    159.779875), ), ((-112.5, 4800.0, -140.220125), ), )), refPointRegion=
    Region(referencePoints=(
    mdb.models['Model-1'].rootAssembly.referencePoints[5], )))
mdb.models['Model-1'].RigidBody(name='Constraint-3', pinRegion=Region(
    edges=mdb.models['Model-1'].rootAssembly.instances['Part-1-1'].edges.findAt(
    ((37.5, 0.0, -140.220125), ), ((0.0, 0.0, 47.279875), ), ((0.0, 0.0,
    -27.720125), ), ((-37.5, 0.0, 159.779875), ), ((37.5, 0.0, 159.779875), ),
    ((-37.5, 0.0, -140.220125), ), )), refPointRegion=Region(referencePoints=(
    mdb.models['Model-1'].rootAssembly.referencePoints[6], )))
mdb.models['Model-1'].RigidBody(name='Constraint-4', pinRegion=Region(
    edges=mdb.models['Model-1'].rootAssembly.instances['Part-1-1'].edges.findAt(
    ((0.0, 3960.0, 88.529875), ), ((0.0, 3960.0, -68.970125), ), ((0.0, 4095.0,
    9.779875), ), ((0.0, 4500.0, -16.470125), ), ((0.0, 4500.0, 36.029875), ),
    )), refPointRegion=Region(referencePoints=(
    mdb.models['Model-1'].rootAssembly.referencePoints[7], )))
mdb.models['Model-1'].RigidBody(name='Constraint-5', pinRegion=Region(
    edges=mdb.models['Model-1'].rootAssembly.instances['Part-1-1'].edges.findAt(
    ((6972.5, 20.0, -140.220125), ), ((6860.0, 20.0, -65.220125), ), ((6897.5,
    20.0, 159.779875), ), ((6747.5, 20.0, 159.779875), ), ((6747.5, 20.0,
    -140.220125), ), )), refPointRegion=Region(referencePoints=(
    mdb.models['Model-1'].rootAssembly.referencePoints[8], )))

### Loading ###
mdb.models['Model-1'].ConcentratedForce(cf2=load1, createStepName='Step-1',
    distributionType=UNIFORM, field='', localCsys=None, name='Load-1', region=
    Region(referencePoints=(
    mdb.models['Model-1'].rootAssembly.referencePoints[5], )))
mdb.models['Model-1'].ConcentratedForce(cf1=load2, createStepName='Step-1',
    distributionType=UNIFORM, field='', localCsys=None, name='Load-2', region=
    Region(referencePoints=(
    mdb.models['Model-1'].rootAssembly.referencePoints[7], )))
mdb.models['Model-1'].ConcentratedForce(cf2=load3, createStepName='Step-1',
    distributionType=UNIFORM, field='', localCsys=None, name='Load-3', region=
    Region(referencePoints=(
    mdb.models['Model-1'].rootAssembly.referencePoints[4], )))


### BC ###
```

```
mdb.models['Model-1'].EncastreBC(createStepName='Step-1', localCsys=None, name=
    'BC-1', region=Region(referencePoints=(
    mdb.models['Model-1'].rootAssembly.referencePoints[6],
    mdb.models['Model-1'].rootAssembly.referencePoints[8], )))

### Mesh Element type ###
mdb.models['Model-1'].rootAssembly.setElementType(elemTypes=(ElemType(
    elemCode=S8R, elemLibrary=STANDARD), ElemType(elemCode=STRI65,
    elemLibrary=STANDARD)), regions=(
    mdb.models['Model-1'].rootAssembly.instances['Part-1-1'].faces.findAt(((
    6860.0, 4320.0, -90.220124), ), ((6860.0, 4320.0, 59.779875), ), ((
    2386.666667, 4500.0, 144.779877), ), ((7780.0, 4500.0, -90.220124), ), ((
    7780.0, 4320.0, 9.779875), ), ((6960.0, 1333.333333, -140.220125), ), ((
    6860.0, 2646.666667, -90.220124), ), ((6910.0, 1333.333333, 159.779875), ),
    ((6760.0, 1333.333333, 159.779875), ), ((6760.0, 1333.333333, -140.220125),
    ), ((6810.0, 3960.0, 109.779876), ), ((6910.0, 3960.0, -90.220124), ), ((
    7780.0, 4500.0, 59.779875), ), ((6810.0, 3960.0, -90.220124), ), ((
    4623.333333, 4140.0, 9.779875), ), ((2386.666667, 4500.0, -25.220125), ), (
    (100.0, 4500.0, 44.779875), ), ((6910.0, 3960.0, 109.779876), ), ((100.0,
    3200.0, -140.220125), ), ((0.0, 3200.0, 59.779875), ), ((-50.0, 3200.0,
    159.779875), ), ((100.0, 3200.0, 159.779875), ), ((-100.0, 3200.0,
    -140.220125), ), ), ))

        # mdb.models['Model-1'].rootAssembly.setElementType(elemTypes=(ElemType(
    # elemCode=S4R, elemLibrary=STANDARD, secondOrderAccuracy=OFF,
    # hourglassControl=DEFAULT), ElemType(elemCode=S3, elemLibrary=STANDARD)),
    # regions=(
        # mdb.models['Model-1'].rootAssembly.setElementType(elemTypes=(ElemType(
    # elemCode=S4, elemLibrary=STANDARD, secondOrderAccuracy=OFF), ElemType(
    # elemCode=S3, elemLibrary=STANDARD)), regions=(

### Seed mesh ###
mdb.models['Model-1'].rootAssembly.seedPartInstance(deviationFactor=0.1,
    minSizeFactor=0.1, regions=(
    mdb.models['Model-1'].rootAssembly.instances['Part-1-1'], ), size=meshSeedSize)

### Mesh Part ###
mdb.models['Model-1'].rootAssembly.generateMesh(regions=(
    mdb.models['Model-1'].rootAssembly.instances['Part-1-1'], ))

### Field Output Request ###
mdb.models['Model-1'].fieldOutputRequests['F-Output-1'].setValues(variables=(
    'U', 'COORD'))

### Create Job ###
```

```
mdb.Job(atTime=None, contactPrint=OFF, description='', echoPrint=OFF,
    explicitPrecision=SINGLE, getMemoryFromAnalysis=True, historyPrint=OFF,
    memory=90, memoryUnits=PERCENTAGE, model='Model-1', modelPrint=OFF,
    multiprocessingMode=DEFAULT, name='LinearBuckling', nodalOutputPrecision=
    SINGLE, numCpus=1, numGPUs=0, queue=None, resultsFormat=ODB, scratch='',
    type=ANALYSIS, userSubroutine='', waitHours=0, waitMinutes=0)

### Copy model ###
mdb.Model(name='Model-2', objectToCopy=mdb.models['Model-1'])

### Editing keywords ###
mdb.models['Model-1'].keywordBlock.synchVersions(storeNodesAndElements=False)
mdb.models['Model-1'].keywordBlock.replace(85, '\n')
mdb.models['Model-1'].keywordBlock.replace(86,
    '\n*Output, field, variables=PRESELECT\n*NODE FILE\nU')
        #'\n*Output, field, variables=PRESELECT\n*FILE FORMAT, ASCII\n*NODE FILE\nU')

elemArr = mdb.models['Model-1'].rootAssembly.instances['Part-1-1'].elements;

### Submit Job ###
mdb.jobs['LinearBuckling'].submit(consistencyChecking=OFF)
mdb.jobs['LinearBuckling'].waitForCompletion()

###### Model-2 ######

odb = openOdb(path = 'LinearBuckling.odb')

STEP = odb.steps.values()[0]

noEl = len(elemArr)

mode = STEP.frames[2].description
eigenValueStr = mode[31:]

f = open('Results\s07Eigen-'+Me+'-'+Ma+'.txt','w+')
f.write('%d,'% noEl)
f.write(eigenValueStr)

eigenValue = float(eigenValueStr)

odb.close()

quit

### Material ###
```

```
del mdb.models['Model-2'].materials['stainless-'+Ma+'-linear']
mdb.models['Model-2'].Material(name='stainless-'+Ma+'-nonlinear')
mdb.models['Model-2'].materials['stainless-'+Ma+'-nonlinear'].Elastic(table=((
    200000.0, 0.3), ))
mdb.models['Model-2'].materials['stainless-'+Ma+'-nonlinear'].Plastic(
    table=(materialGen))

### Section ###
mdb.models['Model-2'].sections['HEA550-tf'].setValues(idealization=
    NO_IDEALIZATION, integrationRule=SIMPSON, material=
    'stainless-'+Ma+'-nonlinear', numIntPts=5, preIntegrate=OFF, thickness=24.0,
    thicknessField='', thicknessType=UNIFORM)
mdb.models['Model-2'].sections['HEA550-tw'].setValues(idealization=
    NO_IDEALIZATION, integrationRule=SIMPSON, material=
    'stainless-'+Ma+'-nonlinear', numIntPts=5, preIntegrate=OFF, thickness=12.5,
    thicknessField='', thicknessType=UNIFORM)
mdb.models['Model-2'].sections['HEB300-tf'].setValues(idealization=
    NO_IDEALIZATION, integrationRule=SIMPSON, material=
    'stainless-'+Ma+'-nonlinear', numIntPts=5, preIntegrate=OFF, thickness=19.0,
    thicknessField='', thicknessType=UNIFORM)
mdb.models['Model-2'].sections['HEB300-tw'].setValues(idealization=
    NO_IDEALIZATION, integrationRule=SIMPSON, material=
    'stainless-'+Ma+'-nonlinear', numIntPts=5, preIntegrate=OFF, thickness=11.0,
    thicknessField='', thicknessType=UNIFORM)
mdb.models['Model-2'].sections['PL10'].setValues(idealization=NO_IDEALIZATION,
    integrationRule=SIMPSON, material='stainless-'+Ma+'-nonlinear', numIntPts=5,
    preIntegrate=OFF, thickness=10.0, thicknessField='', thicknessType=UNIFORM)

### Step ###
del mdb.models['Model-2'].steps['Step-1']
mdb.models['Model-2'].StaticStep(initialInc=ii, maxInc=mi, maxNumInc=mni,
    name='Step-1', nlgeom=ON, previous='Initial')

### BC ###
mdb.models['Model-2'].EncastreBC(createStepName='Step-1', localCsys=None, name=
    'BC-1', region=Region(referencePoints=(
    mdb.models['Model-2'].rootAssembly.referencePoints[6],
    mdb.models['Model-2'].rootAssembly.referencePoints[8], )))
mdb.models['Model-2'].DisplacementBC(amplitude=UNSET, createStepName='Step-1',
    distributionType=UNIFORM, fieldName='', fixed=OFF, localCsys=None, name=
    'BC-2', region=Region(referencePoints=(
    mdb.models['Model-2'].rootAssembly.referencePoints[4], )), u1=UNSET, u2=
    -500.0, u3=UNSET, ur1=UNSET, ur2=UNSET, ur3=UNSET)

### Mesh Element type ###
```

```
mdb.models['Model-2'].rootAssembly.setElementType(elemTypes=(ElemType(
    elemCode=S8R, elemLibrary=STANDARD), ElemType(elemCode=STRI65,
    elemLibrary=STANDARD)), regions=(
    mdb.models['Model-2'].rootAssembly.instances['Part-1-1'].faces.findAt(((
    6860.0, 4320.0, -90.220124), ), ((6860.0, 4320.0, 59.779875), ), ((
    2386.666667, 4500.0, 144.779877), ), ((7780.0, 4500.0, -90.220124), ), ((
    7780.0, 4320.0, 9.779875), ), ((6960.0, 1333.333333, -140.220125), ), ((
    6860.0, 2646.666667, -90.220124), ), ((6910.0, 1333.333333, 159.779875), ),
    ((6760.0, 1333.333333, 159.779875), ), ((6760.0, 1333.333333, -140.220125),
    ), ((6810.0, 3960.0, 109.779876), ), ((6910.0, 3960.0, -90.220124), ), ((
    7780.0, 4500.0, 59.779875), ), ((6810.0, 3960.0, -90.220124), ), ((
    4623.333333, 4140.0, 9.779875), ), ((2386.666667, 4500.0, -25.220125), ), (
    (100.0, 4500.0, 44.779875), ), ((6910.0, 3960.0, 109.779876), ), ((100.0,
    3200.0, -140.220125), ), ((0.0, 3200.0, 59.779875), ), ((-50.0, 3200.0,
    159.779875), ), ((100.0, 3200.0, 159.779875), ), ((-100.0, 3200.0,
    -140.220125), ), ), ))



### Seed mesh ###
mdb.models['Model-2'].rootAssembly.seedPartInstance(deviationFactor=0.1,
    minSizeFactor=0.1, regions=(
    mdb.models['Model-2'].rootAssembly.instances['Part-1-1'], ), size=meshSeedSize)

### Mesh Part ###
mdb.models['Model-2'].rootAssembly.generateMesh(regions=(
    mdb.models['Model-2'].rootAssembly.instances['Part-1-1'], ))

### Job ###
mdb.Job(atTime=None, contactPrint=OFF, description='', echoPrint=OFF,
    explicitPrecision=SINGLE, getMemoryFromAnalysis=True, historyPrint=OFF,
    memory=90, memoryUnits=PERCENTAGE, model='Model-2', modelPrint=OFF,
    multiprocessingMode=DEFAULT, name='NonlinearBuckling',
    nodalOutputPrecision=SINGLE, numCpus=1, numGPUs=0, queue=None,
    resultsFormat=ODB, scratch='', type=ANALYSIS, userSubroutine='', waitHours=
    0, waitMinutes=0)
mdb.jobs['NonlinearBuckling'].setValues(multiprocessingMode=THREADS, numCpus=4,
    numDomains=8, numGPUs=0)

### Keywords ###
mdb.models['Model-2'].keywordBlock.synchVersions(storeNodesAndElements=False)
mdb.models['Model-2'].keywordBlock.replace(69,
    '\n**␣----------------------------------------------------------------
␣␣␣␣\n*IMPERFECTION,␣File=LinearBuckling,␣STEP=1\n2,␣'+str(imp)+'\n6,0.0625\n**
␣␣␣␣\n**␣STEP:␣Step-1\n**')
```

```
### Submit ###
mdb.jobs['NonlinearBuckling'].submit(consistencyChecking=OFF)
```

Listing C.2: Example of the code developed for extracting of the results

```
### General Information
# Developed script for Diploma thesis calculations
# Author: Martin Kapoun
# Contact: martin.kapoun@gmail.com
# Home university: CTU in Prague
# Date: 12/2018
# Developed during ERASMUS exchange program at KTH Royal
# Technical University in Stockholm
###

### Description of the code
# Python script for extracting the results and saving them
# into text file.
###

from abaqus import *
from abaqusConstants import *
import os

execfile('C:/_thesis/s07var.py')

Me = str(Me)
Ma = str(Ma)

session.Viewport(name='Viewport: 1', origin=(0.0, 0.0), width=474.605194091797,
    height=176.388885498047)
session.viewports['Viewport: 1'].makeCurrent()
session.viewports['Viewport: 1'].maximize()
from caeModules import *
from driverUtils import executeOnCaeStartup
executeOnCaeStartup()
session.viewports['Viewport: 1'].partDisplay.geometryOptions.setValues(
    referenceRepresentation=ON)
o1 = session.openOdb(
    name='C:/_thesis/NonlinearBuckling.odb')
session.viewports['Viewport: 1'].setValues(displayedObject=o1)
#: Model: H:/Diploma Thesis/ABAQUS/Model - matlab test/NonlinearBuckling.odb
#: Number of Assemblies:          1
#: Number of Assembly instances: 0
#: Number of Part instances:      1
#: Number of Meshes:              2
#: Number of Element Sets:        1
```

```
#: Number of Node Sets:          7
#: Number of Steps:              1

odb = session.odbs['C:/_thesis/NonlinearBuckling.odb']
session.viewports['Viewport:_1'].setValues(displayedObject=odb)
session.viewports['Viewport:_1'].odbDisplay.display.setValues(plotState=(
    CONTOURS_ON_DEF, ))
odb = session.odbs['C:/_thesis/NonlinearBuckling.odb']
session.xyDataListFromField(odb=odb, outputPosition=NODAL, variable=(('RF',
    NODAL, ((COMPONENT, 'RF1'), (COMPONENT, 'RF2'), (COMPONENT, 'RF3'), )), (
    'U', NODAL, ((COMPONENT, 'U1'), (COMPONENT, 'U2'), (COMPONENT, 'U3'), )),
    ), nodeSets=('REFERENCE_POINT_________1', ))
x0 = session.xyDataObjects['U:U1_PI:_ASSEMBLY_N:_1']
x1 = session.xyDataObjects['U:U2_PI:_ASSEMBLY_N:_1']
x2 = session.xyDataObjects['U:U3_PI:_ASSEMBLY_N:_1']
x3 = session.xyDataObjects['RF:RF1_PI:_ASSEMBLY_N:_1']
x4 = session.xyDataObjects['RF:RF2_PI:_ASSEMBLY_N:_1']
x5 = session.xyDataObjects['RF:RF3_PI:_ASSEMBLY_N:_1']
session.writeXYReport(fileName='C:/_thesis/Results/s07-RF-U-'+Me+'-'+Ma+'.txt',
xyData=(x0, x1, x2, x3, x4, x5))
```

Listing C.3: Example of the code developed for generating the material properties

```
function [V, tit] = s07material(mat)
%%% General Information
% Developed script for Diploma thesis calculations
% Author: Martin Kapoun
% Contact: martin.kapoun@gmail.com
% Home university: CTU in Prague
% Date: 12/2018
% Developed during ERASMUS exchange program at KTH Royal
% Technical University in Stockholm
%%%

%%% Description of the code
% Matlab function written for calculations
% of non-linear material properties based on
% Annex C of EN 1993-1-1
%%%

    switch mat
        case 1
            disp('1.4306')
            fy = 200;
            fu = 520;
            E = 200000;
            tit = '1.4306';
        case 2
            disp('1.4301')
            fy = 210;
            fu = 520;
            E = 200000;
            tit = '1.4301';
        case 3
            disp('1.4401')
            fy = 220;
            fu = 530;
            E = 200000;
            tit = '1.4401';
        case 4
            disp('1.4432')
            fy = 220;
            fu = 550;
            E = 200000;
            tit = '1.4432';
```

```
        case 5
            disp('1.4311')
            fy = 270;
            fu = 550;
            E = 200000;
            tit = '1.4311';
        case 6
            disp('1.4406')
            fy = 280;
            fu = 580;
            E = 200000;
            tit = '1.4406';
        case 7
            disp('1.4318')
            fy = 330;
            fu = 650;
            E = 200000;
            tit = '1.4318';
        case 8
            disp('1.4362')
            fy = 400;
            fu = 600;
            E = 200000;
            tit = '1.4362';
        case 9
            disp('1.4462')
            fy = 460;
            fu = 660;
            E = 200000;
            tit = '1.4462';
        otherwise
            disp('Choose available material!')
    end

    n = 6; %from table 4.1, EN 1993-1-4
    Ey = E/(1+0.002*n*E/fy);
    epsu = 1-(fy/fu);
    m = 1+3.5*(fy/fu);

    sigma1 = linspace(0.01,fy,21);
    sigma2 = linspace(fy,fu,21);

    sigma = [sigma1 sigma2(2:end)];
    eps = [];
    epsTrue = [];
```

```
    for i=1:length(sigma)
        if sigma(i) <= fy
            tempEps = (sigma(i)/E)+0.002*(sigma(i)/fy)^n;
        elseif sigma(i) <= fu
            tempEps = 0.002+(fy/E)+((sigma(i)-fy)/Ey)+epsu*((sigma(i)-fy)/(fu-fy))^m;
        end
        eps = [eps tempEps];
        tempEpsTrue = tempEps-(sigma(i)/(E));
        epsTrue = [epsTrue tempEpsTrue];
    end

    matAbaqus = [transpose(sigma) transpose(epsTrue)];

    V = matAbaqus;
    tit = tit;
end
```

Listing C.4: Example of the code developed for executing the script

```
%%% General Information
% Developed script for Diploma thesis calculations
% Author: Martin Kapoun
% Contact: martin.kapoun@gmail.com
% Home university: CTU in Prague
% Date: 12/2018
% Developed during ERASMUS exchange program at KTH Royal
% Technical University in Stockholm
%%%

%%% Description of the code
% Matlab function written for exectuing
% written python scripts and iterate them.
% Every iteration clear the whole folder.
%%%

clear, clc
mkdir('Results');

tic

%defining variables
meshSeedSizes = 50;
materials = 1:1:9;
maxInc = 0.002;
initialInc = 0.001;
maxNumInc = 200;
imp=33.5; %46.9 or 20.1 or 33.5  +-40%

%creation of variables file and iteration for each mesh size
for i = 1:length(materials)

    %deletion of all files except py scripts
    for d = dir('.\').'
      if(~d.isdir && ~any(strcmp(d.name,{'s07runMeshMaterial.m','s07Buckling.py','s07
        delete(fullfile('.\', d.name));
      end
    end

    %generate material
    [V, mat] = s07material(i);
    matfile = fopen('.\s07material.py', 'w');
```

```
    fprintf(matfile, 'materialGen=');
    V(1,2) = 0; %for abaqus - first plastic strain has to be always zero
    for j = 1:length(V)
        if j ~= length(V)
            formatSpec = '(%18.14f,%18.14f),';
            fprintf(matfile, formatSpec,V(j,1),V(j,2));
        else
            formatSpec = '(%18.14f,%18.14f)';
            fprintf(matfile, formatSpec,V(j,1),V(j,2));
        end
    end

    fclose(matfile);

    %creation of var file
    varfile = fopen('.\s07var.py', 'w');
    fprintf(varfile,'meshSeedSize=%0f\n', meshSeedSizes );
    fprintf(varfile,'Me=%0f\n', meshSeedSizes );
    fprintf(varfile,'Ma=%0s\n', mat(3:6) );
    fprintf(varfile,'mi=%6.3f\n', maxInc);
    fprintf(varfile,'ii=%6.3f\n', initialInc);
    fprintf(varfile,'mni=%0i\n', maxNumInc);
        fprintf(varfile,'imp=%4.2f\n', imp);
    fclose(varfile);

    %execution of abq py script
    system(['abq6141 cae noGUI=.\s07Buckling.py']);
    system(['abq6141 cae noGUI=.\s07NonlinearBucklingResults.py']);
end
toc

%creation of var file into results
varfile = fopen('Results\s07var.txt', 'w');
fprintf(varfile,'S8R');
fprintf(varfile,'meshSeedSize=%0f\n', meshSeedSizes );
fprintf(varfile,'Static step, general');
fprintf(varfile,'mi=%6.3s\n', maxInc);
fprintf(varfile,'ii=%6.3s\n', initialInc);
fprintf(varfile,'mni=%3s\n', maxNumInc);
fprintf(varfile,'imp=%4.2f\n', imp);
fprintf(varfile,'totalTimeAnalysis=%0s\n', toc);
fclose(varfile);
```

Listing C.5: Example of the code developed for generating the material properties

```
%%% General Information
% Developed script for Diploma thesis calculations
% Author: Martin Kapoun
% Contact: martin.kapoun@gmail.com
% Home university: CTU in Prague
% Date: 12/2018
% Developed during ERASMUS exchange program at KTH Royal
% Technical University in Stockholm
%%%

%%% Description of the code
% Matlab function written for processing
% the resulting text files into figures.
%%%

clc,clear
meshSeedSizes = 50;
A=[];
B=[];

materials = 1:1:9;
mxL = [];

hold on
for i = 1:length(materials)
    [V, Ma] = s06material(i);
    Ma = Ma(3:6);
    Me = meshSeedSizes;

    filename = ['Results\s07-RF-U-',num2str(Me),'.0-',Ma,'.txt'];
    delimiterIn = ' ';
    headerlinesIn = 2;
    B = importdata(filename,delimiterIn,headerlinesIn);
    B.textdata = str2double(B.textdata);

    rf = abs(B.textdata(3:end,6))/1000;
    x = B.textdata(3:end,2);
    y = abs(B.textdata(3:end,3));
    z = B.textdata(3:end,4);

    critLoadingNLA = rf;
    mxL = [mxL ; max(critLoadingNLA)];
```

```
    display = [' 1.' Ma ' (' num2str(mxL(i)) ' kN)'];
    h(i) = plot(y,critLoadingNLA, 'DisplayName', display );

end
hold off

legend('Location', 'southeast')
title('P-\delta graph - imp 0%')
ylabel('Load, P_{Cr} (kN)')
xlabel('Displacement, \delta (mm)')
grid on

saveas(gcf,'.\07-Pd-gr.fig')
saveas(gcf,'.\07-Pd-gr.pdf')
```